

NEW METHODS FOR CHARACTERIZING SOLID ACIDITY

By

JOHN PHILIP OSEGOVIC

A DISSERTATION PRESENTED TO THE GRADUATE SCHOOL OF THE  
UNIVERSITY OF FLORIDA IN PARTIAL FULFILLMENT OF THE  
REQUIREMENTS FOR THE DEGREE OF  
DOCTOR OF PHILOSOPHY

UNIVERSITY OF FLORIDA

1999

## ACKNOWLEDGMENTS

I would be strongly remiss if I did not try to mention all of those who contributed to the writing of this work. To start with I would like to acknowledge the faculty and staff of the University of Florida Department of Chemistry for allowing me to continue my research after the passing of Professor Russell S. Drago. I would especially like to single out Professors Russ Bowers and Mike Scott for dealing with and supporting me during a difficult time.

I would not have been able to finish my work if not for the support of all of the members of the Drago, Bowers and Scott groups. Every list must have a start so this one might as well begin with the Burrito Brothers Lunch Brigade (Karen "Captain" Frank, Steve Joerg, Alfredo Mateus, and Ben Gordon) which made lunch interesting during those first formative years. Those Crazy Microporous Guys (William Scott Kassel, J. Michael McGilvray, C. Edwin Webster "Esquire," and Andrew Cottone) who seem to have references for *everything*. The Former Inmates of room CLB 402 (Nick "The Tick" Kob, Siliva Claudia Dias, José A. Dias, Danilo "The Quiet Man" Ortillo, and Krzysztof "The Mad Pol" Jurczyk) who dealt with Emperor John of the Ever Expanding Desk Regime. And finally the Bowers NMR Crew Team and Gymnastics Squad (Vincent Storhaug, Anil Patel, Tony Zook, Gail Fanucci, and Charity Brockman), what more can be said about them that is not already in the title.

I would like to thank Dr. Ion Ghiviriga for all of his help (and patience) in teaching me to use the departmental spectrometers and Randy Duran for giving me the opportunity to travel to the Advanced Photon Source at Argonne National Laboratory.

The true movers in the chemistry department are the secretarial staff. Without them it seems that everything would grind to a halt. I know from experience that if you have a problem with ordering chemicals, formatting text, or just figuring out the right thing to say you go to visit Maribel Lisk. For those days when the University of Florida Faceless Bureaucracy Thugs seems to be in every nook and cranny, Donna Balkom is the woman to call. Her ability to drive the Thugs mercilessly to ground while at the same time soothing the graduate student serfs has saved the sanity of countless individuals (including me several times) over the years. Finally, Amanda Garrigues has been a friendly and supportive face every since she arrived not too long ago.

My most heartfelt thanks are reserved for two people: Professor Russell Drago, and my wife, Karen.

The loss of Doc was like losing a father for the second time. I deeply miss his friendship.

Even though she will not believe it, the most important thing in the world to me is the love and friendship of my wife. I attribute the greatest part of my successes to her.

## TABLE OF CONTENTS

	<u>page</u>
ACKNOWLEDGMENTS.....	ii
LIST OF TABLES.....	vi
LIST OF FIGURES.....	viii
ABSTRACT.....	xi
CHAPTER 1: INTRODUCTION TO THE CHARACTERIZATION OF SOLID ACIDITY.....	1
A Definition of Solid Acidity.....	3
Using Probe Molecules of Measure Acidity.....	6
Calorimetric Measures of Acidity.....	14
CHAPTER 2: A NEW SOLID ACIDITY SCALE.....	23
Experimental.....	28
Results and Discussion.....	31
Conclusions.....	47
CHAPTER 3: THE EFFECTS OF PROTON EXCHANGE ON 12-TUNGSTOPHOSPHORIC ACID AND ITS DERIVATIVES.....	50
Experimental.....	53
Results and Discussion.....	54
Conclusions.....	67
CHAPTER 4: THE ACTIVITY AND ACIDITY OF TWO SULFATED SILICA GELS.....	69
Experimental.....	73
Results and Discussion.....	75
Conclusions.....	81

CHAPTER 5: A NEW SOLID SUPER ACID: SILICA SUPPORTED ANTIMONY PENTACHLORIDE.....	83
Experimental.....	87
Results and Discussion.....	90
Conclusions.....	98
CHAPTER 6: GENERAL CONCLUSIONS.....	99
APPENDIX I: THE BASIC THEORY OF SOLID STATE MAGIC ANGLE SPINNING NMR.....	102
APPENDIX II: OPERATING THE SOLID STATE BRUKER AVANCE 400 MHz NMR SPECTROMETER.....	109
LIST OF REFERENCES.....	120
BIOGRAPHICAL SKETCH.....	130

## LIST OF TABLES

<u>Table</u>	<u>page</u>
Table 1-1 An example of intermolecular interactions that lead to bonding.....	4
Table 1-2 The types of forces measured in calorimetric experiments.....	15
Table 1-3 The Cal-Ad results for 12-tungstophosphoric acid (HPW) in acetonitrile solution and as a solid slurried in cyclohexane.....	18
Table 2-1 The $\Delta\delta$ Scale.....	32
Table 2-2 The inductive effect in Lewis haloacids.....	39
Table 2-3 The Cal-Ad results for HZSM-5.....	43
Table 2-4 The $\Delta\delta$ value of TEPO on several bases.....	44
Table 2-5 The coupling constants ( $J^{31}\text{P}-^{77}\text{Se}$ ) of TMPSe physisorbed on solids.....	48
Table 3-1 Comparison of the Cal-Ad site populations to the position of the protons in the crystal structure of HPW.....	60
Table 3-2 The chemical shift of cesium salts of HPW.....	67
Table 4-1 Retention time of several alcohols and ethers.....	76
Table 4-2 The acidity of two sulfated catalysts measured by calorimetry.....	77
Table 5-1 Retention times of various hydrocarbon families.....	89
Table 5-2 The ECW model can be used to predict the strength of donor-acceptor interactions.....	91
Table 5-3 $E_a$ and $C_a$ parameters for a variety of Lewis acids.....	92
Table 5-4 Assignment of the FTIR peaks of adsorbed pyridine on (silica gel) $_n$ Sb $^V$ Cl $_3$ .....	93

Table 5-5	The results of alkylation reactions with silica supported antimony pentachloride and aluminum chloride.....	96
-----------	---	----

## LIST OF FIGURES

<u>Figure</u>	<u>page</u>
Figure 1-1 An example of site density.....	5
Figure 1-2 The effect of magic angle spinning (MAS) on the NMR spectra of solids.....	7
Figure 1-3 Weakening of the phosphorous-oxygen bond.....	9
Figure 1-4 Resonance forms of mesityl oxide in Brønsted acid solutions.....	12
Figure 1-5 Energy diagrams for slurry and gas phase calorimetries.....	16
Figure 1-6 Only Brønsted sites can be probed by 2,6-di(2-methylpropyl) pyridine..	18
Figure 1-7 A Born-Haber cycle relating Cal-Ad to gas phase calorimetry.....	21
Figure 2-1 The three chemical shifts of adsorbed trimethylphosphine.....	25
Figure 2-2 Transfer of electron density from a base to an acid.....	27
Figure 2-3 The correlation between calorimetry and $\Delta\delta$ .....	34
Figure 2-4 Phosphorus-31 MAS NMR of TEPO on (silica gel) <sub>n</sub> Sb <sup>V</sup> Cl <sub>3</sub> .....	37
Figure 2-5 Phosphorus-31 MAS NMR of TEPO adsorbed on TaCl <sub>5</sub> .....	38
Figure 2-6 A comparison of two different methods of measuring of solid acidity.....	41
Figure 2-7 Phosphorus-31 MAS NMR of trimethylphosphine oxide on zeolite TS-1.....	43
Figure 2-8 The chemisorbed chemical shift of trimethylphosphine oxide compared to calorimetric measures of acidity.....	45
Figure 2-9 An MO diagram for the <i>acid</i> TEPO interacting with KOH.....	46
Figure 2-10 Phosphorus-31 MAS NMR of TEPO on potassium hydroxide.....	46



Figure 2-11	The $^{31}\text{P}$ MAS spectrum of TMPSe on tungstic acid ( $\text{H}_2\text{WO}_4$ ).....	48
Figure 3-1	The structure of the Keggin anion.....	51
Figure 3-2	Delocalization of charge in 12-tungstophosphoric acid.....	52
Figure 3-3	The $^{31}\text{P}$ MAS NMR of 12-tungstophosphoric acid.....	55
Figure 3-4	The $^{31}\text{P}$ MAS NMR of 0.24 mmol pyridine on 1 gram of 12-tungstophosphoric acid.....	56
Figure 3-5	The chemical shift of the central phosphate changes with cesium loading.....	57
Figure 3-6	The XRD data for 12-tungstophosphoric acid.....	58
Figure 3-7	The XRD data for 12-tungstophosphoric acid with one pyridine molecule adsorbed per acid site.....	58
Figure 3-8	A representation of the unit cell of 12-tungstophosphoric acid.....	61
Figure 3-9	A representation of site one for pyridine titration of HPW.....	62
Figure 3-10	A representation of fully titrated HPW.....	62
Figure 3-11	The $^{31}\text{P}$ MAS NMR spectrum of $\text{CsH}_2\text{PW}$ .....	65
Figure 3-12	The $^{31}\text{P}$ MAS NMR spectrum of $\text{Cs}_2\text{HPW}$ .....	65
Figure 3-13	The $^{31}\text{P}$ MAS NMR spectrum of $\text{Cs}_{2.5}\text{H}_{0.5}\text{PW}$ .....	66
Figure 3-14	The $^{31}\text{P}$ MAS NMR spectrum of $\text{Cs}_3\text{PW}$ .....	66
Figure 4-1	The effect of solid acidity on the reaction of tertiary butanol with methanol.....	70
Figure 4-2	The mechanism for the catalytic production of MTBE from methanol and <i>t</i> -butanol.....	70
Figure 4-3	The reaction mechanism for the production of dimethyl ether from methanol.....	72
Figure 4-4	The transition states for ether production.....	72
Figure 4-5	Hydrolysis of a tethered sulfate group from a surface.....	74

Figure 4-6	Amount of MTBE and <i>t</i> -butanol in the product stream from TSC over the life span of the catalyst.....	78
Figure 4-7	Amount of MTBE and <i>t</i> -butanol in the product stream from BSC over the life span of the catalyst.....	79
Figure 4-8	The products of the reaction change as the acidity of the catalyst deteriorates.....	80
Figure 5-1	Examples of super acids.....	84
Figure 5-2	The reaction mechanism for the alkylation of isobutane to octane.....	85
Figure 5-3	The FTIR of pyridine on (silica gel) <sub>n</sub> Sb <sup>V</sup> Cl <sub>3</sub> .....	93
Figure 5-4	Titration of (silica gel) <sub>n</sub> Sb <sup>V</sup> Cl <sub>3</sub> with pyridine in cyclohexane.....	95
Figure 5-5	The proposed acid sites of (silica gel) <sub>n</sub> Sb <sup>V</sup> Cl <sub>3</sub> .....	97

Abstract of Dissertation Presented to the Graduate School  
of the University of Florida in Partial Fulfillment of the  
Requirements for the Degree of Doctor of Philosophy

## NEW METHODS FOR CHARACTERIZING SOLID ACIDITY

By

John Philip Osegovic

May 1999

Chairman: Dr. Clifford R. Bowers  
Major Department: Chemistry

Liquid acids are very important catalysts that are used to make many types of products. However, the waste from industrial facilities that use liquid acids has contributed to many environmental problems such as ozone depletion. Replacement of these hazardous liquids with reusable solid acids is the key to developing green industrial processes. Unfortunately, the complex interactions of a molecule with a solid acid site is not fully understood, preventing the rapid and wide spread replacement of liquid acids with new solid acids.

Current methods for characterizing solid acidity include many different types of spectroscopic and calorimetric techniques. Many of these methods rely on observing the changes that occur in probe molecules interacting with the acid site. Generally, adsorption of the probe molecule onto the acid site results in the formation of an adduct bond between the probe and the acid site. The change in the electronic state of

triethylphosphine oxide upon adsorption to an acid site can be measured with Phosphorus-31 MAS NMR.

The position of the spectral line(s) of the adduct can be used to identify the relative acidity of multiple acid sites on a surface. The combination of this new method with activity tests and calorimetry can be used to describe the total acidity of a solid.

Additional methods can be used to determine how the probe molecule reacts with the surface of a solid. In the case of the important catalyst 12-tungstophosphoric acid and its cesium derivatives, several techniques were used to characterize the surfaces of the solids. Penetration of the lattice by small molecules is apparently limited by the energy cost associated with opening the crystal lattice to include the molecule. The result is that only a small fraction of the available acid sites of these solids are available for interaction with the reactant.

The development of new solid acid characterization techniques will help to increase the level of understanding of these important catalysts. The new insights gained will lead to an increase in the pool of solid acids available to replace liquid acids, reducing the burden placed on the environment by industrial processes.

## CHAPTER 1

### INTRODUCTION TO THE CHARACTERIZATION OF SOLID ACIDITY

The replacement of hazardous liquid acid catalysts with solid analogs is one of the most important goals for the modernization of industrial processes. This substitution is driven by economic and environmental factors. Removal of acidified waste from effluent streams would lower the amount of sulfate and other waste products that are dumped into watercourses by millions of tons per year.<sup>1</sup> Solids are also easier to transport, store, handle, and are (generally) recyclable, resulting in a significant reduction in cost. Finding a solid that is capable of catalyzing a current industrial process under laboratory conditions is only the first step in the development of an industrially viable replacement for liquid acids. The subsequent steps include up scaling catalyst synthesis and reaction size and retooling or constructing production facilities.

The replacement of a liquid acid with a solid is the result of years of testing and retesting. Much of this time is spent in the initial steps of identifying which reaction(s) a candidate solid is capable of catalyzing. These initial steps include activity tests and various measures of acidity, usually beginning with a screening process.<sup>2,3</sup> One method of screening catalysts starts with measuring the activity of a series of solids toward a certain reaction. The catalysts that do not perform well are discarded, and the successful solids are further tested to determine their life span or to isolate the components that make them successful to help in the generation of another set of catalysts for testing. A

second screening method initially tests the solid acid to predict the type of reactions it will be capable of catalyzing. The solid is then tested for its ability to catalyze reactions in this range of acidity. Such a test is often used to estimate acidity through calorimetric or spectroscopic techniques. This second method is more common when only a small number of solids have been synthesized and require testing.

The use of solid acids has been driven by the need to separate products from catalysts and to replace toxic liquids with less hazardous solids. A reaction driven by a liquid acid has three major shortcomings. The first problem is how to store large volumes of dangerous liquids. For example, handling hydrofluoric acid is not a simple, inexpensive, or safe operation. The acid is produced on site and piped to the reaction vessel as a gas where it is condensed. A small leak of HF can stop the production of a large plant, as well as pose a significant health risk to the local community and environment. The second problem is how to separate the product from the spent acid. This is often performed by distillation or neutralization procedures.<sup>4</sup> Finally, the cost to regenerate acidified waste is more than the cost to produce fresh acid, resulting in a large increase of waste. For example, production of methylmethacrylate results in several tons of ammonium sulfate that must be disposed of for every ton of product.<sup>1</sup> This salt is often dissolved and dumped into the environment.

Solid acids address each of these problems in a favorable way.<sup>2</sup> Storage and handling of solid acids is a simple task. They can be stored in bags or containers, and require only a mask to avoid getting the particles in the eyes and lungs. Separation of the catalysts from reaction products is an easy procedure: filtration or reactive distillation, where a chemical reaction occurs simultaneously and concurrently with fractionalization

of products.<sup>5</sup> Finally, many solid acids can be regenerated, extending their lifetime indefinitely.<sup>6</sup>

### A Definition of Solid Acidity

Solid acids are invaluable as catalysts in industrial reactions. The interaction of a solid acid with a base can be described using Lewis acid-base theory--the sharing of an electron pair.<sup>7-9</sup> The intermolecular interactions involved can be distinguished from other forms of intermolecular bonding through the use of some examples. If we allow two non-acidic, non-basic molecules to interact, such as two helium atoms, the strength of the interaction can be described using only van der Waals forces.<sup>10</sup> The same forces can be used to describe the interaction of a basic molecule, such as pyridine, interacting with a non-acidic solid such as silicalite. The magnitude of this interaction, measured through the enthalpy of adsorption, has been determined to be  $-19.1 \text{ kcal mol}^{-1}$ .<sup>11</sup> However, if we exchange the silicalite with its acidic isomorph, HZSM-5, we must describe the bonding as containing both a van der Waals and an acid-base interaction.<sup>12</sup> The total enthalpy of this interaction has been measured to be  $-47.8 \text{ kcal mol}^{-1}$  that can be separated into a van der Waals component of  $-19.1 \text{ kcal mol}^{-1}$  and an acid-base component of  $-28.7 \text{ kcal mol}^{-1}$ . To truly describe a solid acid we must also rule out interactions that oxidatively lead to the formation of a covalent or ionic bond (Table 1-1).

### Describing Solid Acids

Solid acids are described in three ways: (1) the number of types of acid sites and their site density, (2) the acid strength possessed by each type of site, and (3) the activity of the solid toward acid catalyzed reactions. The overall strength of a solid acid (points 1 and 2) is perhaps its most significant characteristic. The maximum strength tells

Table 1-1. An example of intermolecular interactions that lead to bonding.

Reaction	Type of Interaction leading to the Product
$\frac{1}{2} \text{H}_2 + \text{Ar} \rightarrow \text{HAr}^+ + \text{e}^-$	Redox reaction
$\text{H}^+ + \text{Ar} \rightarrow \text{HAr}^+$	Brønsted Acid-Base
Argon + Water $\rightarrow$ Argon Clathrate	Dipole-Induced Dipole
$\text{NH}_3 + \text{HCl} \rightarrow \text{NH}_4\text{Cl}$	Brønsted/Lewis Acid-Base
$\text{C}_2\text{H}_4 + \text{H}_2\text{O} \rightarrow \text{CH}_3\text{CH}_2\text{OH}$	Addition Reaction
$n\text{Cl}_2 + 2n\text{Na} \rightarrow \text{Sodium Chloride}$	Redox to a Ionic Bond
$\text{NH}_3 + \text{BF}_3 \rightarrow \text{H}_3\text{N}:\text{BF}_3$	Lewis Acid-Base

researchers and engineers what kind of reactions the solid is capable of catalyzing. It may also give the researcher some idea of how well the catalyst will carry out that reaction.<sup>3</sup> Site density is the second consideration (Figure 1-1).<sup>13</sup> Site density is different from normal density,  $\rho$ , in that it is a measure of the number of acid sites available for interaction with a specific probe molecule for a given mass of solid. Site density is probe dependent and is usually reported in units of mmol of acid site per gram of solid acid, or simply  $\text{mmol g}^{-1}$ .

It is important to stress that site density is probe dependent.<sup>14</sup> For example, the two solids shown in Figure 1-1 might report the results of a single solid that was titrated with two different probe molecules, one of which could not interact with the Type 1 sites. Such differences can be related to the size, or steric requirement, and basicity of the probe molecule.



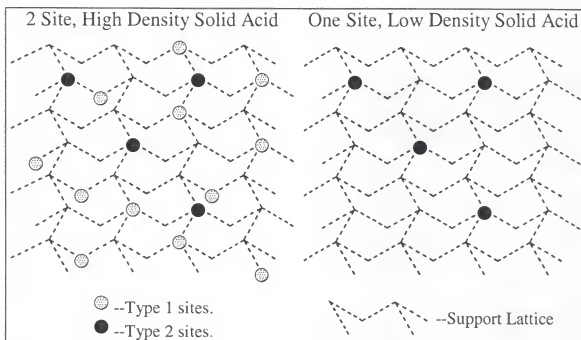


Figure 1-1. An example of site density. The diagram on the left shows a high-density solid acid with two different types of acid sites. The diagram on the right shows a one site, low-density solid acid. A reaction that can be catalyzed by either type of acid site will be better performed by the high-density, two site solid. Tests of acidity that can only detect the Type 2 sites cannot be used to distinguish one solid from the other—they will have identical results.

The combination of site density and acidity are the dominant factors in determining the usefulness of the catalyst. Both a low density solid with very strong acid sites and a high density solid with very weak acid sites will be poor catalysts. They may be capable of catalyzing a reaction, but only at a very limited rate. Additionally, the stability of the acid sites is also very important.<sup>15</sup> If the acid sites are easily destroyed, for example, by water hydrolysis, the catalyst will be of limited use in reactions where complete removal of water is difficult.

### Using Probe Molecules to Measure Acidity

Acidity is often characterized by measuring spectral line shifts of an adsorbed probe molecule.<sup>16</sup> Techniques based on IR,<sup>17-21</sup> UV,<sup>22</sup> EPR<sup>23</sup> and NMR (to be discussed later) have been developed. The shift of the spectral line(s) is compared to the shift of the spectral line(s) of the same probe molecule on other solid acids with different acidity to generate a scale of relative acidity. A relatively larger shift of the spectral line indicates higher acidity. When several different spectral lines from a probe on one solid acid are observed, the additional spectral lines are taken to be additional acid sites with different strengths.<sup>24</sup> By monitoring the changes in intensity of the different spectral lines as the total amount of adsorbed probe is varied, the amount of each acid site present in the solid can be determined.

The technique for obtaining a useful NMR spectrum of a solid is called magic angle spinning (MAS). (The basic theory behind MAS NMR can be found in the Appendix.) Without MAS, the NMR signal of a solid is typically broad and the determination of the position of the isotropic spectral line(s) is inaccurate. The line width of a solid sample can be in the tens of kilohertz.<sup>25</sup> For example, a 10 kHz line for phosphorus-31 on a 400 MHz spectrometer will be approximately 62 ppm wide, while in solution the line representing the same feature might only be 0.1 ppm in width (16 Hz). The extreme broadening is due to the large number of rigid dipolar couplings in the solid state. The use of MAS allows the acquisition of moderately high resolution NMR spectrum of a solid, where the spectral line or lines are resolved and their chemical shifts can be determined. Figure 1-2 shows a graphical representation of the effects of MAS. Figure 1-2a is an example of the NMR of solid adamantane without MAS. Adamantane

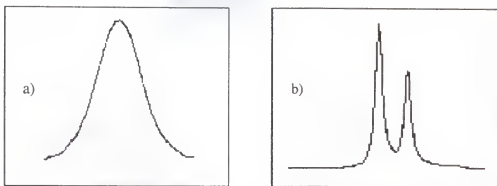


Figure 1-2. The effect of magic angle spinning (MAS) on the NMR spectra of solids. Figure 1-2a represents the NMR spectra of a solid adamantane. Figure 1-2b represents the NMR spectra of the same solid while spinning on the magic angle. The line width has been significantly decreased allowing for the observation of two spectral lines. (Adapted from "Modern NMR Spectroscopy 2<sup>nd</sup>" by J. K. M. Sanders and Brian K. Hunter.)<sup>26</sup>

is a symmetrical bicyclic organic compound with two types of carbon atoms in a 2:1 ratio. However, the static NMR spectrum shows only one featureless peak. Figure 1-2b is of the same sample but acquired under MAS conditions. The line width has been greatly reduced and two spectral lines of roughly 2:1 intensity can now be resolved.<sup>26</sup>

Phosphorus-31 MAS NMR is well suited for solid acid characterization. The large gyromagnetic ratio and 100% natural abundance of phosphorus-31 allows detection of very small amounts of probe molecules, which is advantageous when attempting to observe the limited number of acidic sites present on the surface of a solid acid. Previously reported phosphorus-31 MAS-NMR studies over the past decade have focused primarily on trimethylphosphine as the adsorbate probe of choice.<sup>27-34</sup> Trimethylphosphine has been used to identify the number of different sites on the solid, the density of each site, and the nature of each site as either Lewis or Brønsted.<sup>34</sup> Unfortunately, the small variation of the phosphorus-31 chemical shift of trimethylphosphine in solids of wide ranging acidity limits the utility of this probe for the

determination of acidity. For Brønsted acids the range of acidity correlates with chemical shifts over a 5 ppm range, with an error in measurement of 0.5 ppm. For Lewis acids, the range is covered in only 3 ppm, with an error of measurement of 1 ppm.

The most promising use of trimethylphosphine is for the determination of densities of the Lewis and Brønsted sites on the surface. Work performed using  $^{15}\text{N}$  pyridine has shown  $\delta^{15}\text{N}$  of that probe can be used to give similar information to  $\delta^{31}\text{P}$  from trimethylphosphine.<sup>35-39</sup>

Liquid acids have been previously characterized using triethylphosphine oxide (TEPO), upon which the acceptor number scale is based.<sup>19,30,40-42</sup> The phosphorus-31 isotropic chemical shift of TEPO can identify the relative acidity of solutions. However, while this and similar probe molecules have been used to distinguish multiple types of acid sites on the surface of several solids,<sup>28,43-44</sup> no attempt has been made to use TEPO to form a scale of solid acidity. A scale based on the change in chemical shift of this probe would be advantageous due to the speed at which the characterization can be performed.

The origin of the phosphorus-31 chemical shift of chemisorbed TEPO is the shift of electron density from the basic probe to the acid site.<sup>42</sup> The interaction of the phosphoryl oxygen atom with the acid site gives rise to a weakening of the phosphorus-oxygen bond (Figure 1-3). Evidence for the weakening of this bond can be obtained from the vibrational, or infrared, spectroscopy investigation of solvent acidity.<sup>17,19-20</sup> As the acidity of the solution is increased, the phosphorus-oxygen stretching frequency can be seen to decrease, indicating a weakening of the bond. Positive charge develops at the phosphorus center while negative charge builds up at the acid site. The stronger the acid site, the greater the shift of electron density and the greater the charge build up. This

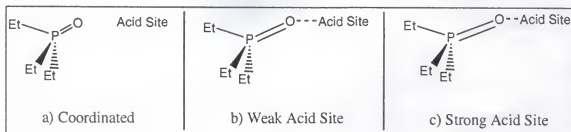


Figure 1-3. Weakening of the phosphorus-oxygen bond. The phosphorus-oxygen bond of uncoordinated triethylphosphine oxide lengthens upon coordination to an acid site. Figure 1-3b represents coordination to a weak acid site such as a hydrogen bonding site. Figure 1-3c represents bonding to an extremely powerful acid site.

Note: The nature of the phosphorus-oxygen bond in trialkylphosphine oxides is not understood.<sup>45</sup> Due to the short length of this bond measured through crystallography and other means, this bond has been characterized as a double bond. However, calculations have shown that it is possible to represent the bonding as a single bond with a full positive charge at the phosphorus and a full negative charge at the oxygen. The work here can not add to this debate and the choice to show the phosphorus-oxygen bond as a double bond throughout this dissertation is for clarity only.

shift in electron density causes a change in the chemical shielding factor,  $\sigma$ , at the phosphorus nucleus. The resulting change in the chemical shift can be readily observed using MAS NMR.

It has been reported that the  $^{31}\text{P}$  chemical shift of triphenylphosphine oxide is dependent upon the Al-O(P) distance in aluminum coordination complexes.<sup>46</sup> This bond distance was noted to decrease with increasing electrophilicity (acidity) of the aluminum center. While the P-O bond distance was observed to increase slightly, the correlation to  $\delta^{31}\text{P}$  was poor.

Since each acid catalyzed reaction requires a certain range of acidity, a researcher can quickly determine what reactions a new solid acid will be suitable for. If the catalyst causes TEPO to have a small shift in its  $^{31}\text{P}$  MAS NMR signal, it will be suited to perform reactions that require little acidity, such as the dehydration of tertiary butanol to

isobutene, an important chemical building block. If the shift is large, the catalyst can be tested with reactions that require much greater acidity, such as the conversion of butane to octanes, the major component of gasoline. Using the methods described in this dissertation, a researcher can focus on optimizing the catalyst for a catalytic process, or attempt to synthesize a new catalyst to perform the desired reaction.

#### Carbon-13 Probes of Solid Acids.

Several studies of solid acids using carbon-13 labeled ketones have been reported. The work of Biaglow *et al.*<sup>47-50</sup> and others<sup>51</sup> focuses on the perturbation of the chemical shift of 2-<sup>13</sup>C acetone to simultaneously determine the relative acidity and Brønsted or Lewis nature of acids sites in HZSM-5 and Faujasites.<sup>48</sup> A chemical shift of about 220 ppm (relative to TMS) was reported to represent acetone adsorbed on the Brønsted acid sites of the solids, and slight variations about this shift were taken to indicate changes in the strength of the hydrogen bond. The stoichiometric adsorption complexes of antimony pentachloride with the Brønsted acid sites of zeolite HZSM-5 were studied separately.<sup>50</sup> The magnitude of the shift in this solid was larger than in clean HZSM-5. The shift was enhanced due to the coordination of the antimony halide to the oxygen atom at the acid site similar to the large increase in acidity observed in two component super acids over either component alone. Treating the solid at 700 K resulted in dealumination of the zeolite and a larger chemical shift for acetone, approximately the same as measured in a magic acid solution (249.5 ppm). Additional work on other molecular sieve solids showed that the chemical shift of acetone in these structures was largely invariant and that the shift might even be correlated to the size of the cavity of the solids studied.<sup>47</sup> The change in chemical shift of acetone on silica supported aluminum chloride was used to

assert that the acidity of that solid was greater than HZSM-5.<sup>39</sup> The overall picture for characterizing acidity with acetone is a cloudy one. Acetone appears to be sensitive to the strength of the acid site, but the relationship is not well known. It may also be sensitive to size of the pore the acid site is located within and will have different, overlapping chemical shift ranges depending on whether it is bound to a Brønsted or Lewis site.

Farcasiu *et al.* and others have developed a scale for Brønsted acids based on the difference in shift of the carbons of mesityl oxide (4-methyl-3-pentene-2-one) in solution.<sup>52-56</sup> The  $\beta$  carbon of Mesityl oxide (Figure 1-4) showed a large dependence on the acidity and polarity of solutions,<sup>52-55</sup> but it was less sensitive to the acidity of solid acids.<sup>56</sup>

#### Using <sup>27</sup>Al and <sup>29</sup>Si MAS NMR to Determine the Structure of Molecular Sieves.

Aluminum-27 and Silicon-29 MAS NMR are invaluable tools for studying the structure of silica/alumina molecular sieve catalysts.<sup>57</sup> The structures of these catalysts are a series of tetrahedral silicon atoms linked into regular repeating ring structures of varying sizes. The substitution of aluminum for a silicon atom (up to a certain limit: there can be no Al-O-Al linkages in zeolites) results in a change in the chemical shift of the nearest neighbors and results in the potential for acid sites to exist. A single chemical shift can be measured for silicon atoms with zero, one, two, three or four adjoining aluminum centers *in the framework* and the population of each type of silicon atom can be obtained from integration.<sup>58-59</sup> The bulk silicon/aluminum ratio includes non-framework aluminum atoms (present predominantly as alumina, Al<sub>2</sub>O<sub>3</sub>) and a comparison of the two ratios can be used to determine the purity of the sample. Additionally, the

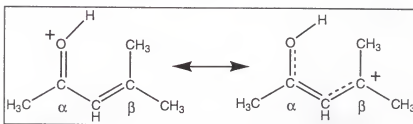


Figure 1-4. Resonance forms of mesityl oxide in Brønsted acid solutions. The chemical shift of the  $\alpha$  and  $\beta$  of mesityl oxide carbons are both sensitive to protonic media.

extent of dealumination can be measured with  $^{27}\text{Al}$  NMR.<sup>60-66</sup> Aluminum-27 ( $I = 5/2$ , natural abundance = 100%) is a quadrupolar nucleus, so the spectral lines observed are a mixture of both quadrupolar coupling and chemical shift of the aluminum centers.<sup>67</sup> Essentially, only two peaks will be observed in the MAS spectra: one due to tetrahedral framework aluminum and one due to octahedral extra framework alumina (virtually all non-spherically symmetric  $^{27}\text{Al}$  signals will be lost due to rapid quadrupolar relaxation).<sup>60</sup> The amount of dealuminated material can be determined by comparing the intensity of each signal. By combining both the  $^{27}\text{Al}$  and  $^{29}\text{Si}$  MAS NMR of a molecular sieve the possible ordering schemes of the solid can be derived that show the possible location of the aluminum atoms in the unit cell.<sup>57</sup> Additionally, Huggins and Ellis showed that lateral surface diffusion of surface protons on aluminas causes an electric field gradient that provides an efficient quadrupolar relaxation mechanism resulting in a loss of signal intensity that increases with surface area.<sup>67</sup>

#### Methods Using $^1\text{H}$ MAS NMR

Proton NMR has been used to label the chemical shift of acidic protons on surfaces.<sup>39,67-71</sup> The chemical shift of protons varies tremendously with the type of solid and whether or not the proton is acidic. A scale based on simulating the static  $^1\text{H}$  NMR



of  $\text{H}_3\text{O}^+$  relative to the total number of protons at 4K was proposed to distinguish between the acidic protons from hydrogen bonding protons and non-acidic protons and rank zeolite acidity.<sup>70-71</sup> The scale that was developed, however, ranked the acidity of zeolite HZSM-5 lower than both HY and H-Mordenite in contradiction to all other scales of acidity. Pearson<sup>68</sup> used MAS NMR to identify two different types of protons, chemisorbed and physisorbed, on the surface of various transition-aluminas (the different transitions of alumina can be obtained through heat and pressure treatments). It was also reported that 83% of the acidic protons can be found in defect sites in the first two layers of the surface.

In addition to labeling the acidic protons in zeolites, Anderson *et al.*<sup>69</sup> utilized the change in  $^1\text{H}$  chemical shift of  $\text{CD}_3\text{OH}$  to measure the proton donating ability (rather than the acid strength) of molecular sieves. The origin of the shift is due to the formation of a strong Brønsted-alcohol hydrogen bond or the formation of the oxonium ion ( $\text{CD}_3\text{OH}_2^+$ ). This change in shift was greatest in HZSM-5 (9.4 ppm) while in silicalite (a non-acidic isomorph of HZSM-5) the resonance was at 3.8 ppm. Solids with acidities between these two extremes generally resonated between 4 and 6 ppm. It was clearly demonstrated that the observed chemical shift was dependent on synthesis technique and silica/aluminum ratios by using two separate methods for preparing HZSM-5. The two different solids differed in the  $^1\text{H}$  chemical shift of adsorbed  $\text{CD}_3\text{OH}$  by almost 2.4 ppm!

### Summary

A basic description of NMR and the theory behind magic angle spinning can be found in Appendix I. Chapters 2 and 3 will use MAS NMR to help characterize solid acidity. Chapter 2 will focus on the use of triethylphosphine oxide to develop a new

scale to characterize solid acidity. A brief description of the use of other phosphine chalcogenide probes will also be discussed. The scale developed in Chapter 2 will be applied to the characterization of a new solid acid in Chapter 5. The location of the acid sites in the crystalline solid 12-tungstophosphoric acid will be determined with the help of MAS NMR in Chapter 3.

#### Calorimetric Measures of Acidity

The measurement and determination of the acidic properties of solids is of great interest. Calorimetry is a common method used in the characterization of solid acidity. As it applies to solid acid characterization, calorimetry can be described as a measure of the initial and final enthalpy of a free or solvated probe molecule upon adsorption onto a surface.<sup>72</sup> The enthalpy change of the probe molecule as it adsorbs or desorbs from a surface causes a measurable change in the temperature of the surroundings. The degree to which the temperature is changed is dependent upon the strength and type of interaction of the probe with the surface (Table 1-2). In the case of a basic probe molecule adsorbing onto a clean (unsolvated) non-acidic surface, only the energy due to van der Waals forces will be measured. For the same system in the presence of a solvent the difference in the van der Waals forces due to probe-solid and solvent-solid interactions can be obtained. However, if the solid is acidic, then the clean solid will have an enthalpy equal to the sum of the van der Waals forces and the donor-acceptor forces. In the case of a solvated, acidic solid, the extent to which the van der Waals forces are measured depends on the difference between the van der Waals forces for the solvent and probe interacting with the surface.

Table 1-2. The types of forces measured in calorimetric experiments.

Type of Surface	Forces Present		Example
	van der Waals	Donor-Acceptor	
Clean Non-Acidic	Yes	No	Carbonaceous Solid
Solvated Non-Acidic	Reduced	No	Wet Graphite
Clean Acidic	Yes	Yes	Aluminum Trichloride
Solvated Acidic	Reduced	Yes	$\text{Al}_2\text{Cl}_6$ in alkanes

The measured energetics of adsorption of a probe molecule onto a surface varies with the technique used. In gas phase adsorption calorimetry the energy measured is the total of the non-specific van der Waals interaction of the probe with the surface plus the donor-acceptor interaction of the probe with the acid site.<sup>72</sup> The magnitude of the van der Waals probe-surface interaction can be as high as 40% of the measured enthalpy.<sup>11</sup>

A second type of calorimetry is performed in the presence of a non-participating solvent. This method of calorimetry is called solution calorimetry if the compound under study is dissolved in the solvent or slurry calorimetry if the compound is suspended in the solvent. For slurry calorimetry, the non-specific van der Waals contribution to the enthalpy measured in gas phase calorimetry is reduced or canceled by the energy required to displace a solvent molecule from the surface (Figure 1-5).<sup>73</sup> The complete cancellation of the van der Waals component relies on the selection of a solvent molecule that is approximately the same size as the probe molecule, therefore having essentially the same van der Waals contribution.

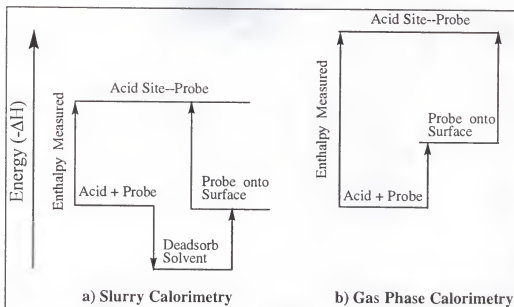


Figure 1-5. Energy diagrams for slurry and gas phase calorimetries. The energetics of adsorption for a) slurry and b) gas phase calorimetries. The enthalpy observed during slurry calorimetry is due only to the donor-acceptor interaction of the probe with the surface. The observed enthalpy from gas phase calorimetry contains both the specific and non-specific enthalpies of adsorption.

An additional step is often added that measures the amount of base adsorbed.

This addition is especially useful for solids where adsorption is far from complete. It allows a more accurate description of the acid sites. The method of tracking the amount of adsorbed probe is generally determined by taking the difference between the amount of free probe and the total amount of probe in the system as measured through UV or IR spectroscopy. The Cal-Ad method is an example of such a method.

Cal-Ad combines the data obtained from slurry adsorption calorimetry with a UV adsorption isotherm.<sup>39,73-83</sup> A least square fit to the data allows a determination of the number of discrete acid sites and the population, acid strength, and equilibrium constant for adsorption of the probe for each site. The probe typically used to perform Cal-Ad is

pyridine dissolved in either *n*-hexane, cyclohexane, or acetonitrile. Additional information about the solid can be obtained by varying the probe molecule. For example, comparing the results of a titration using pyridine with the results of an experiment using 2,6-di(2-methylpropyl) pyridine, a site can be designated as Lewis or Brønsted in nature.<sup>73,80</sup> The presence of the 2 methylpropyl arms will prevent the 2,6-di(2-methylpropyl) pyridine from interacting with a Lewis acid site (Figure 1-6). Many solids have been successfully characterized by this method, and a Cal-Ad scale of solid acidity has been proposed. Table (1-3) shows the results from the Cal-Ad experiment for 12-tungstophosphoric acid dissolved in acetonitrile<sup>77</sup> and slurried in cyclohexane.<sup>83</sup> In both cases the titrant was pyridine.

The following description of a typical solution or slurry calorimetric experiment is adapted in part from an article authored by Jose A. Dias, John P. Osegoovic and Russell S. Drago.<sup>83</sup> It is the method followed for all of the calorimetry reported in this dissertation, and is the general method practiced by the Drago laboratory. As such, similar descriptions can be found in many publications.<sup>73-83</sup> The repetition here is for completeness.

Samples are weighed (typical sample mass: 1.0 g) and transferred to an insulated calorimetric cell with an internal mirrored coating containing a stir bar. For each titration, 100ml of solvent is added to the cell. A calibrated syringe, filled with a solution of known concentration of base (e.g., 0.1 mol L<sup>-1</sup>) is inserted into the cell along with a thermistor and a heater coil. The thermistor and heater coil are connected to an electronic bridge and a computer.<sup>83</sup> The completed cell is allowed to reach thermal equilibrium with the environment. After thermal equilibrium is met, the experiment is begun. The

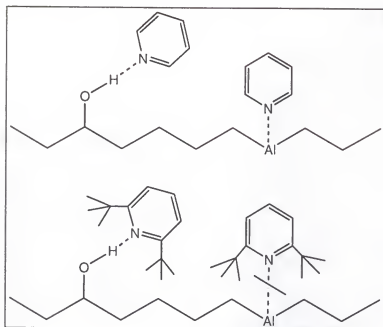


Figure 1-6. Only Brønsted sites can be probed by 2,6-di(2-methylpropyl) pyridine. The alkyl arms on 2,6-di(2-methylpropyl) pyridine (bottom), a slightly stronger base than pyridine, prevent the formation of an acid-base bond at the Lewis site in this diagram. Pyridine (top) can freely interact with either site. The Cal-Ad data for each solid would show one fewer site when titrated with 2,6-di(2-methylpropyl) pyridine.

Table 1-3. The Cal-Ad results for 12-tungstophosphoric acid (HPW) in acetonitrile solution<sup>77</sup> and as a solid slurried in cyclohexane.<sup>83</sup>

Site	HPW Dissolved in Acetonitrile			Solid HPW in Cyclohexane Slurry		
	$-\Delta H$ (kcal mol <sup>-1</sup> )	Density <sup>a</sup> (mmol g <sup>-1</sup> )	K <sup>b</sup>	$-\Delta H$ (kcal mol <sup>-1</sup> )	Density <sup>a</sup> (mmol g <sup>-1</sup> )	K <sup>b</sup>
1	21.0	0.33	$2.1 \times 10^3$	32.7	0.079	$3.7 \times 10^5$
2	11.8	0.33	$2.4 \times 10^2$	19.6	0.16	$2.9 \times 10^3$
3	18.6	0.33	$4.1 \times 10^1$	-	-	-

<sup>a</sup> All of the protons are available for titration in solution; however, only about 25% of the protons of solid HPW are available for reaction.

<sup>b</sup> Equilibrium Constant for adsorption.

thermistor is calibrated with the heater coil prior to or immediately after each titration. A set of 12 calibrated brass stops is used for the additions of the titrant. After each addition the heat evolved from reaction of the base with the sample is measured. The calorimetric data generates an isotherm of total heat evolved versus the total moles of base added.

#### A Current Example of the Application of Calorimetric Methods

In a recent paper,<sup>11</sup> the analysis of the interaction of pyridine with HZSM-5 by the Cal-Ad method<sup>73</sup> was called into question. A discrepancy of  $22.9 \text{ kcal mol}^{-1}$  between the value derived from gas phase adsorption calorimetry and Cal-Ad was believed to be due to a flaw in the Cal-Ad technique, and Savitz *et al.*<sup>11</sup> concluded that Cal-Ad was unsuitable for the characterization of the acidity of HZSM-5. Gas-solid calorimetry (GSC) results were directly compared to the average enthalpy of the two acid sites described by Cal-Ad without insuring that the two HZSM-5 samples were prepared identically. The authors had also arrived at the conclusion that there is only one type of acid site present in HZSM-5 despite a variety of papers that disagree.<sup>73,84-90</sup> In their response to the Savitz article, Webster *et al.*<sup>91</sup> pointed out that they failed to accurately describe the differences in the experimental procedures and sample preparation methods.

It was shown<sup>91</sup> that several considerations could reduce the discrepancy between the Cal-Ad and GSC results. The first reduction made originated when accounting for the change in temperature between the two experiments. The heat absorbed by pyridine gas, as the temperature of the experiment is changed from 298 K (Cal-Ad is performed at ambient temperatures) to 473 K (the gas phase calorimetry experiment is performed at elevated temperatures to ensure homogenous adsorption of the pyridine),<sup>11,92</sup> is  $4.06 \text{ kcal mol}^{-1}$ . Webster *et al.* assumed that the heat absorbed by the zeolite during the

temperature increase from 298 K to 473 K canceled the heat released by the zeolite-pyridine adduct during the temperature reduction from 473 K to 298 K and left this step out of their consideration.

Reports have shown that there are *n*-hexane molecules specifically bound to the acid sites of HZSM-5.<sup>93</sup> Every pyridine that interacts with the acid site must displace a coordinated *n*-hexane.<sup>91</sup> The desorption of a sufficient amount of *n*-hexane to allow pyridine to occupy all of the acid sites resulted in a calculated enthalpy of 19.6 kcal mol<sup>-1</sup>.

Sample preparation procedures for zeolite HZSM-5 directly affect the amount of heat observed.<sup>94</sup> The sample procedure used by Savitz *et al.* was not reported; however, other preparation procedures used by the same group are very mild.<sup>95</sup> Drago *et al.*<sup>73</sup> used a very harsh treatment condition designed to emulate the procedures used to prepare HZSM-5 for industrial use. In their survey of the literature Webster *et al.* discovered gas phase heats of adsorption for both *n*-hexane and pyridine onto HZSM-5 prepared in a similar manner to the sample used in the Cal-Ad method.<sup>84,93</sup> When both the enthalpies for *n*-hexane and pyridine adsorption were used in place of the values reported in Reference 11, the difference between the two measures was reduced to -2.7 kcal mol<sup>-1</sup>. The discrepancy between Savitz *et al.*<sup>11</sup> and Drago *et al.*<sup>73</sup> is almost certainly due to differences in the preparation of the solid. A Born-Haber cycle helps to illustrate the thermodynamic arguments used (Figure 1-7).

Calorimetric methods of characterization are very useful tools for exploring solid acidity. There are a wide variety of procedures that are available to suit the researchers' needs. However, due to the extreme dependence on sample preparation and experimental parameters, care must be taken when comparing the results of two different types of



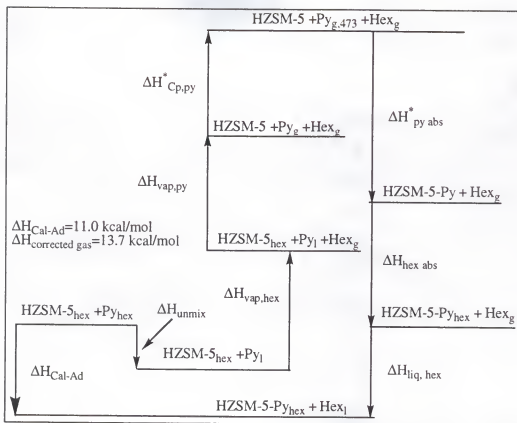


Figure 1-7. A Born-Haber cycle relating Cal-Ad to gas phase calorimetry. The Born-Haber cycle used to relate the gas phase adsorption of pyridine onto HZSM-5 to the Cal-Ad experiment. The \* on an enthalpy denotes that the value was changed by Webster *et al.* from those used by Savitz *et al.* These values were changed because the new values were obtained from HZSM-5 samples that were treated in a very similar manner to the one described by the Cal-Ad method.

experiments. An understanding of slurry calorimetry is all that is necessary to interpret the enthalpies reported throughout this dissertation.

Characterizing solid acidity is important for the further development of environmentally friendly processes that employ acid catalyst. The work in this dissertation describes several new solid acids and a new method for their characterization. The first part of the dissertation will focus on the use of MAS NMR to describe solid acidity in two ways by 1) introducing a new method for using probe

molecules to measure the acidity of a solid and 2) by assigning locations to the acid sites in a crystalline solid.

Chapter 2 will describe a new method for qualifying the acidity of solid acids. This chapter will focus on the use of the phosphorus-31 solid state NMR to measure the acidity of surfaces. The behavior of the probe molecule on solid acids of all strengths as well as bases and neutrals will be discussed.

The third chapter will detail the efforts made to characterize the acidity of an important series of solid acid catalysts. Spectroscopic methods will be combined with calorimetry to help to understand the behavior of these solids. With the aid of a crystal structure diagram, the location of the acid sites within the structure will be determined.

In Chapter 4 the relationship between structure and activity will be explored by comparing the activity of two very similar sulfate catalysts for the production of methyl *t*-butyl ether from methanol and *t*-butanol. This reaction will be shown to be an ideal model reaction system for monitoring the changes in acidity of a catalyst throughout its lifetime.

Chapter 5 will focus on the characterization of a new solid acid, silica supported antimony pentachloride. Calorimetry, activity, and  $^{31}\text{P}$  MAS NMR will be used to describe this catalyst as a new solid super acid.

## CHAPTER 2

### A NEW SOLID ACIDITY SCALE

Identifying the total acidity of a solid acid is a complex process, involving the use of activity tests, calorimetric titrations, and many spectroscopic methods. Magic angle spinning NMR of chemisorbed basic probe molecules is a very important step in this characterization process. Probe molecules can be used to classify the acid sites of a solid as Brønsted or Lewis in nature and measure relative acidity. To this end, a new scale based on the chemical shift of the spectral lines of chemisorbed triethylphosphine oxide is reported here.

Several NMR probes that have been used to study solid acids including 2- $^{13}\text{C}$  acetone,<sup>47-51</sup> 4- $^{13}\text{C}$  mesityl oxide,<sup>53-56</sup> and  $^{15}\text{N}$  pyridine.<sup>35-39</sup> Unfortunately, due to the low population of acid sites on the surface, the low sensitivity of these nuclei requires either extensive signal averaging or the use of labeled materials. To avoid both of these problems, a probe molecule including a more sensitive nucleus at or near the basic site is highly desirable. An ideal replacement probe would contain phosphorus-31. The gyromagnetic ratio and natural abundance of phosphorus-31 is much greater than either  $^{13}\text{C}$  or  $^{15}\text{N}$  resulting in an order of magnitude increase in the NMR signal that can be observed. The relative sensitivity of  $^{31}\text{P}$  compared to  $^{13}\text{C}$  and  $^{15}\text{N}$  at natural abundance is approximately 700 and 2400 respectively.<sup>96</sup> The very high sensitivity allows for the

detection of small amounts of phosphorus containing compounds adsorbed on the acid sites of a solid without the use of expensive enriched samples.

Over the past few years, the spectral probe molecule of choice for the study of solid acids by MAS NMR has been trimethylphosphine.<sup>27-34</sup> Coordination of trimethylphosphine to an acid site results in a characteristic shift of the spectral line that depends primarily on the Brønsted or Lewis nature of the acid site (Figure 2-1). The similar chemical shift of Lewis bound and physisorbed trimethylphosphine results in difficulty for using this probe to unambiguously determine the presence and population of Lewis sites. Despite this shortcoming, trimethylphosphine has been widely used to determine the total population of Brønsted sites on a surface. The strong basicity of phosphines results in the formation of a protonated base upon coordination to any Brønsted site. The chemical shift of this characteristic system is about -4 ppm (all <sup>31</sup>P chemical shifts in this dissertation are referenced to 85% phosphoric acid) and is largely invariant with the strength of the acid site.

The basicity of trialkylphosphine oxides is on the same order of magnitude as trimethylphosphine. However, the removal of the phosphorus atom from the base site leads to a wide range of chemical shifts that vary with the strength of the acid site.<sup>40</sup> The most prominently used trialkylphosphine oxides are triethylphosphine oxide (TEPO) and trimethylphosphine oxide. Both have seen limited use as probes of solid acids.<sup>28,29,31,44</sup> The most well known use of TEPO is as a probe of solvent acidity. Meyer and Guttman proposed the Acceptor Number scale based on the chemical shift of TEPO extrapolated to infinite dilution in an acidic solvent ( $\delta^{31}\text{P}_{\text{infinite dilution}}$ ).<sup>40</sup> Normal hexane was assigned an

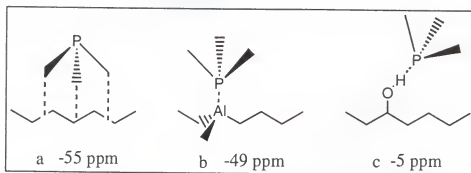


Figure 2-1. The three chemical shifts of adsorbed trimethylphosphine. The chemical shift of trimethylphosphine a) physisorbed (van der Waals forces only) b) Lewis<sup>+</sup> chemisorbed and c) Brønsted chemisorbed.

Acceptor Number value of 0.0 and  $\text{SbCl}_5$  was assigned a value of 100. The acceptor number of any solvent can be determined by using Equation 2-1:<sup>68</sup>

$$\text{Acceptor Number} = 2.348 \cdot \delta^{31}\text{P}_{\text{infinite dilution}} \quad (2-1)$$

This scale has been criticized for the observation that even neutral and basic solvents can have significant Acceptor Number values that have been attributed to van der Waals interactions.<sup>42</sup>

Recently, Rakiewicz *et al.*<sup>44</sup> characterized the acid sites of amorphous silica-alumina; zeolites HY, dealuminated HY, and USY; and  $\gamma$ -alumina with trimethylphosphine oxide. They were able to distinguish several acid sites on these materials, and then measure the population of those sites through spin counting experiments. It was also reported that this probe could differentiate Lewis and Brønsted sites. A small negative shift of the spectral line (compared to physisorbed trimethylphosphine oxide) on dry  $\gamma$ -alumina was observed. This feature disappeared upon exposure to water. It is known that water destroys the Lewis acid sites of  $\gamma$ -alumina. From these observations, the negative shift was taken to indicate the presence

of Lewis acid sites. This trend of assigning shift ranges for Lewis or Brønsted bound phosphine oxides includes work by Lunsford<sup>31</sup> and Baltusis.<sup>28</sup> However, each author has assigned a different region to the chemical shifts for the Lewis chemisorbed probe.

Triethylphosphine oxide has been previously used only twice for the characterization of solid acids: to identify two different acid sites on  $\gamma$ -alumina and to identify several acid sites on zeolite HY.<sup>29,31,44</sup>

The change in position of a spectral line through the chemisorption of a basic probe molecule onto an acidic site is primarily due to electronic changes in the probe molecule leading to a change in the local magnetic field about the nucleus.<sup>42,68</sup> Electron density flows from the base to the acid site (Figure 2-2) upon formation of an adduct bond with the acid site. Coordination of the phosphoryl oxygen of a trialkylphosphine oxide creates overlap between the electron deficient orbital on the acid site (LUMO), be it Brønsted or Lewis, and one of the orbitals on the oxygen that contains a lone pair of electrons (HOMO). The resulting adduct bond causes a loss of electron density from the probe that can be observed by a change in the phosphorus-31 NMR. As the strength of a Brønsted acid site is increased, the acid site-probe adduct will begin to resemble an ion pair. However, once the base is fully protonated (acid site<sup>+</sup>:H-probe<sup>+</sup>) no further change in chemical shift will be observed by increasing the acidity of the site. Instead, the same chemical shift will be observed for any stronger acid sites. At a Lewis site, coordination of a probe will result in the formation of an adduct bond. In the case of a phosphine oxide, the oxygen atom acts as a bridge between the Lewis site and the phosphorus center. The strength of the acid site will be directly related to the strength of the adduct

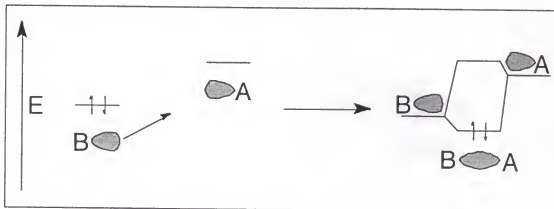


Figure 2-2. Transfer of electron density from a base to an acid. Overlap of the LUMO on A (the acid site) with the HOMO of B (the base) results in the formation of a molecular orbital (BA). The component of B in BA is reduced from B alone and as the strength of A increases so will its share of the electrons in BA.

bond. At very high acid strength electron transfer may occur forming an ion pair. Again, no further change in the chemical shift is expected, unless oxygen atom transfer occurs. Transfer of the oxygen atom will result in an oxidized acid site and the reduction of the trialkylphosphine oxide to the corresponding trialkylphosphine.

By comparing the shift of a physisorbed base to that of a chemisorbed base, the contribution of the van der Waals forces to the chemical shift is reduced or removed.<sup>28</sup> The chemical shift of physisorbed TEPO has been observed to be approximately 50 ppm. By referencing the chemisorbed chemical shift to this value, the relative acidity of a solid acid site can be measured. The change in the chemical shift of TEPO has an excellent correlation with calorimetric measurements of acidity except in the case of 12-tungstophosphoric acid (*vide infra*).

Currently there is debate as to the acid strength of the crystalline solid acid 12-tungstophosphoric acid (HPW). Many reports have been issued with conflicting

measurements of its acidity.<sup>97-112</sup> HPW is composed of large anions called Keggin units with a secondary structure composed of  $\text{H}_5\text{O}_2^+$  counter ions.<sup>113-115</sup> The Keggin unit is composed of four  $\text{W}_3\text{O}_{12}$  groups called  $\text{W}^3$  triplets.<sup>116</sup> These triplets are linked by shared corners about a central  $\text{PO}_4$  tetrahedron. The acidity of this solid is believed to come from the large size of this anion and from the high proton conductivities that spread any buildup of anionic charge throughout the solid.

For a probe to penetrate the crystalline HPW structure, the lattice must expand. Evidence of this can be seen by comparing the lattice constants of HPW samples obtained from X-ray diffraction analysis before and after loading with the base pyridine.<sup>83,117</sup> Expansion of the lattice to incorporate a guest molecule requires energy, reducing the enthalpy observed by methods based on differential measurements of heats of adsorption and resulting in a lower estimation of acidity.

Reported in this chapter is new a method for the determination of the global acidity of a solid acid. Chemisorption of the probe TEPO results in a chemical shift that is only dependent on the strength of the acid site and not the Brønsted or Lewis nature of the site. We discuss the observed static acidity of HPW compared to acidity determined by calorimetric titration of this solid. The chemical shift behavior of TEPO on solid neutrals and bases is also discussed.

### Experimental

The solid acids and bases were loaded with TEPO by combining a known mass of 1.0 M TEPO in anhydrous pentane solution with a known mass of the solid. The loading is determined by the ratio of the moles of TEPO, determined by using a solution density of  $0.679 \text{ g ml}^{-1}$  and the molar mass of TEPO of  $134.16 \text{ g mol}^{-1}$ , to the mass of the solid.



For example, a TEPO loading of 0.74 mmol TEPO g<sup>-1</sup> solid was obtained by combining approximately 100 mg of the TEPO solution to 200 mg of the solid. A volume of 2 ml of anhydrous pentane was also added to the samples to facilitate mixing. The slurries were allowed to equilibrate for twenty to thirty minutes with additional time for the zeolite samples. The samples were then dried in a vacuum oven maintained at 50°C. Our preferred method, however, was to individually mix a small mass of TEPO dissolved in 4-5 ml anhydrous pentane with the solid, allowing twenty to thirty minutes for equilibrium to be established, and then treating the sample in the vacuum oven.

The MAS spectrum of each sample was acquired on either a Varian Unity 500 MHz spectrometer operating at 202.270 MHz or a Bruker Avance 400 MHz spectrometer operating at 161.976 MHz. Both spectrometers were equipped with Jakobsen style MAS probes operated at spinning speeds of 4-6 kHz (Unity) or 10-12 kHz (Avance). A simple one pulse-acquire sequence was employed with a pulse corresponding to the 90° flip angle of 22 μs (Unity) or 3.0 μs (Avance). A recycle delay of 30 s was found to allow complete spin lattice relaxation between pulses. The spectra were referenced to an 85% phosphoric acid external standard.

#### Preparation of the Solids

Many of the solid acids used in this report were supported on a treated silica gel. The preparation of this silica gel can be found in Chronister *et al.*<sup>74</sup> The preparation includes washing the silica with aqueous HCl, 30% hydrogen peroxide, and deionized water followed by a heat treatment. This preparation procedure is believed to increase the number and strength of silanol sites on the silica surface.<sup>74</sup>

Silica supported aluminum chloride,<sup>118,119</sup> (silica-gel)<sub>n</sub>Al<sup>III</sup>Cl<sub>2</sub>, is a strong Brønsted acid that was prepared by refluxing the silica gel described above with anhydrous aluminum chloride in carbon tetrachloride. This solid was prepared and stored under an inert atmosphere. The antimony (V) analog, (silica-gel)<sub>n</sub>Sb<sup>V</sup>Cl<sub>3</sub>, was prepared in an identical manner, except trichloromethane was used as the solvent.

Silica supported sulfated tungsten oxide, (silica-gel)<sub>n</sub>WO<sub>3</sub>SO<sub>3</sub>, is also a strong Brønsted acid.<sup>78</sup> The preparation of this solid was performed in two steps. The first step was refluxing tungsten hexachloride with silica gel for 24 hours. The solid was then collected and dried in a 140 °C oven for one day. The supported tungsten oxide was cooled to room temperature and then washed with 1 M sulfuric acid. It was activated at 200 °C in flowing air prior to use.

The sulfated silica gel solid was prepared by washing silica gel with 1 M sulfuric acid. This solid was activated at 200 °C in flowing air prior to use.

The sol-gel sample was prepared by hydrolyzing tetraethyl ortho silicate in the presence of a catalytic amount of HCl at 80 °C. The resulting gel was crushed and calcined at 400 °C. This solid was found to have a very small number of weak acid sites. It had a surface area of approximately 400 m<sup>2</sup> g<sup>-1</sup>.<sup>82</sup>

Zeolites HZSM-5 and H-Mordenite were prepared by ion exchanging the solids with 3 M ammonium chloride in deionized water. Both solids were then treated at 400 °C in flowing air for four hours and then for 12 hours under vacuum. The furnace was then cooled and filled with dry nitrogen and the samples were taken to an inert atmosphere glove box where they were stored until used. Zeolite TS-1 was prepared by heating it to

200 °C in flowing air for two hours, and then in vacuum for twelve. The furnace was cooled and transferred to the glove box as described above.

The preparation of 12-tungstophosphoric acid will be described in detail in Chapter 3.

The method of preparing the 1:1 adduct of TEPO with  $\text{SbCl}_5$  was similar to one found in the literature for the preparation of a 1:1 adduct of  $\text{SbCl}_5$  with triphenylphosphine oxide.<sup>120</sup> In separate vials 0.124 g of TEPO and 0.276 g  $\text{SbCl}_5$  were dissolved in hot anhydrous  $\text{CCl}_4$ . After full dissolution, the hot  $\text{CCl}_4$ /TEPO solution was transferred by syringe to the vial containing the hot  $\text{CCl}_4$ / $\text{SbCl}_5$  solution. A clear white solution formed that contained a brown oil. The oil was extracted by syringe, allowed to cool, and the  $\text{CCl}_4$  was evaporated. Both the solution and the oil yielded a white solid that was stable in air. The oil yielded the bulk of the solid, and this portion was used for the NMR studies. The same procedure was followed to produce the 1:1 adduct of TEPO with  $\text{TaCl}_5$  (0.128 g TEPO and 0.309 g  $\text{TaCl}_5$ ) and the 2:1 adduct with  $\text{Al}_2\text{Cl}_6$  (0.305 g TEPO and 0.155 g  $\text{Al}_2\text{Cl}_6$ ). The  $^1\text{H}$  MAS NMR of 2:1 TEPO: $\text{Al}_2\text{Cl}_6$  showed only the ethyl protons.

## Results and Discussion

### The Acidity Scale

A new solid acidity scale based on the change in the chemical shift of chemisorbed TEPO has been discovered.<sup>121</sup> This scale is based on the change in  $^{31}\text{P}$  MAS NMR chemical shift of TEPO from the shift of physisorbed TEPO, a  $\Delta\delta$  value. The  $\Delta\delta$  value is calculated by subtracting the chemical shift of physisorbed TEPO, estimated as 50.0 ppm, from the chemisorbed chemical shift. The  $\Delta\delta$  values for all of the solid

acids measured are reported in Table 2-1. By referencing all the shifts to physisorbed TEPO the van der Waals forces component of the chemical shift is significantly reduced, making this an excellent, one parameter measure of the donor-acceptor interaction between TEPO and the acid site.

Table 2-1. The  $\Delta\delta$  Scale.

Acid or Adduct		$\Delta\delta$
(silica-gel) <sub>n</sub> Sb <sup>V</sup> Cl <sub>3</sub>	Site 1	66.6
	Site 2	48.0
	Site 3	36.4
	Site 4	22.6
(silica-gel) <sub>n</sub> Al <sup>III</sup> Cl <sub>2</sub>		52.0
1:1 TEPO:TaCl <sub>5</sub>		51.3 <sup>a</sup>
		46.3 <sup>a</sup>
		~42.2 <sup>a,b</sup>
		41.8 <sup>a</sup>
		38 <sup>a</sup>
HPW		45.8
1:1 TEPO:SbCl <sub>5</sub>		41.7 <sup>c</sup>
		37.5
Supported Sulfated Tungsten Oxide		41.7
HZSM-5	Site 1	39
	Site 2	7
2:1 TEPO:Al <sub>2</sub> Cl <sub>6</sub>		36.6
Sulfated Silica Gel		35.9
Tungstic Acid Hydrate	Site 1	27.6
	Site 2	13.4
H-Mordenite <sup>d</sup>		25.6
Silica Gel		6.0
Sol-Gel		4.5
NaCl*6H <sub>2</sub> O		2.7
NaOH		-1.2

<sup>a</sup> Various solids with different acidities.

<sup>b</sup> Identified through the spinning side bands.

<sup>c</sup> This is a minor peak with less than 10% of the total intensity.

<sup>d</sup> TEPO can probably only access the large cavities where the weaker of two acid sites can be found.

The comparison of the  $\Delta\delta$  scale to calorimetric measures of acidity results in a linear relationship (excluding 12-tungstophosphoric acid *vide infra*). The correlation of  $\Delta\delta$  to the Cal-Ad and slurry calorimetry scales is not fortuitous (Figure 2-3). Both experiments measure the extent of interaction of a basic probe molecule with a solid acid site. Stronger acid sites will cause greater interactions with the probe, decreasing the electron density about the central phosphorus atom in TEPO or increasing the enthalpy of interaction with pyridine. The chemical shift of TEPO will consistently increase with the acid strength until oxygen atom transfer or full protonation occurs. In the case of oxygen atom transfer, chemical shifts similar to that expected for triethylphosphine should be observed. In the case of full protonation, no further increase in the chemical shift will occur, as the conjugate acid of TEPO, HTEPO<sup>+</sup>, can no longer easily donate electron density.

Fitting the points where one acid site was detected resulted in a straight line with an excellent  $r^2$  value of 0.9855. The correlation of these single points allows us to assume with a degree of certainty that both the pyridine and TEPO are probing the same acid sites (i.e., the strongest site detected by pyridine on a particular solid is the same as the strongest site detected by TEPO). The correlation considering all of the acid sites is improved slightly over the previous trend:  $r^2 = .9862$ . The use of a second order (or higher) polynomial results in a better fit ( $r^2 = .9879$ ); however, within experimental error it cannot be distinguished from a first order fit, leading to a choice of the linear fit.

The derivation of a relationship between the change in chemical shift and enthalpy of adsorption is not known. However, there are two empirical methods to justify a relationship between the two values. The first comes from Drago's E and C method.<sup>122</sup>

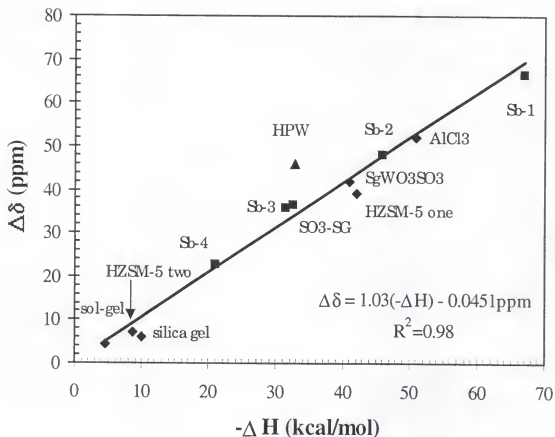


Figure 2-3. The correlation between calorimetry and  $\Delta\delta$ . The acids are: sol-gel, a low acidity silica solid; silica gel, a typical silica gel; HZSM-5 one and two, the acid sites of zeolite HZSM-5; Sb-1 through Sb-4, the four acid sites of silica supported antimony pentachloride; SO3-SG, sulfuric acid washed silica gel; SgWO3SO3, silica supported sulfated tungsten oxide; HPW, 12-tungstophosphoric acid; AlCl3, silica supported aluminum trichloride. The  $\blacklozenge$  points are enthalpies derived from the Cal-Ad method, while the  $\blacksquare$  are derived from slurry calorimetry alone. The  $\blacktriangle$  represents 12-tungstophosphoric acid. The line was fit without 12-tungstophosphoric.

E and C uses two parameters to describe the donor-acceptor interaction between two molecules (Equation 2-2):<sup>123</sup>

$$\Delta\chi = E_a E_b + C_a C_b - W \quad (2-2)$$

The nature of  $\Delta\chi$  can be enthalpies of reaction, spectral shifts, or even rate constants. The first set of parameters,  $E_a$  and  $E_b$ , represent the electrostatic component of the interaction, while the second set,  $C_a$  and  $C_b$ , represent the covalent interaction. The  $W$  term accounts for any barrier that must be overcome to allow the acid and base to interact, such as the breaking of a dimer. The E and C model indicates that the same factors that lead to an evolution of an enthalpy of interaction will lead to a proportional change in the spectral parameters.<sup>122</sup>

Literature precedence has established a second link between acidity measured by enthalpies of interaction and changes in chemical shift. It can be shown that acidity is proportional to strength of the acid-base bond formed (Equation 2-3):<sup>11,72-73,77,94</sup>

$$-\Delta H_{\text{acid-base}} \propto \text{acid-base bond strength} \quad (2-3)$$

And that the change of chemical shift of TEPO or 2-<sup>13</sup>C acetone in solution is proportional to the bond strength of the donor-acceptor pair in the solution (Equation 2-4).<sup>40-42,44,51,69</sup>

$$\Delta\delta^{31}\text{P}, \Delta\delta^{13}\text{C} \propto \text{acid-base bond strength} \quad (2-4)$$

These two equations allow the relationship between chemical shift, a spectral parameter, and enthalpy of interaction, a thermodynamic parameter to be written:

$$\Delta\delta^{31}\text{P}, \Delta\delta^{13}\text{C} \propto \text{acid-base bond strength} \propto -\Delta H_{\text{acid-base}} \quad (2-5)$$

This relationship allows us to look for a correlation between  $\Delta\delta$  and calorimetry.

### Evidence for the Measurement of Global Acidity

The  $\Delta\delta$  scale is a global acidity scale<sup>34</sup>--it measures acidity without regard for the type of acid site the probe is bound to. The total donor-acceptor interaction is the primary contribution to the observed change in chemical shift. The  $^{31}\text{P}$  MAS NMR spectra of TEPO on the solid acid (silica gel) $_{\text{n}}\text{Sb}^{\text{V}}\text{Cl}_3$  (Figure 2-4) demonstrates this phenomenon. This solid contains four acid sites, at least one of which is a Lewis site as determined by pyridine adsorption IR.<sup>124</sup> Additionally, the  $\Delta\delta$  of the four acid sites observed all correlate with differential heats of pyridine adsorption obtained from slurry calorimetry (reported in Chapter 5).

Additional evidence for a global measurement of acidity comes from TEPO adsorbed on a series of Lewis acids. The spectrum of the adducts formed between TEPO and tantalum pentachloride (TEPO: $\text{TaCl}_5$ ) is presented in Figure 2-5. Each adduct measured ( $\text{TaCl}_5$ ,  $\text{SbCl}_5$ ,  $\text{Al}_2\text{Cl}_6$ ) had a positive  $\Delta\delta$  at a different chemical shift. The position of this peak indicates that the Lewis region predicted by Rakiewicz *et al.*<sup>44</sup> (a small, negative  $\Delta\delta$ ) for trimethylphosphine oxide cannot be extended to TEPO. Such negative  $\Delta\delta$  values can be shown to be the very weak Lewis acid TEPO interacting with strong basic sites on the surface (*vide infra*).

By changing the loading of TEPO on  $\text{TaCl}_5$ , a new of shift can be observed. The variation in shift is attributed to the nearest neighbor effect. In samples with less than a 1:1 TEPO:  $\text{TaCl}_5$  ratio, induction effects that will increase the acidity of the acid site are likely to be observed. Two different loadings of TEPO on  $\text{TaCl}_5$  demonstrate this effect (Table 2-2).



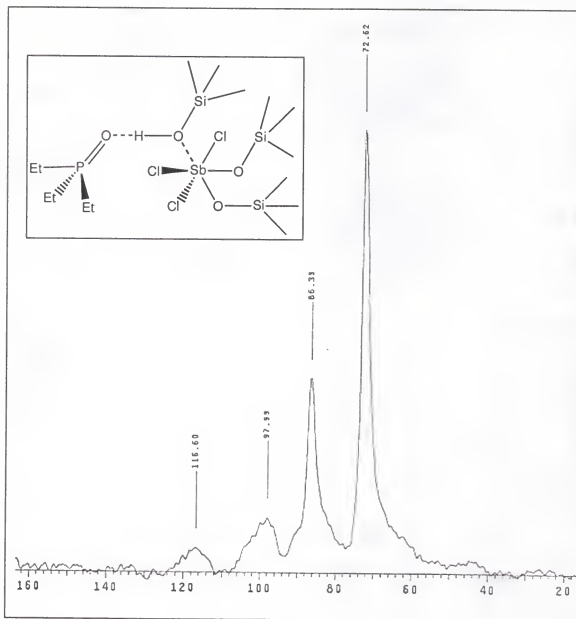


Figure 2-4. Phosphorus-31 MAS NMR of TEPO on  $(\text{silica gel})_n\text{Sb}^{\text{V}}\text{Cl}_3$ . The four acid sites observed correspond to the four acid sites detected by slurry calorimetry. Additionally, this solid contains both Lewis and Brønsted acid sites. One of the proposed Brønsted acid sites appears in the inset.

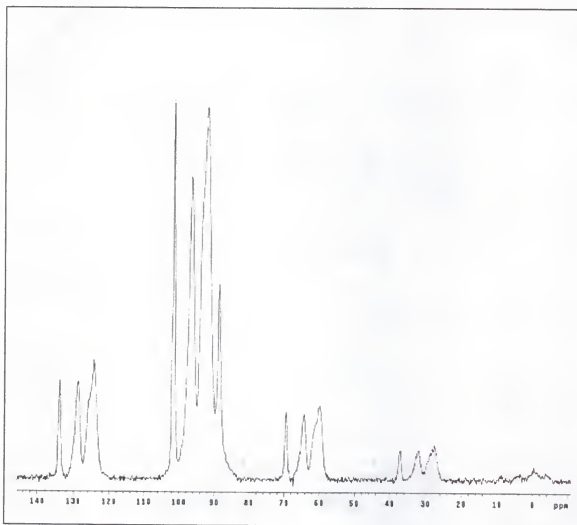


Figure 2-5. Phosphorus-31 MAS NMR of TEPO adsorbed on  $\text{TaCl}_5$ . The four lines observed are each a different solid form of the adduct with different bonding between the metal and the phosphine oxide. A fifth spectral line can be identified through the spinning side bands.

Table 2-2. The inductive effect in Lewis haloacids.

Compound	Compound Observed	Chemical Shift (ppm)	$\Delta\delta$ (ppm)
1:1 TEPO:SbCl <sub>5</sub>	TEPO:SbCl <sub>5</sub>	87.5	37.5
		91.7	41.7
2:1 TEPO:Al <sub>2</sub> Cl <sub>6</sub>	TEPO:AlCl <sub>3</sub>	86.6	36.6
1:1 TEPO:TaCl <sub>5</sub>	Various TEPO:TaCl <sub>5</sub> Crystals	88.0	38
		91.8	41.8
		~92.2	~42.2
		96.3	46.3
		101.3	51.3
1:10 TEPO:TaCl <sub>5</sub>	TEPO:TaCl <sub>5</sub>	101.6	51.6
	TEPO:TaCl <sub>5</sub> -TaCl <sub>5</sub>	110.2	60.2

### Static and Differential Measures of Acidity

Chemisorption of a probe molecule results in a static measurement of acidity. This static interaction is a measurement of the acidity of the site that a molecule experiences while bound to it. Differential heats of adsorption may indicate a different acidity than such a static measure depending on the acid under study. The acidity of 12-tungstophosphoric acid has been measured calorimetrically both in solution<sup>77</sup> and in the solid state (Table 1-3).<sup>83</sup> Most results indicate that HPW is a powerful solid acid; however, there is much dispute over the true strength of this solid. The Cal-ad acidity of the strongest site is 32.7 kcal mol<sup>-1</sup>, the expected  $\Delta\delta$  is therefore 33.6 ppm. The observed

$\Delta\delta$  of HPW, however, is 45.8 ppm (predicted enthalpy of 44.5 kcal mol<sup>-1</sup>), much greater than the expected value. The  $\Delta\delta$  scale predicts that HPW is a much stronger acid than measured by the Cal-ad techniques.

The source of this discrepancy between calorimetry and  $\Delta\delta$  can be readily accounted for with an understanding of the nature of the two experiments. The heat measured from slurry calorimetry is the heat of interaction of the base with the acid site less the heat required to displace a solvent molecule from the acid site, less the heat required, in this case, to open up the lattice for the basic probe to enter (Figure 2-6). The heat of interaction of the base with the acid site contains contribution from both donor-acceptor interactions and van der Waals forces. It can be shown that with the correct choice of basic probe and solvent, the van der Waals component can be removed from the measured enthalpy by the displacement of the solvent molecule.<sup>73,123</sup>

The reduction of the measured enthalpy by opening the lattice cannot be accounted for without a measure of the lattice energy of the initial and final states. The reduction of the exothermic energy by the opening of the lattice will lower the estimate of the acidity of the solid by the amount of energy required to open the lattice. The initial adsorption of TEPO contains all of these energetic steps, but the measure of the acidity by <sup>31</sup>P MAS NMR occurs after all of these processes have been completed. The  $\Delta\delta$  is a measure of the static interaction of TEPO with the acid site after the lattice is opened and the molecule is fully adsorbed at the site. The difference between the enthalpy estimated from the change in chemical shift of TEPO and the enthalpy measured by the Cal-Ad method leads to an estimated energy of 11.8 kcal mol<sup>-1</sup> required to open the HPW lattice to include a pyridine sized molecule

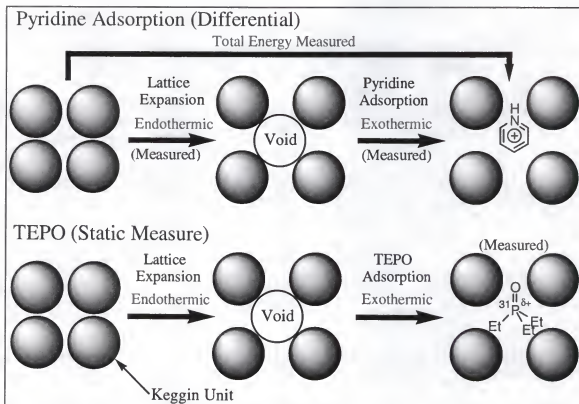


Figure 2-6. A comparison of two different methods of measuring solid acidity. The top scheme demonstrates the energy changes measured during differential calorimetry of 12-tungstophosphoric acid (HPW) with pyridine. The first step is the endothermic opening of the lattice to accommodate the probe molecule. The second step is the exothermic enthalpy for adsorption of the probe. The total energy measured is the sum of both these steps. The lower scheme is for the measurement of the chemical shift of chemisorbed triethylphosphine oxide. Only the interaction between the probe and the acid site is measured.

### Triethylphosphine Oxide in Zeolites

Previous measurements of trimethylphosphine oxide in zeolites HY and dealuminated HY have been carried out by Zalewski *et al.*<sup>32</sup> and Rakiewicz *et al.*<sup>44</sup> and of zeolite USY by Rakiewicz *et al.* They report that the shift observed is very sensitive to the type of acid site to which the probe is adsorbed. We extend their observations of phosphine oxide behavior to include the measurement of zeolites HZSM-5 and H-Mordenite with TEPO and zeolite TS-1 with trimethylphosphine oxide.

The  $^{31}\text{P}$  MAS NMR spectrum of 0.1 mmol  $\text{g}^{-1}$  TEPO on zeolite HZSM-5 demonstrates the presence of two acid sites. The structure of HZSM-5 is large enough to allow complete penetration by the probe into the large chambers and channels;<sup>125</sup> however, a significant amount of time is required to allow TEPO to penetrate the pores of the zeolite. The first acid site is a low population strong site that has been assigned as a Brønsted site through pyridine IR adsorption and Cal-Ad.<sup>73</sup> The second site has been shown to be a weaker hydrogen bonding site of significantly larger population. The acidity determined for these two sites are in good agreement with results from calorimetric measurements (Table 2-3).

The spectra of TEPO adsorbed on H-Mordenite shows the presence of only one acid site. The  $\Delta\delta$  value for this moderate strength site is 25 ppm. It is probable that TEPO cannot penetrate the small channels of H-Mordenite where additional acid sites are believed to exist.

Zeolite TS-1 is a very weakly acidic zeolite.<sup>79</sup> The acidity of TS-1 arises from defect sites resulting in tricoordinate  $\text{Ti}^{4+}$ . The acidity of this solid was measured with trimethylphosphine oxide. Two overlapping spectral lines were observed (Figure 2-7).

Table 2-3. The Cal-Ad and  $\Delta\delta$  results for HZSM-5.<sup>80</sup>

	Site 1	Site 2
$-\Delta H_{\text{ave}}$ (kcal mol <sup>-1</sup> )	$42.1 \pm 0.8$	$8.6 \pm 3.8$
Population (mmol g <sup>-1</sup> )	$0.0415 \pm 0.0057$	$0.53 \pm 0.01$
K	$4.9 \pm 2.3 \times 10^6$	$2.3 \pm 2.0 \times 10^6$
$\Delta\delta$ (ppm)	39	7

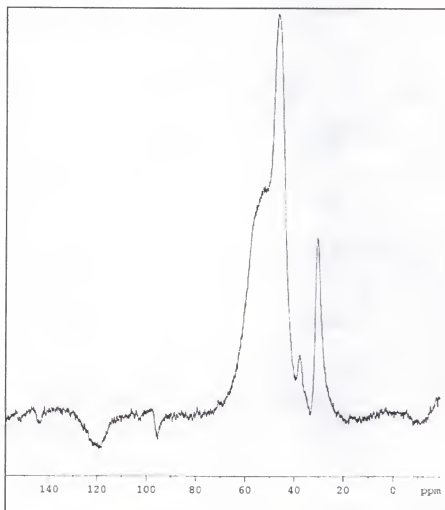


Figure 2-7. Phosphorus-31 MAS NMR of trimethylphosphine oxide on zeolite TS-1. The peak at about 30 ppm corresponds to physisorbed trimethylphosphine oxide.

From limited studies of the behavior of trimethylphosphine oxide on solid acids (Figure 2-8), the change in the chemical shift of trimethylphosphine oxide can be roughly compared to the  $\Delta\delta$  values for TEPO but with a chemical shift for the physisorbed probe of ~30-34 ppm. This assumption leads to the conclusion that the acidity of TS-1 is very mild, and arises from titanium sites scattered throughout the structure (there are twelve different types of titanium centers in TS-1) and possibly from surface silanols.

#### Interaction of Triethylphosphine Oxide with Solid Bases

The adsorption of a large amount of TEPO onto a strong, basic solid results in a small negative  $\Delta\delta$  shift (Table 2-4). The shift is only observed at very high loadings. It is

Table 2-4. The  $\Delta\delta$  value of TEPO on several bases.

System	$\Delta\delta$ (ppm)
NaOH	-1.36
KOH	-0.90
	-1.66
CaO	-0.56
	-1.63
$\gamma$ -alumina	-1.35

believed that the cause of the shift is an acid base interaction between the TEPO and the basic sites of the solid. In this case, TEPO is acting as a very weak acid and accepting a small amount of electron density from the basic site (Figure 2-9). A similar result is



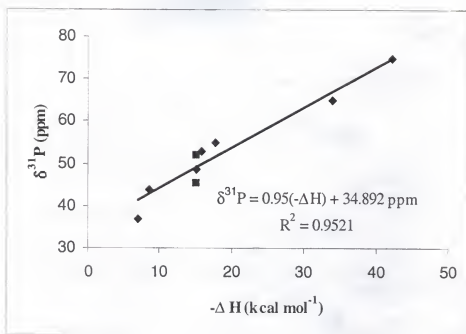


Figure 2-8. The chemisorbed chemical shift of trimethylphosphine oxide compared to calorimetric measures of acidity. The two chemical shifts of trimethylphosphine oxide interacting with zeolite TS-1 (represented by ■) were averaged together to estimate the shift of the acid site found by Cal-Ad for this solid. The Cal-Ad method cannot separate two sites that have similar acidity. The chemical shifts reported by Rakiewicz *et al.* (54) for zeolite HY were used for this solid.

reported for trimethylphosphine oxide adsorbed on  $\gamma$ -alumina,<sup>44</sup> although the shift was attributed to adsorption onto a Lewis acid site. Upon exposure to water, the resonance observed in Rakiewicz *et al.* disappeared. Exposure to water destroys the Lewis acid sites of  $\gamma$ -alumina, as reported, but will also greatly diminish the basicity of the solid.

Figure 2-10 is the spectrum of TEPO adsorbed on potassium hydroxide.

#### The Use of Trimethylphosphine Selenide to Explore Solid Acidity

The use of trimethylphosphine selenide (TMPS<sub>e</sub>) to measure solid acidity was explored. It was hoped that both the <sup>31</sup>P and <sup>77</sup>Se chemical shift information could be

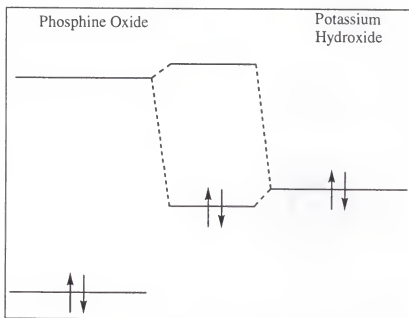


Figure 2-9. A MO diagram for the *acid* TEPO interacting with KOH. The negative  $\Delta\delta$  observed for TEPO adsorbed on the solids  $\gamma$ -alumina, potassium hydroxide, calcium hydroxide, and sodium hydroxide to be representative of an interaction with a basic site.

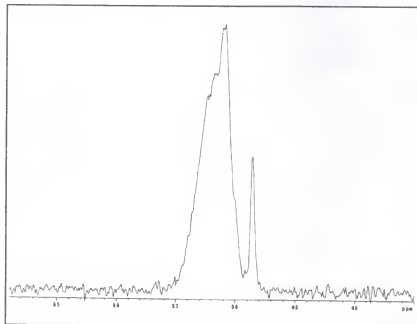


Figure 2-10. Phosphorus-31 MAS NMR of TEPO on potassium hydroxide. The small peak at around 48.5 ppm represents TEPO interacting with a basic site.

obtained from one probe molecule. However, the solid was unstable, decomposing at various rates depending on the components of the solid it was adsorbed on producing an insidious fine red powder (polymeric selenium?) and a stench (trimethylphosphine). All attempts to measure solids with any sulfur content failed due to exchange of the selenium with the sulfur moiety of the acid. The use of TMPSe must be restricted to solids without sulfur, and serves only to detect the presence of acidity, not as a measure of acid strength. The coupling constants of physisorbed TMPSe may be a measure of the surface polarity, and further research into this phenomenon would help to improve understanding of the physiochemical properties of surfaces.

The chemical shift of TMPSe chemisorbed on a solid appears to be limited to one shift at about 30 ppm. However, chemical shifts from the decomposition products (trimethylphosphine and trimethylphosphine oxide) can be observed (Figure 2-11).

Information can be gained from the study of the coupling constant,  $J(^{31}\text{P}-^{77}\text{Se})$ , of physisorbed TMPSe. The coupling constant is very sensitive to the distance between the coupled nuclei. Polarization of the phosphorus-selenium bond will lead to small changes in the bond length that will be observable in the change of  $J(^{31}\text{P}-^{77}\text{Se})$ . Since the coupling constants varied with the adsorbent (Table 2-5), they may prove useful as a measure of the polarity of a surface.

### Conclusions

The basic probe molecule triethylphosphine oxide is capable of measuring the acidity of solid acids using simple one pulse  $^{31}\text{P}$  MAS NMR. The shift of TEPO has been shown to correlate well with acidities measured with Cal-ad or slurry calorimetry. The nature of the acid site, as Lewis or Brønsted, does not affect the shift of TEPO. The value

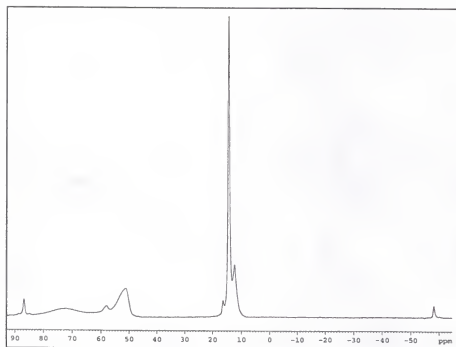


Figure 2-11. The  $^{31}\text{P}$  MAS spectrum of TMPSe on tungstic acid ( $\text{H}_2\text{WO}_4$ ). The peaks at 51, 58 and 72 ppm are decomposition products. The spinning side bands are at -60 ppm and 88 ppm. The peak at 14 ppm is assigned to physisorbed TMPSe and shows coupling to  $^{77}\text{Se}$  ( $J = 662$  Hz).

Table 2-5. The coupling constants ( $J$   $^{31}\text{P}$ - $^{77}\text{Se}$ ) of TMPSe physisorbed on solids.

Solid	$J$ ( $^{31}\text{P}$ - $^{77}\text{Se}$ )
Crystallized TMPSe	638 Hz
Silica Gel	644 Hz
HZSM-5	646 Hz
Tungstic acid ( $\text{H}_2\text{WO}_4$ )	662 Hz

of measuring acidity through several techniques has been demonstrated by a comparison of the acidity measured by differential heats of adsorption to the static method involving  $^{31}\text{P}$  NMR to determine a "lattice penetration" energy for pyridine into HPW. Reports of a Lewis acid region observed for TMPO have been shown to be inappropriate for TEPO. Small, negative  $\Delta\delta$  values have been demonstrated to be interactions with basic sites. Overall, this is a powerful, accurate and fast tool for characterizing and exploring solid acidity.

Triethylphosphine oxide is an ideal probe for the measurement of the global acidity of solid acids. It is capable of identifying different strength acid sites on the surface. However, simple one pulse experiments are incapable of identifying the nature of the acid site. TEPO lacks the chemical shift ranges dependent upon the nature of the acid site observed for TMP. It has been demonstrated elsewhere<sup>44</sup> that the population of acid sites can be determined with phosphine oxides. The combination of all of these traits makes phosphine oxides ideal for the characterization of solid acids.

### CHAPTER 3

#### THE EFFECTS OF PROTON EXCHANGE ON 12-TUNGSTOPHOSPHORIC ACID AND ITS DERIVATIVES

Interest in heteropoly acid catalysts has been raised by their interesting results in laboratory scale work and their industrial applications. Their use as homogeneous and heterogeneous catalysts for redox and acid catalyzed reactions have been extensively reviewed.<sup>16,126-132</sup> Promising use of heteropoly acids in the synthesis of fine chemicals and for biological applications has extended the range of use of these acids.<sup>133-134</sup>

The crystal structure of 12-tungstophosphoric acid (HPW) hexahydrate has been determined by X-ray<sup>113-114</sup> and neutron diffraction<sup>115</sup> analysis. The Keggin anion is highly symmetrical and can be considered a tetrahedron about the central  $\text{PO}_4$  group. The central phosphate is surrounded by twelve  $\text{WO}_6$  octahedra. These octahedra are arranged in four groups of three edge-shared  $\text{W}_3\text{O}_{13}$  groups called  $\text{W}_3$  triads (Figure 3-1).<sup>116</sup> The Keggin anions are close packed on a body centered lattice with the central anion turned 90 degrees to its eight neighbors. The counter ions to the -3 charge on each Keggin ion of HPW are  $\text{H}_5\text{O}_2^+$  located in the tetrahedral vertices. Extensive dehydration will leave a proton in the same position as the  $\text{H}_5\text{O}_2^+$  ion.<sup>127</sup>

An additional feature of the solid HPW hydrates are their high proton conductivities. The proton conduction in solid HPW is comparable to the proton conduction of water. The low activation energy for conduction is attributed to the location of waters of crystallization and hydrated protons in the interstices of the large,

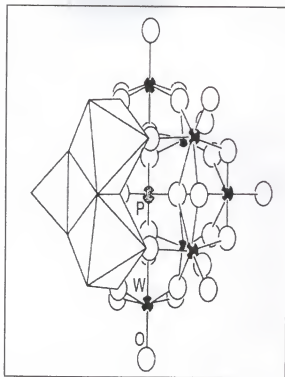


Figure 3-1. The structure of the Keggin anion. This particular Keggin ion,  $\text{PW}_{12}\text{O}_{40}$  has a negative 3 charge.

globular anions.<sup>135-137</sup> The high mobility of the proton is thought to increase the acidity of this compound by distributing any anionic charge built up throughout the solid (Figure 3-2). The catalytic properties of this solid can be tailored at atomic and molecular levels by exchanging the hydrated protons with other cations. Changing the counter cation modifies the properties of the heteropoly acid and can result in a change in both structure and activity.

Recently,  $\text{Cs}_x\text{H}_{3-x}\text{PW}_{12}\text{O}_{40}$  derivatives (abbreviated as  $\text{Cs}_x\text{H}_{3-x}\text{PW}$ ) have gained attention because of their claimed super acidity and shape-selectivity in alkylations reactions.<sup>138-140</sup> Unlike HPW, the  $\text{Cs}_x\text{H}_{3-x}\text{PW}$  salts have limited solubility in water or organic solvents and are used exclusively as heterogeneous catalysts. The cesium salts

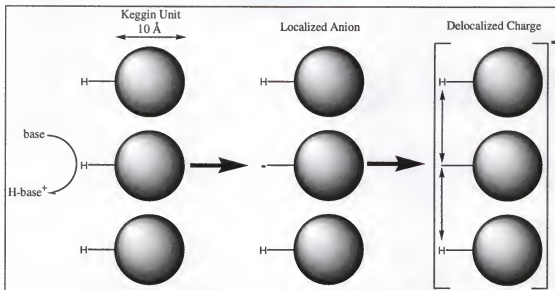


Figure 3-2. Delocalization of charge in 12-tungstophosphoric acid. Abstraction of a proton by a base results in a negative charge that is distributed throughout the solid by proton conduction.

show higher catalytic activity and higher thermal stability in some reactions than HPW.<sup>126</sup> The cesium salts are thought to have a similar structural motif as HPW.

The structure of  $\text{Cs}_3\text{PW}$  is the same as HPW but with  $\text{Cs}^+$  in place of the  $\text{H}_5\text{O}_2^+$  groups and larger lattice constants from the larger spaces between Keggin units. The structure of the other  $\text{Cs}_x\text{H}_{3-x}\text{PW}$  compounds is not completely established. The proposed structures of cesium complexes with  $x < 3$  are reported to be mixtures of HPW and  $\text{Cs}_x\text{H}_{3-x}\text{PW}$ . A study of the precipitates from the titration of HPW with  $\text{Cs}_2\text{CO}_3$  concluded that in the range of  $0 < x \leq 2$  the solid is mainly a mixture of HPW and  $\text{Cs}_2\text{HPW}$ .<sup>142</sup> Compounds prepared in the range of  $2 < x \leq 3$  are mixtures of  $\text{Cs}_3\text{PW}$  and HPW, although  $\text{Cs}_{2.5}\text{H}_{0.5}\text{PW}$  is considered to be a mixture of  $\text{Cs}_2\text{HPW}$  and  $\text{Cs}_3\text{PW}$ . Reported XRD patterns for  $\text{Cs}_x\text{H}_{3-x}\text{PW}$  ( $x = 0, 1, 2$ , and  $3$ )<sup>143</sup> claim that  $\text{CsH}_2\text{PW}$  is a mixture of HPW and  $\text{Cs}_2\text{HPW}$  which is transformed into a nearly homogeneous acidic



salt after thermal treatment of the precipitate at 300 °C. The lattice constants for those cesium salts indicate all of them belong to cubic systems.<sup>141</sup>

The cesium salts were studied by  $^{31}\text{P}$  NMR.<sup>39</sup> Each loading of cesium has been found to have a distinct MAS NMR spectrum. Literature reports that the  $^{31}\text{P}$  spectrum of  $\text{Cs}_2\text{HPW}$  is composed of four peaks, which were interpreted as a mixture of four species ( $x = 0, 1, 2$ , and  $3$ ). Results for  $\text{Cs}_{2.5}\text{H}_{0.5}\text{PW}$  also claim that this compound is a mixture of  $\text{Cs}_2\text{HPW}$  and  $\text{Cs}_3\text{PW}$ . Supported HPW on  $\text{Cs}_3\text{PW}$  presents the same  $^{31}\text{P}$  spectrum as  $\text{Cs}_{2.5}\text{H}_{0.5}\text{PW}$ ,<sup>139</sup> indicating in homogenous exchange between  $\text{H}^+$  and  $\text{Cs}^+$  during the heating process. In those studies<sup>141-143</sup> the cesium derivatives were prepared similarly, although the thermal treatment before analysis of the solids was not always the same.

The location of the pyridine binding sites in HPW will be identified. Pyridine will be shown to be incapable of completely penetrating the solid, but that it can cause the widening of certain crystalline layers allowing for an interaction with various protons in the structure. The effect of cation exchange on the phosphorus-31 chemical shift of the cesium salts will be reported.

### Experimental

#### Materials Preparation

The solids studies were prepared by J6se A. Dias,<sup>83</sup> but since the method of preparation is of critical importance the relevant experimental steps will be summarized here. Elemental analysis of the HPW (Aldrich) revealed 16 moles of water per mole of HPW, therefore a drying procedure is required to obtain the hexahydrate. The drying procedure was to heat the solid at 160 °C for 4 hours under vacuum. It has been shown that heating HPW at that temperature yields the anhydrous acid.<sup>77</sup>

### Spectral Analysis

The  $^{31}\text{P}$  MAS NMR spectra of the solids were taken on a Varian Unity 500 NMR operating at 202.264 MHz. The magic angle was tuned using  $\text{K}^{79}\text{Br}$ . A recycle delay of 2 seconds was used. The acquisition time was set to 0.02 ms. Signals were indirectly referenced to 85% phosphoric acid. At least ten minutes of signal averaging were allowed for all spectra.

### Calorimetric Titrations and Adsorption Measurements

Jóse A. Dias performed all calorimetric titrations. The methods he used can be found in his dissertation<sup>81</sup> or in Reference 83, a paper co-written by this author. The calorimetric data is instrumental in the data analysis presented in this chapter, particularly for HPW. The exact experimental procedure does not differ significantly from the calorimetric procedure presented in Chapter 1. Cyclohexane was chosen as the solvent to make the slurry because it is a non-interacting solvent in which the solids are insoluble. Time dependent UV adsorption experiments were performed to insure that equilibrium of the pyridine with HPW was achieved in the time scale of the calorimetric titration.

### Results and Discussion

#### Spectroscopic Results of $^{31}\text{P}$ MAS NMR and XRD for HPW and $\text{Cs}_5\text{H}_{3-x}\text{PW}$

The  $^{31}\text{P}$  MAS NMR spectra of HPW and several Py-HPW species with different ratios of pyridine to the total number of acid sites were obtained. The spectrum of anhydrous HPW shows a single peak at -12.0 ppm (Figure 3-3), corresponding to literature values of -10.9 ppm,<sup>141</sup> -12.4 ppm,<sup>144</sup> and -11.1 ppm.<sup>98</sup> The product spectrum of the first two sites titrated with pyridine, 1.04:0.24 mol ratio of HPW to pyridine, gives only a single resonance at -17.5 ppm (Figure 3-4), which changes to -16.5 ppm upon

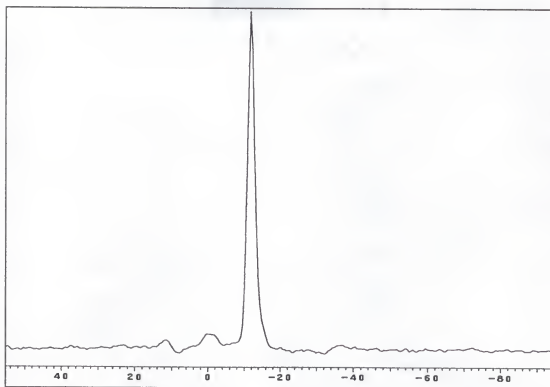


Figure 3-3. The  $^{31}\text{P}$  MAS NMR of 12-tungstophosphoric acid. There is only one peak (-12.0 ppm), the other peaks are spinning side bands.

exposure to water. Proton conduction acts to distribute the anionic charge throughout the structure, making the electron density on all the Keggin units similar on the time scale of the NMR experiment. Spectra of 1.04:0.08 and 1.04:0.12 mole ratio of HPW to pyridine also show a single peak at -17.5 ppm providing further evidence that the protons are mobile in the structure.

Exchange of protons for less acidic cesium atoms causes a small increase in the electronic density at the phosphorus core. The resulting increase in electron density can be observed in the  $^{31}\text{P}$  MAS NMR of the solids  $\text{Cs}_x\text{H}_{3-x}\text{PW}$  ( $x=0, 0.9, 1.8, 2.4, 2.7$ ). Each

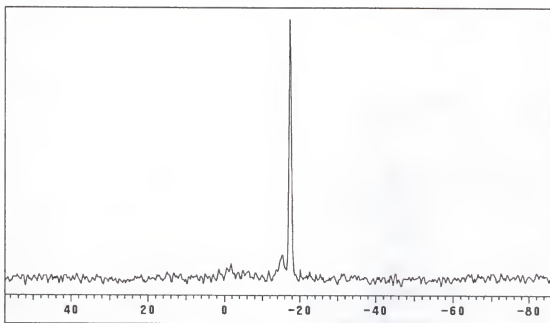


Figure 3-4. The  $^{31}\text{P}$  MAS NMR of 0.24 mmol pyridine on 1 gram of 12-tungstophosphoric acid.

spectrum shows a single peak that shifts to lower field going from HPW to  $\text{Cs}_3\text{PW}$ . The presence of only one narrow peak in the NMR, unlike the reported literature results,<sup>141</sup> demonstrates that the method of preparation produces homogenous compounds.

The chemical shift of the cesium salts changes regularly with increasing cesium substitution (Figure 3-5). The shift is due to the increasing electron density on the Keggin units due to the greater charge separation afforded by the larger cesium cations. In essence, the cesium cations hold a larger portion of a positive charge than the solvated protons, allowing for a greater negative charge to build up on the Keggin units. The result of this buildup can be observed through the shielding of the phosphorus atoms. Increasing the amount of cesium in the structure results in a gradual decrease in the chemical shift.

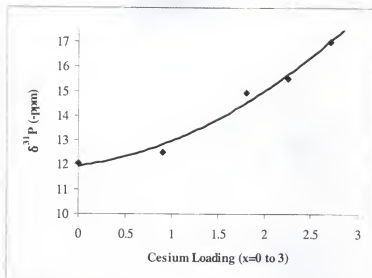


Figure 3-5. The chemical shift of the central phosphate changes with cesium loading. The data can be fit by a second order (or higher) polynomial indicating that there are at least two factors which influence the chemical shift (*vide infra*).

#### Locating the Acid Sites in the HPW Crystal Structure

The XRD spectra of HPW gives a pattern similar to that reported in the literature.<sup>117</sup> The main peaks, related to the strongest reflections, are present at  $2\theta = 10.4^\circ$ ,  $25.4^\circ$ , and  $33.5^\circ$  (Figure 3-6). The broader peaks indicate loss of crystallinity, as reported for HPW dried at different conditions.<sup>105,145</sup> The XRD from the reaction of 1.04 mmol of HPW with 0.24 mmol of pyridine shows a few new peaks (Figure 3-7). The most intense peak at  $2\theta = 10.4^\circ$  splits up into two less intense shoulders at  $2\theta = 10.30^\circ$  and  $10.52^\circ$ . Two new reflections at  $2\theta = 9.27^\circ$  and  $9.98^\circ$  are present in the powder pattern. These smaller angle reflections indicate a larger d-spacing in the unit cell to accommodate the pyridine molecules attached to the protons. Other reflections shifted slightly with significant changes in intensity. No large-scale change was observed in the

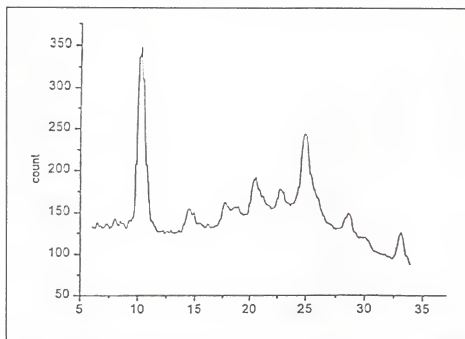


Figure 3-6. The XRD data for 12-tungstophosphoric acid.

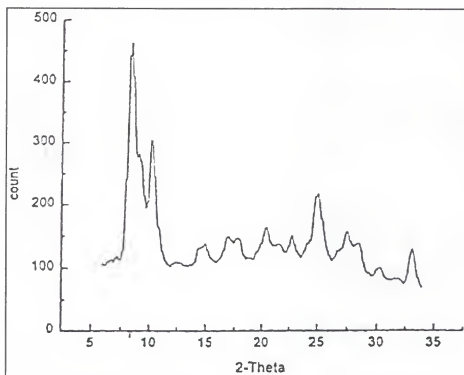


Figure 3-7. The XRD data for 12-tungstophosphoric acid with one pyridine molecule adsorbed per acid site. The smaller  $2\theta$  values compared to pure HPW indicate an expansion of the lattice.

XRD pattern when enough pyridine was adsorbed onto HPW to account for all of the strong acid sites determined by Cal-Ad.<sup>83</sup>

The Cal-Ad results for HPW<sup>83</sup> (reported previously in Table 1-3) demonstrate that the heat evolved from adsorption of pyridine indicates that only a fraction of the 1.04 mmol of protons in one gram of HPW are titrated. After 0.24 mmol of pyridine was added (about 24% of the moles of protons in a gram of solid), heat evolution essentially stopped along with the adsorption of pyridine by the solid. The number of surface protons reported for solid HPW is 0.008 mmol g<sup>-1</sup>.<sup>146</sup> This value can also be calculated by assuming that the Keggin ions are spherical and that the surface area is 5 m<sup>2</sup> g<sup>-1</sup> (calculated 0.0079 mmol surface sites per gram HPW). Thus, in addition to reacting with the surface protons, pyridine also penetrates into regions of the solid. This result is consistent with Misono<sup>131</sup> who reports that the adsorption of polar molecules by HPW leads to catalytic reactions in the bulk of the crystal as well as on the surface. This behavior is analogous to a concentrated solution and is described as a pseudoliquid phase<sup>131,147</sup> where non-polar molecules are not absorbed.

In order to make sure that the incomplete reaction was not caused by forming a layer of product on the surface that could not be penetrated by pyridine, the sample was ground to finer particles inside an inert atmosphere box and titrated with pyridine.<sup>83</sup> An identical isotherm was produced demonstrating that diffusion due to restrictions of particle size is not a problem, and suggesting that pyridine was not able to access certain protons.

In the tertiary structure, the protons are located at the center of each edge and face, while the Keggin anions are arranged in a cubic body centered manner. The unit

cell (Figure 3-8) consists of a total of two anions (8 anions centered on the vertices and 1 anion in the center of the cube) and six protons (6 positioned on the center of the faces and 12 at the edges). The ratio of anions to protons (2:6) corresponds to the molecular formula. The Cal-Ad results suggest that the total number of protons titrated (0.24 mmol per gram) could be assigned to the number of protons in every even plane of the lattice (E00). The Cal-Ad determined first site would be the face-centered proton, corresponding to about 8% of the total protons in the cell. Summing over all the face protons in the even planes in one gram of HPW would yield 0.08 mmol of protons for this site (Figure 3-9). The second site closely corresponds to the edge protons in this plane (Figure 3-10). These edge protons represent 16% of the protons of each unit cell. Again, summing over all the edge protons in the even planes in one gram of HPW would yield 0.16 mmol of sites. Both the individual components and the total number of moles determined in this manner correspond with the Cal-ad results of  $n_1 = 0.08 \text{ mmol g}^{-1}$  and  $n_2 = 0.16 \text{ mmol g}^{-1}$  (Table 3-1).

Table 3-1. Comparison of the Cal-ad site populations to the position of the protons in the crystal structure of HPW.

	Bulk Crystal <sup>a</sup>	Even Planes <sup>a</sup> (E00)	Cal-ad Population <sup>c</sup>
Site One (mmol g <sup>-1</sup> ) <sup>b</sup>	0.35	0.08	0.079 ± 0.002
Site Two (mmol g <sup>-1</sup> ) <sup>b</sup>	0.69	0.16	0.16 ± 0.05

a. Site one for the Bulk Crystal and the Even Planes are the face centered protons. Site two represents the edge protons.

b. To convert from mmol site (gram HPW)<sup>-1</sup> to mmol site (mmol HPW)<sup>-1</sup> multiply each value by 2.880 g mmol<sup>-1</sup> HPW.

c. The units for Cal-ad Population are the number of acid site of a particular type that interact with the probe molecule pyridine for an average gram of material (from Reference 83).



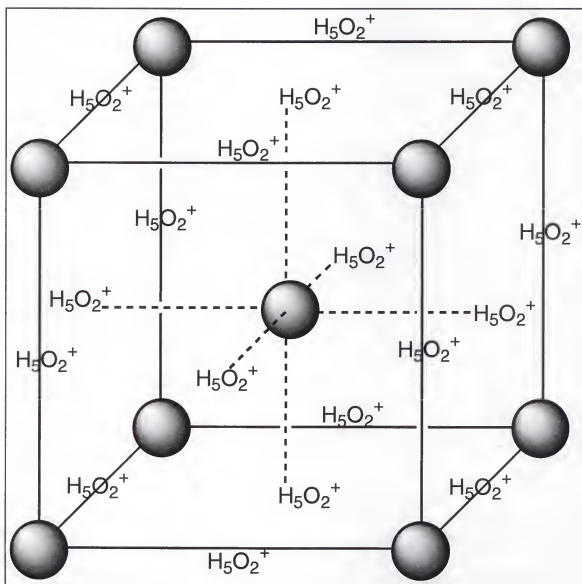


Figure 3-8. A representation of the unit cell of 12-tungstophosphoric acid. The shaded spheres represent the Keggin anions.

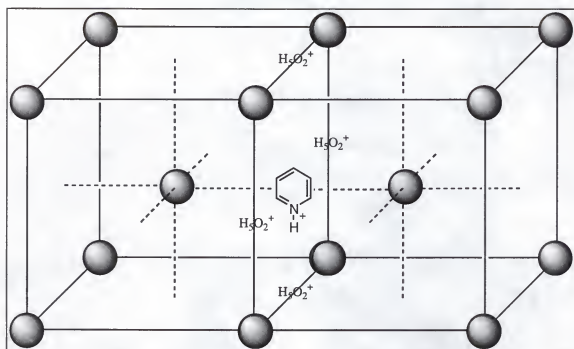


Figure 3-9. A representation of site one for pyridine titration of HPW. Pyridine can only interact with the face protons of every even lattice plane.

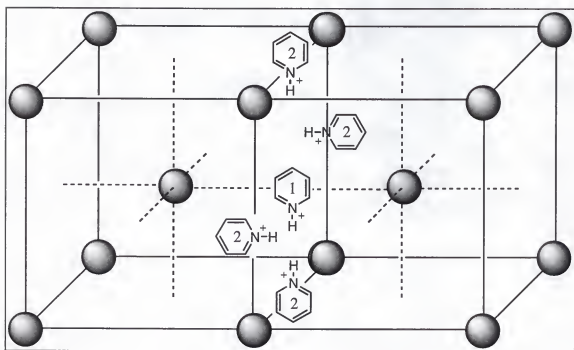


Figure 3-10. A representation of fully titrated HPW. The site two protons are all the edge protons in the even planes.

The assignment of the protons that can react with pyridine to the faces and edges of the unit cell account for the two sites found in the titration of HPW. The unit cell of this preparation is thought to be identical to that of the hexahydrate, bcc. Pyridine initially reacts with one of the six available face protons, producing site 1 of the titration. With one equivalent of pyridine attached to the structure, additional pyridine is in effect titrating  $(C_5H_5NH)^+ H_2PW^-$ . The second site has a lower enthalpy,  $\Delta H_2 = -19.6 \text{ kcal mol}^{-1}$  but a higher site density. Considering the fraction that each proton shares in the unit cell, the ratio of face protons to edge protons (1:2) titrated by pyridine gives the Cal-Ad ratio of  $n_1$  to  $n_2$  (1:2). The lower enthalpy for site two is probably due to a loss or lowering of the proton conduction due to the nearby pyridinium cation. The sum of the  $n_1$  and  $n_2$  value from Cal-Ad,  $0.24 \text{ mmol g}^{-1}$ , confirms that protons have reacted and are located inside the solid as well as on the surface.

The chemical interaction of the probe molecule with the solid is of great importance. In studies conducted using microcalorimetry of gaseous ammonia adsorption,<sup>107-109</sup> all of the protons in HPW were observed to react. The complete penetration of ammonia into HPW can be attributed to its small size. The HPW lattice will not have to be distorted for an ammonia molecule to enter and displace a water molecule from the  $H_5O_2^+$  cations. Additionally, the stronger basicity of ammonia will help to drive the reaction to completion.

#### Homogeneity of Cesium Distribution in Cesium-HPW Salts

Literature reports have shown that the cesium salts of HPW are mixtures of HPW with  $Cs_3PW$ . Phosphorus-31 MAS NMR has shown multiple peaks indicating the complex nature of the precipitated, uncalcined solids. However, a thermal treatment

process developed in the Drago lab can be shown to produce a homogenous distribution of the cesium ions throughout the structure.

For  $\text{CsH}_2\text{PW}$  only 3% of the available protons in the solid are titrated which is lower than the 24% titrated for HPW. Coupled with the  $^{31}\text{P}$  NMR (Figure 3-11) results which lacks a peak for HPW, it can be concluded that the surface is coated with cesium ions which prevent access to most of the protons in the solid. However, the bulk solid has a regular substitution of cesium ions for protons. The location of the pyridine binding sites in this solid, nor for any of the other cesium salts, can be determined as for HPW. The blocking of the surface by the cesium ions prevents even penetration of the pyridine into the structure.

The  $^{31}\text{P}$  MAS NMR spectrum of  $\text{Cs}_2\text{HPW}$  (Figure 3-12) has only one signal that is at a different chemical shift from pure HPW. This indicates that the bulk solid has a homogenous distribution of cesium ions. A previous report found that  $\text{Cs}_2\text{HPW}$  was a mixture of four different species of  $\text{Cs}_x\text{H}_{3-x}\text{PW}$  ( $x = 0, 1, 2, \text{ and } 3$ ).<sup>141</sup> The preparation of this salt in aqueous solution might generate a series of equilibria in solution involving up to four different species, and when the solid precipitates all four species are present in the solid. After thermal treatment the solvated protons and the cesium ions are completely homogenized into the solid  $\text{Cs}_2\text{HPW}$  structure.

Like  $\text{Cs}_2\text{HPW}$ , solid  $\text{Cs}_{2.5}\text{H}_{0.5}\text{PW}$  is reported to be a mixture of two compounds:  $\text{Cs}_2\text{HPW}$  and  $\text{Cs}_3\text{PW}$ .<sup>141</sup> Our results from  $^{31}\text{P}$  MAS NMR (Figure 3-13) again demonstrate that a thermal treatment results in a homogenous solid. Neither a spectral line for  $\text{Cs}_2\text{HPW}$  or  $\text{Cs}_3\text{PW}$  (Figure 3-14) was observed.

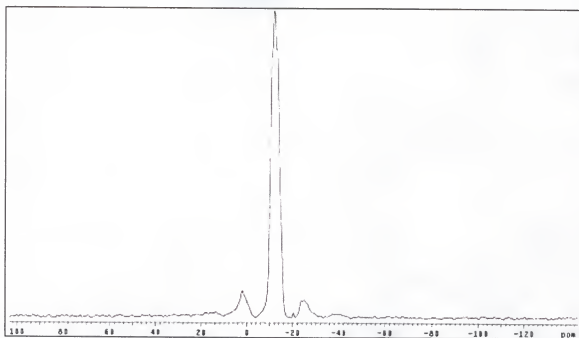


Figure 3-11. The  $^{31}\text{P}$  MAS NMR spectrum of  $\text{CsH}_2\text{PW}$ . The peak at 14.9 ppm is the isotropic peak while the other peaks are spinning side bands.

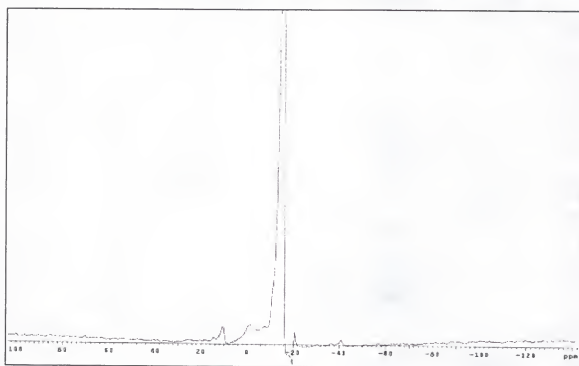


Figure 3-12. The  $^{31}\text{P}$  MAS NMR spectrum of  $\text{Cs}_2\text{HPW}$ . The signal near -20 ppm is the transmitter signal.

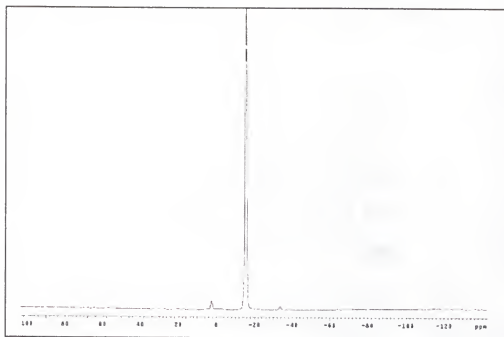


Figure 3-13. The  $^{31}\text{P}$  MAS NMR spectrum of  $\text{Cs}_{2.5}\text{H}_{0.5}\text{PW}$ .

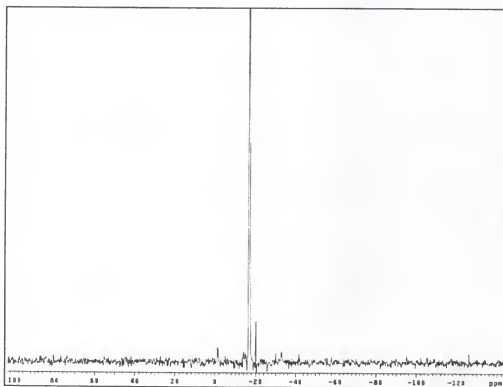


Figure 13-14. The  $^{31}\text{P}$  MAS NMR spectrum of  $\text{Cs}_3\text{PW}$ . The line at -20 ppm is the transmitter spike.

The single chemical shift observed for each solid indicates that thermal treatment results in a homogenous distribution of the cesium units throughout the solid. The change in chemical shift is probably due to a combination of electronic effects concomitant with cesium substitution and changes in the surface area, and hence the space between the Keggin anions (Table 3-2).

Table 3-2. The chemical shift of cesium salts of HPW.

	Number of Cesiums <sup>a</sup>	Surface Area (m <sup>2</sup> g <sup>-1</sup> )	$\delta^{31}\text{P}$ (ppm)
HPW	0	5	12.05
CsH <sub>2</sub> PW	.9	1	12.5
Cs <sub>2</sub> HPW	1.8	63	14.9
Cs <sub>2.5</sub> H <sub>0.5</sub> PW	2.2	119	15.5
Cs <sub>3</sub> PW	2.7	72	17.0

<sup>a</sup> Determined from ICP-MS.

### Conclusions

Spectroscopic methods have led to a better understanding of the behavior of HPW and its cesium salts. For HPW, the large number of sites (0.24 mmol g<sup>-1</sup>) found by titration with pyridine compared to the number of surface protons (0.008 mmol g<sup>-1</sup>) demonstrates penetration of the solid by pyridine. XRD results confirm the opening of the lattice as pyridine absorbs on sites 1 and 2 of solid HPW. By comparing the Cal-Ad results to the crystal structure of HPW, the limitation that pyridine can only interact with every other plane of the HPW lattice was discovered. The proper thermal treatment of

the cesium derivatives was found to result in a homogenous solid as determined by  $^{31}\text{P}$  MAS NMR, in conflict with literature reports. The change in the isotropic  $^{31}\text{P}$  chemical shift with increasing cesium loading is probably due to a combination of electronic and structural changes due to the large size of this counter cation.



## CHAPTER 4

### THE ACIDITY AND ACTIVITY OF TWO SULFATED SILICA GELS

The activity of a solid acid catalyst is proportional to its acidity.<sup>3,148-150</sup> A more acidic solid is generally able to catalyze a reaction faster than a weaker solid or at a lower temperature. However, there is a minimum acidity that is necessary to drive any catalytic pathway. For the production of methyl *t*-butyl ether (MTBE) from methanol (MeOH) and *t*-butanol an acid which is both capable of dehydrating *t*-butanol to isobutene and then alkylating it with methanol is necessary.<sup>149</sup> Until, recently, MTBE was considered a safe oxygenate to help increase the octane number of automobile fuel.<sup>15,150</sup> The dehydration of tertiary butanol occurs on fairly weak acids with the coupling reaction to MTBE occurring under more rigorous conditions. The dehydrative coupling of two methanols to form dimethyl ether occurs under very acidic conditions. This reaction system gives an ideal handle for an activity test measure of acidity. A stream of methanol and *t*-butanol can be exposed to a surface and the products can be utilized to measure the current acidity of the solid (Figure 4-1). If the products are monitored as a function of time, then the acidic lifecycle of a catalyst can be determined.

The reaction mechanism for the production of MTBE (Figure 4-2) starts with the dehydration of *t*-butanol to isobutene.<sup>149</sup> The isobutene can then be protonated to form the *t*-butyl cation, and the electrophilic central carbon is then attacked by a MeOH. Loss of a proton returns the acid site to the initial condition and allows the MTBE to diffuse

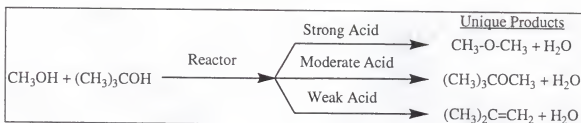


Figure 4-1. The effect of solid acidity on the reaction of tertiary butanol with methanol. Strong acids can catalyze the formation of dimethyl ether, while moderate strength solids produce MTBE, and the weakest solid can only dehydrate *t*-butanol.

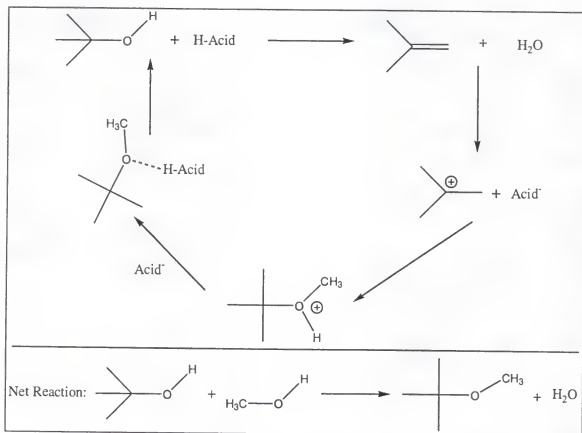


Figure 4-2. The mechanism for the catalytic production of MTBE from methanol and *t*-butanol.

away. The production of dimethyl ether is the most prominent side reaction.<sup>4</sup> The mechanism for this dehydration reaction is very similar to the production of MTBE; however, there is no initial dehydration step. The first step is the protonation of the methanol to form an oxonium ion (Figure 4-3). The oxonium ion is intimately associated with the acid site. A second methanol can then approach and in a concerted reaction a water molecule is produced and the ether linkage is formed. Transfer of a proton back to the acid site allows the dimethyl ether to diffuse away from the surface.

The current process for the synthesis of MTBE is the alkylation of isobutene by methanol carried out over a sulfonic acid resin, Amberlyst 15.<sup>150</sup> Tertiary butanol cannot be used in place of isobutene with this system as the water produced reduces the acidity of the solid (requiring higher temperatures) and eventually leads to deactivation of the surface and corrosion of the reactor.<sup>5</sup> An efficient process for producing MTBE from alcohol feed stock was devised by Nicolaides *et al.*<sup>149</sup> Nicolaides *et al.* used isobutyl alcohol in their feed in stead of *t*-butanol or isobutene. Due to the association of the protonated isobutyl alcohol with the acid site, the methanol was forced to attack the primary carbon producing methyl isobutyl ether (MIBE), an undesirable product. It was discovered that two separate catalyst beds were necessary to produce MTBE from this system. If the isobutanol is first dehydrated to isobutene over one catalyst and then alkylated with methanol by a second, the primary product was MTBE. The shift in product specificity is due to the location of the carbocation of isobutene at the central carbon. Methanol attack at the central carbon results in production of MTBE (Figure 4-4).



Deactivation of a catalyst can occur in many ways. In the presence of acid sites, alkenes can polymerize and block the surface from interaction with reactants. The common method used to remove the polymer and other carbonaceous deactivators include dissolving them in organic solvents or burning them off in an oxygen stream at elevated temperatures. A second, more disastrous deactivation pathway occurs through the loss of the acid site. Sintering of a mixed metal oxide results in loss of surface homogeneity and the properties that resulted in the acidity of the solid, metal A in close proximity to metal B, are lost. Dealumination of a zeolite catalyst is a special type of sintering that results in the loss of the internal acid sites of the solid and the creation of weaker alumina sites. For catalysts which rely upon sulfate groups hydrolysis of the sulfate linkage to the surface by water (Figure 4-5) results in the production of sulfuric acid which is lost from the surface and is a corrosion problem.<sup>15</sup> In the MTBE reaction, all of the reaction pathways result in the production of water, which makes this system ideal for studying the loss of sulfate functionality from an acid surface.

Two solid acids that derive their acidity from surface sulfate groups have been developed and characterized. These solids have had their acidity tested by both calorimetric and activity tests. They both have been found to be of similar acid strength. It was discovered that inclusion of the sulfate group into the silica lattice increases the life span of the catalyst without sacrificing acidity.

### Experimental

#### Preparation of the Catalysts

The bridging sulfate catalyst (BSC) was prepared by mixing 23 ml diethyl sulfate with 30 ml tetraethyl ortho silicate in a Teflon container (The synthesis procedure was

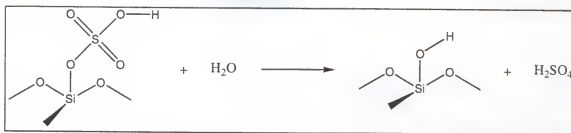


Figure 4-5. Hydrolysis of a tethered sulfate group from a surface. The sulfuric acid produced is swept out of the reactor by the carrier gas.

devised by John Michael McGilvray<sup>151</sup> who also supplied the bulk of the BSC sample). Ethanol was added and the solution was stirred for twenty minutes. The solution was diluted with 20 ml of deionized water, followed by the addition of ~0.1 ml of sulfuric acid. The Teflon container was sealed in an autoclave and heated at 80 °C for five days. The resulting gel was crushed and heated in a tube furnace, under flowing air, at 400 °C for three days.<sup>151</sup> These conditions were reported to remove any residual organic compounds, water, and sulfuric acid.

The tethered sulfate catalyst (TSC) was prepared by washing acid and peroxide treated silica gel with 1M sulfuric acid. The catalyst was heated to 200 °C before use.

### Activity Tests

Activity tests were performed in a gas flow reactor with 0.5 g of catalyst. Glass beads were packed over the catalyst bed to vaporize the incoming liquid reactants. Dry nitrogen was used as the carrier gas with flow rates of 5 ml min<sup>-1</sup>. The addition of reactants was accomplished with the use of a syringe pump. The liquid alcohols were vaporized on the hot glass beads then carried through the catalyst bed. Temperature control was accomplished by monitoring the temperature of the catalyst bed with a K

type thermocouple. The thermocouple was attached to an Omega Temperature Control unit that regulated the bed temperature to 150 °C unless otherwise noted.

Additional tests were performed in a glass bomb reactor. These were prepared by loading 0.5 g of catalyst into a 250 ml bomb reactor. A solution of methanol and *t*-butanol was then poured into the bomb. The bomb was then sealed and placed into an oil bath operating at either room temperature or 50 °C.

### Calorimetry

Calorimetry was performed on TSC by slurring 1.0 g of the solid into 100 ml of anhydrous cyclohexane. The solution was titrated with a 0.10 M or 0.18 M pyridine in anhydrous cyclohexane solution. Cal-Ad experiments were performed on BSC by John Michael McGilvray.<sup>151</sup>

All analyses were performed on a Hewlett Packard Model 5890 gas chromatograph operating at 70 °C equipped with an FID detector and a Hewlett Packard HP3394 Integrator. The retention times of several compounds under these conditions can be found in Table 4-1. The effluent gases were sampled with a gas-tight syringe. Infrared spectra of the catalysts were obtained using a KBr pellet on a Nicolet 5PC FTIR.

Surface area and pore volume measurements were performed on a Micromeritics ASAP 2000.<sup>151</sup>

## Results and Discussion

### The Acidity of the Solids

The TSC solid was characterized by pyridine adsorption slurry calorimetry. This solid can be classified as a moderate strength solid acid, with acidity that is slightly less than zeolite HZSM-5. The Cal-Ad procedure was used to characterize BSC (Table 4-

Table 4-1. Retention time of several alcohols and ethers.

Compound	Retention Time (min)
dimethyl ether	3.42
Methanol	5.12
<i>t</i> -butanol	7.07
MTBE	10.42
MIBE	11.5

2).<sup>151</sup> BSC was found to be slightly less acidic than TSC. However, the small difference in acidity (4 kcal mol<sup>-1</sup>) is not likely to be of great significance unless the acidic threshold--the minimum acidity required to drive a reaction--occurs in this range. Porosimetry was performed, with the TSC having a surface area of 240 m<sup>2</sup>/g and BSC having a surface area of 540 m<sup>2</sup>/g.

#### Results of the Activity Tests

Further testing of the catalysts began with a simple test to determine their stability. Three containers containing identical *t*-butanol/methanol solutions were set up. TSC was placed in one of the containers, BSC in the second, and a small amount of sulfuric acid was placed in the last. One hour was allowed for the reactions to progress, and then the solutions were analyzed by GC. All three catalysts had the same products and product distributions, notably an excess of methyl iso-butyl ether. Leaching of the sulfate functionality by water in the solvents to form sulfuric acid caused the identical results for all three systems. More reactions were undertaken using dry solvents and sealed from the atmosphere by using a bomb reactor. Results were significantly different



Table 4-2. The acidity of two sulfated catalysts measured by calorimetry.

Catalyst	$n_1$ (mmol g <sup>-1</sup> )	$-\Delta H_1$ (kcal mol <sup>-1</sup> )	$n_2$ (mmol g <sup>-1</sup> )	$-\Delta H_2$ (kcal mol <sup>-1</sup> )
TSC <sup>a</sup>	0.2	32	0.7	17
BSC <sup>b</sup>	0.1	28.5	0.9	17

<sup>a</sup> Pyridine adsorption slurry calorimetry in cyclohexane.

<sup>b</sup> Cal-Ad results from J. M. McGilvray (151).

from the wet reactions or the sulfuric acid standard, primarily producing MTBE and isobutene with maximum conversion of methanol.

More ambitious testing of the catalysts was performed in the gas phase. The product of the reaction of a methanol and *t*-butanol stream is strongly dependent on the acidity of the catalyst used. Strong acids are capable of dehydratively coupling methanol to form dimethyl ether and water. Acids of fairly weak to moderate strength dehydrate the alcohols to form MTBE. Weak acids are capable of dehydrating *t*-butanol to form isobutene.

Tests using this alcohol system were performed using various ratios of methanol/*t*-butanol at 150°C in a flow reactor unless otherwise noted. Initial testing began with 10% (mol/mol) methanol in *t*-butanol. TSC converted all of the methanol to MTBE and MIBE and 95% of the remaining *t*-butanol to isobutene. The catalyst lasted for twenty hours before losing activity and was dead by fifty hours (Figure 4-6). The rapid deactivation of this catalyst was probably due to loss of the sulfate moiety as sulfuric acid. BSC showed complete conversion of the methanol to MTBE with high selectivity (MTBE/MIBE>20) and nearly complete conversion of *t*-butanol to isobutene.

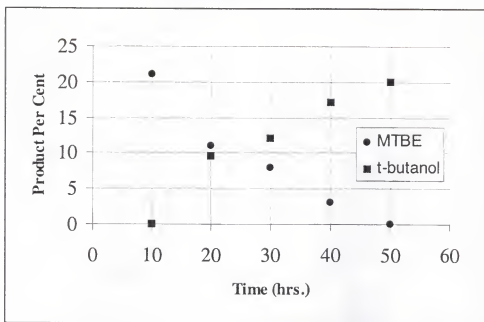


Figure 4-6. Amount of MTBE and *t*-butanol in the product stream from TSC over the life span of the catalyst.

The initially high activity dropped off slowly starting at fifteen hours but was still producing a significant amount of MTBE at 120 hours (Figure 4-7).

MTBE forms an undesirable azeotrope with both *t*-butanol and methanol. In an attempt to find out if we could avoid formation of the azeotrope, we tried to determine if BSC could stoichiometrically convert methanol and *t*-butanol to MTBE and/or isobutene. A 50% (mol/mol) methanol in *t*-butanol solution was prepared from solvents dried over 4Å molecular sieves (only excess water was eliminated; water is produced by the reaction). Initial results showed 100% conversion of *t*-butanol to isobutene, and 25% conversion of methanol to dimethyl ether. After four hours, the reactants began to be converted to MIBE. After seven hours, MTBE production was observed. MTBE production plateaued at 10% of the products. Greater than 20% conversion of methanol was achieved with 100% conversion of *t*-butanol (>80% selectivity to isobutene). Small

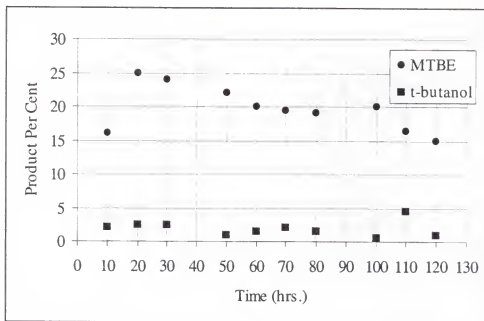


Figure 4-7. Amount of MTBE and *t*-butanol in the product stream from BSC over the life span of the catalyst.

amounts of water were added to attempt to force the *t*-butanol dehydration equilibrium towards *t*-butanol, but little effect was observed. A similar activation pattern was observed for TSC.

The products produced by the catalyst allow us insight into how the catalyst changes during the reaction (Figure 4-8). Both catalysts start very acidic, producing dimethyl ether for the first few hours of reaction. The catalysts then begin to lose acidity as can be seen by the production of methyl isobutyl ether. The production of methyl isobutyl ether from *t*-butanol or isobutene requires a strong enough acid to stabilize a primary carbocation. As the acidity continues to decrease, we see MTBE production begin. Isobutene and MTBE are the primary products of both catalysts during the middle

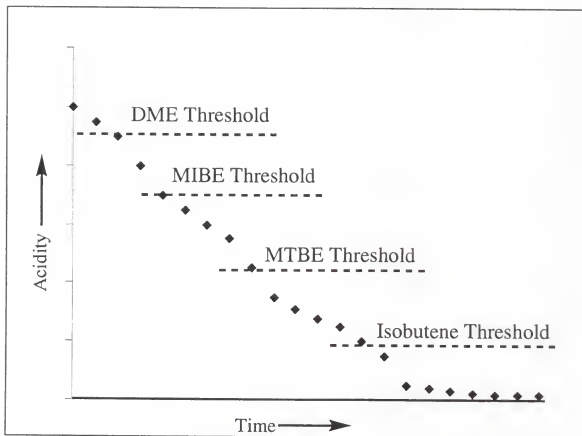


Figure 4-8. The products of the reaction change as the acidity of the catalyst deteriorates. At the start of the reaction the catalysts are strong enough to produce dimethyl ether. However, the acidity quickly deteriorates to the point where MIBE production begins. As the reaction continues, MTBE production begins and MIBE production fades. Finally, the solid can no longer catalyze MTBE formation and only isobutene is observed.

portion of their lifetimes. The TSC, however, quickly begins to lose activity. Soon this solid can no longer catalyze the production of MTBE. The BSC catalyst loses its activity toward this reaction much more slowly.

#### Threshold Acidity for Heptane Isomerization

Both catalysts were used to isomerize *n*-heptane. The small difference in acidity between the two solids resulted in different product streams. The TSC catalyst was found to have no activity towards isomerization, while the BSC was found to have a small activity toward *n*-heptane isomerization. From these two observations the threshold acidity for heptane isomerization can be said to be slightly less than the BSC catalyst, or  $-32.5 \text{ kcal mol}^{-1}$  measured by pyridine adsorption slurry calorimetry.

#### Structure of the Solids

The structure of the acid site of the two solids is very different. Fourier transform IR of both catalysts shows a distinct difference in the nature of the bonding about the sulfate group. The BSC solid was shown to be a bridging group by the presence of the characteristic band at  $1057 \text{ cm}^{-1}$ ,<sup>151,152</sup> while the TSC lacks this band. The stability of BSC over TSC is due to this structural difference. The bridging sulfate group of the BSC catalyst results in a more stable sulfate moiety. A double hydrolysis reaction must occur to remove this sulfate from the solid, and a longer life span is to be expected.

#### Conclusion

Further research into obtaining a wide range of solids of varying acidity is required. They are important for the further discovery of threshold and optimum acidities. The methanol/*t*-butanol system is offered as a new system for characterization of solid acidity. Monitoring the products is a good method for determining the overall

strength of the catalyst and may give insight on how that catalyst deactivates. Further study with other acids may prove this system to be a general method for broad classification of acids.

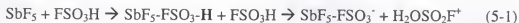
The structure of solid acids has been shown to be of great importance. The stability of the bridging sulfate catalyst (BSC) when compared to the very similar tethered sulfate catalyst (TSC) is impressive. Stabilization of future catalysts may use this incorporation system to improve lifetime and increase resilience.

## CHAPTER 5

### A NEW SOLID SUPER ACID: SILICA SUPPORTED ANTIMONY PENTACHLORIDE

Conventional strong acids can be used as inspiration for new strong solid acids. For example, Drago *et al.* supported aluminum chloride, a conventional strong Lewis acid, on a silanol rich silica gel, a Brønsted acid, to produce a solid that was significantly stronger than either component alone.<sup>154-155</sup> However, their goal was not to form a solid with Lewis acid sites, but instead to form an even more powerful Brønsted acid. The interaction of a powerful Lewis acid with a Brønsted acid leads to the enhancement of the acidity of the Brønsted site.<sup>156,157</sup> In the case of Drago's catalyst, the interaction between the unsaturated aluminum center with the oxygen of a silanol promoted the acidity of the solid such that it can be labeled as a solid super acid (Figure 5-1).<sup>39</sup>

The ability of a Lewis acid to enhance the acidity of a Brønsted acid is due to the inductive effect. The coordination of the Lewis acid to the Brønsted site leads to a further reduction in electron density at the proton. The net effect is the weakening of the O-H bond, and in extreme cases, the protonation of the Brønsted acid occurs. In the case of Magic Acid, antimony pentafluoride in fluorosulfonic acid, the super acid formed is capable of protonating fluorosulfonic acid (Equation 5-1):



The protonated fluorosulfonic acid is then capable of forming carbonium ions from hydrocarbons.

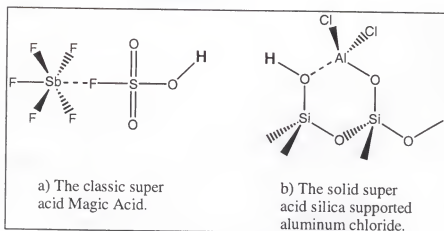


Figure 5-1. Examples of super acids. A super acid is formed, primarily, through the interaction of a strong Brønsted acid with a strong Lewis acid. a) Antimony pentafluoride in fluorosulfonic acid, a classic super acid. b) The solid super acid silica supported aluminum chloride.

Since super acids are capable of protonating alkanes to form carbonium ions, they are ideal for performing certain petroleum reforming reactions.<sup>148</sup> The alkylation of isobutane and butane to higher molecular weight hydrocarbons is important for creating a value-added product from these materials. The mechanism (Figure 5-2) for this reaction begins with an initiation step. The isobutene present in the stream is protonated by a strong Brønsted acid forming the *t*-butyl cation. The *t*-butyl cation can then interact with another isobutene to form a variety  $C_8$  carbocations. These carbocations then abstract a hydride from isobutane to produce another *t*-butyl cation continuing the catalytic cycle. Side reactions that occur include isomerization, polymerization, cracking, and disproportionation. Isomerization of the  $C_8$  carbocations to a more stable form may occur before hydride abstraction. Polymerization occurs if the  $C_8$  carbocations comes into contact with an alkene, thus the concentration of the alkene must be kept high enough to initiate and sustain the alkylation reaction, but low enough to prevent polymerization



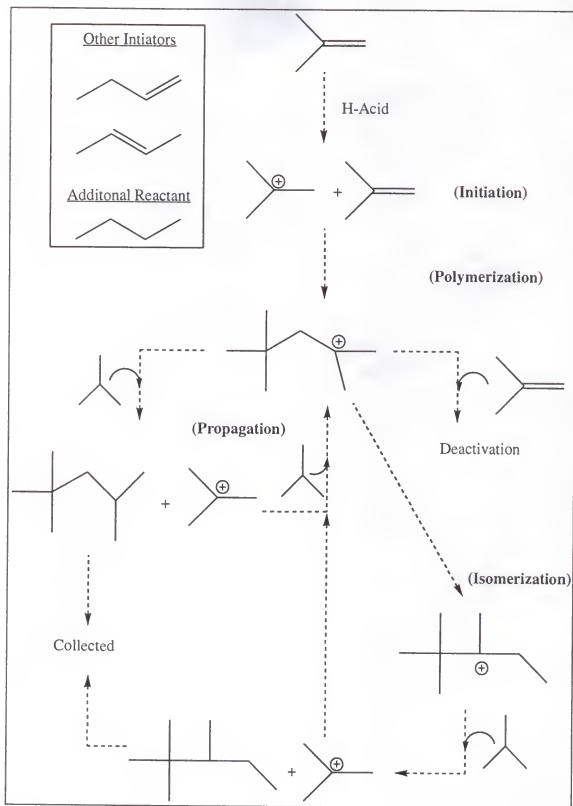
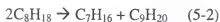


Figure 5-2. The reaction mechanism for the alkylation of isobutane to octane. The catalyst is deactivated by the build up of polymer on its surface.

which leads to catalyst deactivation. Disproportionation is a bimolecular interaction that results in one hydrocarbon abstracting a methyl group from another hydrocarbon (Equation 5-2). Cracking of a hydrocarbon results in two smaller fragments, one of which is an alkene (Equation 5-3).



The activity of a catalyst towards each of these reactions is related to its acidity. The more acidic the solid the lower the temperature it can carry out each reaction. By comparing two (or more) catalysts at the same temperature, the relative acidity can be found by comparing the activity. Strong catalysts, such as Drago's aluminum chloride catalyst, can perform alkylations (little or no cracking, isomerization, or disproportionation) with high selectivity at 0 °C.

The growing importance of solid acid catalysis and the correlation of activity with acidity has lead to a surge in the development of new, strong solid acid catalysts. A new solid acid that uses antimony pentachloride as an acidity promoter has been developed. The acidity of this catalyst has been measured through a new method (reported in Chapter 2). The synthesis and characterization of this new solid super acid will be reported. The acidity and activity of this solid will be shown to be greater than that of Drago's silica supported aluminum chloride catalyst.

## Experimental

### Materials

Davisil silica gel (mesh 100-200, surface area  $250 \text{ m}^2 \text{ g}^{-1}$ ) was purchased from Aldrich. It was washed with 1M HCl three times (about 20 ml 1M HCl per 10 grams silica gel), then with deionized water three times, followed by a 35% hydrogen peroxide wash three times, and finally several washes with deionized water before drying it in an oven at  $140^\circ\text{C}$  overnight. The silica gel was removed from the oven and allowed to adsorb water from the atmosphere for 24 hrs.

### Synthesis of the Catalyst

The catalyst is prepared by slurring silica gel in dry chloroform (carbon tetrachloride or methylene chloride can be used, but the best results were obtained with chloroform). The slurry is heated to  $35^\circ\text{C}$  with stirring under a slowly flowing  $\text{N}_2$  atmosphere. Enough  $\text{SbCl}_5$  (Aldrich) was added to make  $0.5 \text{ mmol SbCl}_5 (\text{g}^{-1} \text{ SiO}_2)$ . This was accomplished by loading a syringe with  $\text{SbCl}_5$  (98%, Aldrich) in a dry box. The syringe was capped and removed from the  $\text{N}_2$  glove box.  $\text{SbCl}_5$  was added dropwise into the slurry by injection through a septum. The solution immediately turned brown. Passing the  $\text{N}_2$  purge gas through a water bubbler collects the HCl gas produced during the reaction. Titration of the water trap with  $0.0469 \text{ M NaOH}$  shows that  $1.8 \pm 0.1 \text{ mol HCl}$  was produced for every mol of  $\text{SbCl}_5$  reacted. Substituting  $\text{PCl}_5$  for  $\text{SbCl}_5$  produced the phosphorus analog.

### Activity Tests

Alkylation reactions were performed in a glass batch reactor by loading, in an inert atmosphere glove box, one gram of each solid into a separate 250 ml glass reactor

bomb. The pressure head was attached before removing the assembly from the box. The bomb was cooled in a dry ice/acetone bath (after sealing and removing from the glove box). Butane was condensed (10 ml) into the bomb, followed by 0.2 ml of isobutene. The isobutene is necessary as an initiator, however excess isobutene will polymerize and deactivate the catalyst by covering the surface with a polymer. The system was removed from the dry ice/acetone bath and placed in an ice water bath. The reaction was then allowed to proceed for thirty minutes. At that point the products were filtered off, 2 ml of *n*-pentane was added as an internal standard, and the residual butane and isobutene were allowed to boil off.

#### Analysis

Analysis of the reaction products were performed on a Hewlett Packard 5890 Gas Chromatograph equipped with a FID detector and a Hewlett Packard HP3394 Integrator. A temperature ramp was used to separate the products of the reaction:

- 1) Initial Temperature 35°C.
- 2) Initial time 10 minutes.
- 3) Increase by 5 °C min<sup>-1</sup> to 200°C
- 4) Hold at 200 °C for 10 minutes.

The retention time of various standards can be found in Table 5-1.

The solid state NMR experiments were described in Chapter 2. The sample was prepared and loaded into the rotor in an inert atmosphere glove box.

#### Calorimetry

The procedure used to perform calorimetry is standard and was described in Chapter 1. The highest heats of interaction were observed when a small amount of

Table 5-1. Retention times of various hydrocarbon families.

Family	Retention Time (min)
Butanes	6.92
Isobutene	5.35
Pentanes <sup>a</sup>	12.52
Hexanes	20
Heptanes	27
Octanes	32
Nonanes	38

<sup>a</sup> Internal standard.

carbon tetrachloride was used to wet the solid prior to removing it from the glove box. The  $\text{CCl}_4$  serves to protect the solid from moisture that will enter the calorimetry cell during the period between removing the cell from the glove box and covering the sample with anhydrous cyclohexane. Antimony pentachloride is very halophilic and covering the solid with  $\text{CCl}_4$  protects the solid from reacting with atmospheric water. The  $\text{CCl}_4$  occupies the open coordination site on the antimony center preventing hydrolysis. However, the interaction is very weak and the  $\text{CCl}_4$  dissolves into the cyclohexane solvent. The coordination of the  $\text{CCl}_4$  results in a dark brown solid that turns to a light brown when slurried in cyclohexane (the color of the unreacted solid). Titration with pyridine results in the formation of a coordination compound. The resulting solid is bright purple and is air stable  $[(\text{silica-gel})_n\text{Sb}^{\text{V}}\text{Cl}_3\text{-pyridine}]$ .

### Results and Discussion

From Drago's work, it is already known that the acidity of silica gel is susceptible to enhancement through the coordination of a strong Lewis acid.<sup>39,153,156</sup> However, aluminum chloride is not the strongest Lewis acid that can be used. Other, stronger, Lewis acids may also be used to enhance the acidity to a larger extent. An estimate of the strength of such a solid can be qualitatively obtained through the ECW model.

The ECW method is a two-parameter scale that separates the total interaction of two molecules into electrostatic (E) and covalent (C) terms. The E parameter is a measure of the propensity of a molecule to form acid-base bonds that are ionic in nature. The C parameter measures the propensity of a molecule to form covalent acid-base bond. The E and C parameters of both the acid and the base are combined in the Drago equation (Equation 5-4) to predict the total strength of the interaction.

$$\text{Bond Strength} = \Delta\chi = E_a E_b + C_a C_b \quad (5-4)$$

Where  $\Delta\chi$  is a measure of the acidity (calorimetry, IR or NMR shifts, Acceptor Numbers, etc.). When  $\Delta\chi$  is an enthalpy of interaction,  $E_b$  and  $C_b$  are used. When  $\Delta\chi$  is from a spectroscopic measure,  $E_b^*$  and  $C_b^*$  are used to designate that a conversion factor is included in these parameters (if the acid is the probe then reverse notation is used). From inspection, it can be seen that a donor (b) with a high  $C_b/E_b$  ratio will not have a large interaction with an acceptor (a) with a low  $C_a/E_a$  ratio (Table 5-2). (For a thorough review of ECW theory see Reference 122.)

Since the super-acid interaction is really an acid-base reaction between a Lewis acid and a lone pair of electrons on the Brønsted acid, the strength of that interaction will be proportional to the acidity enhancement. For a given solid, such as Drago's silica gel

Table 5-2. The ECW model can be used to predict the strength of donor-acceptor interactions.

Reaction	Acceptor			Donor			$E_a E_b + C_a C_b$
	$E_a$	$C_a$	$C_a/E_a$	$E_b$	$C_b$	$C_b/E_b$	$-\Delta H$ (kcal mol <sup>-1</sup> )
$\text{Al}(\text{CH}_3)_3 + \text{CH}_3\text{Cl}$	8.66	3.68	0.47	2.54	0.10	0.04	22.4
$\text{SbCl}_5 + \text{CH}_3\text{Cl}$	3.64	10.42	2.9	2.54	0.10	0.04	10.28
$\text{Al}(\text{CH}_3)_3 + \text{NH}_3$	8.66	3.68	0.47	2.31	2.04	0.88	27.5
$\text{SbCl}_5 + \text{NH}_3$	3.64	10.42	2.9	2.31	2.04	0.88	29.7
$\text{Al}(\text{CH}_3)_3 + \text{pyridine}$	8.66	3.68	0.47	1.78	3.54	2.0	28.4
$\text{SbCl}_5 + \text{pyridine}$	3.64	10.42	2.9	1.78	3.54	2.0	43.4

catalyst, the  $C_b$  and  $E_b$  parameters of the silanols on the surface will remain constant as the acid is changed. The  $C_b/E_b$  ratio of a silanol has never been measured, however, the  $C_a/E_a$  has been measured to be 1.04, and if the trend observed for alcohols can be extended to silanols, the  $C_b/E_b$  can be assumed to be greater than 1.<sup>74</sup> If this assumption is correct then substituting a Lewis acid with a higher  $C_a$  value than aluminum chloride will result in a significantly stronger solid, provided that the  $E_a$  values are similar. A list of the  $E_a$  and  $C_a$  parameters for several solid acids are presented in Table (5-3). Under these limitations ( $C_b/E_b > 1$  for silanols), the strongest acid by far is antimony pentachloride. The interaction between the silanol and the Lewis center will be maximized and the inductive effect, that leads to super acid character, will be larger than for the aluminum chloride catalyst (assuming that the acidity of  $\text{AlCl}_3$  is not tremendously greater than  $\text{Al}(\text{CH}_3)_3$ ). This phenomenon is observed in the heat of

Table 5-3.  $E_a$  and  $C_a$  parameters for a variety of Lewis acids.

Acid	$E_a$	$C_a$
$Al(CH_3)_3$	8.66	3.68
$Ga(CH_3)_3$	6.95	1.48
$BF_3$	6.10	2.87
$SbCl_5$	3.64	10.42

interaction of the two catalysts. The estimated enhancement when employing antimony pentachloride in place of aluminum chloride is strongly dependent on the ratio of  $C_b/E_b$  for the silanols (Equation 5-5):

$$\text{Enhancement} = (E_{a,Sb} + C_{a,Sb}C_b/E_b)/(E_{a,Al} + C_{a,Al}C_b/E_b) \quad (5-5)$$

The value of  $C_b/E_b$  in equation 5-5 is between 1.1 and 1.4. By using  $E_a$  and  $C_a$  parameters for monomeric aluminum chloride of 10 and 3.5 respectively, the enhancement varies between 1.1 and 1.22. Through both calorimetry and the change in chemical shift of triethylphosphine oxide the enhancement observed is 1.28 which is a good approximation of the theoretical range considering all of the assumptions necessary (the  $C_b/E_b$  for silanols and the estimate of the  $E_a$  and  $C_a$  parameters for monomeric aluminum chloride).

#### Characterization of the New Solid

Investigation of the solid via FTIR spectroscopy of adsorbed pyridine resulted in the classification of this sample as both a Brønsted and Lewis acid (Figure 5-3).<sup>124</sup> A list of the peaks and their assignments can be found in Table 5-4. A calorimetric



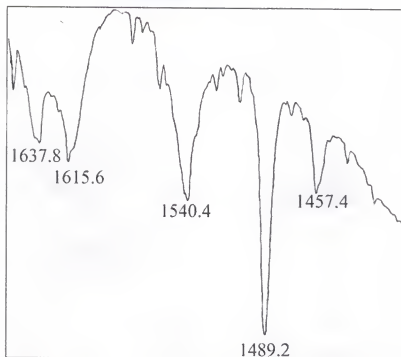


Figure 5-3. The FTIR of pyridine on  $(\text{silica gel})_n\text{Sb}^{\text{V}}\text{Cl}_3$ . The peaks can be used to assign this solid as both a Brønsted and a Lewis acid.

Table 5-4. Assignment of the FTIR peaks of adsorbed pyridine on  $(\text{silica gel})_n\text{Sb}^{\text{V}}\text{Cl}_3$ .

Peak ( $\text{cm}^{-1}$ )	Assignment
1457	Lewis Site
1489	Brønsted or Lewis
1540	Brønsted Site
1652	Lewis Site
1638	Brønsted Site

investigation of the acidity was performed using pyridine as the adsorbent probe. The solid was slurried in cyclohexane and exposed to small doses of pyridine. The heat of interaction was converted to a concentration dependant enthalpy of interaction. The plot of the enthalpy against the amount of total pyridine added results in a titration curve that shows four acid sites (Figure 5-4). The heats of interaction for each of these sites is -65.5, -48, -31, and  $-22 \pm 1.5 \text{ kcal mol}^{-1}$ . The  $^{31}\text{P}$  MAS NMR technique presented in Chapter 2 was also used to characterize this solid. It was found that there were four different acid sites with  $\Delta\delta$  values of 66, 48, 36.4 and 22.6 ppm. The correlation between the acidity measured for these sites using both methods was excellent,  $r^2 = 0.9778$ . The low population of the first two sites was also observed in the  $^{31}\text{P}$  MAS NMR of chemisorbed triethylphosphine oxide. Exposure of the solid to any amount of water resulted in a loss of the first acid site. A calorimetric titration was performed on a solid that had been briefly exposed to the atmosphere prior to formation of the slurry. The curve shows a complete loss of the strong acid site observed when the surface was protected from water. Additional exposure to water leads to the destruction of the remaining acid sites.

#### Activity Tests

In addition to the calorimetric and spectroscopic methods, this solid was tested against a benchmark activity test. The alkylation of butane to octane is an important process. This reaction converts low value butane into octane, a value-added product. Strong solid acids are necessary to catalyze this transformation at low temperatures, so the activity of a solid can be compared to other solid acids by measuring reactivity at a given temperature. In previous work, the acidity and activity of  $(\text{silica-gel})_n\text{Al}^{\text{III}}\text{Cl}_2$ , has

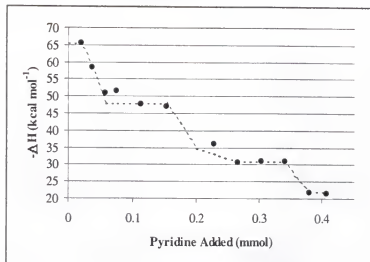


Figure 5-4. Titration of (silica gel)<sub>n</sub>Sb<sup>V</sup>Cl<sub>3</sub> with pyridine in cyclohexane. The four acid sites of this catalyst can be observed with slurry calorimetry. Exposure to water results in the loss of the strongest site.

been used to characterized this solid as a super acid.<sup>75,118,153,154</sup> The Cal-Ad results for this solid have shown that the strong acid site has an enthalpy of interaction with pyridine in a cyclohexane slurry of -51 kcal/mol acid.<sup>75</sup> This is significantly less than the antimony solid because of the smaller covalent acidity of aluminum chloride. Comparison of the activity of these two solid acids will make it possible to determine if the acidity determined by calorimetry and TEPO is a true measure of the acidity of this solid.

The antimony catalyst was run side by side with the aluminum catalyst. The results of the two reactions have been summarized in Table 5-5. The aluminum catalyst produced a large amount of octane isomers with high conversion and selectivity. The antimony catalyst produced almost no octanes, but a variety of lower molecular weight hydrocarbons were observed.

Table 5-5. The results of alkylation reactions with silica supported antimony pentachloride and aluminum chloride.

	% Conversion (silica gel) <sub>n</sub> Al <sup>III</sup> Cl <sub>3</sub>	% Conversion (silica gel) <sub>n</sub> Sb <sup>V</sup> Cl <sub>5</sub>
Cracked	< 5%	>95%
Alkylated	>95%	Trace
Disproportionated	Trace	1.1

The production of lower molecular weight hydrocarbons is possible only if the catalyst first alkylates the butane to octane. The catalyst then cracks the octane to smaller mass hydrocarbons in the same amount of time that the aluminum catalyst produced only octane isomers.

The cracking of octane by this catalyst was also observed in the gas phase. For these reactions the catalyst was placed in a flow reactor similar to the one designed in Chapter 4, and dry octane was fed into a nitrogen carrier stream. The catalyst was maintained at room temperature. The results of this reaction showed that at low flow rates the primary reaction is the cracking of octane to lower molecular weight hydrocarbons with little disproportionation or isomerization observed. When the octane was replaced with heptane, the primary reaction was isomerization with smaller amounts of cracking.

#### The Structure of the Acid Sites

The acid sites are probably a mixture of Brønsted coordinated antimony (V) trichloride and uncoordinated antimony (V) trichloride. The strongest sites are Brønsted in nature, as these are required to perform alkylation and cracking reactions (Figure 5-5).

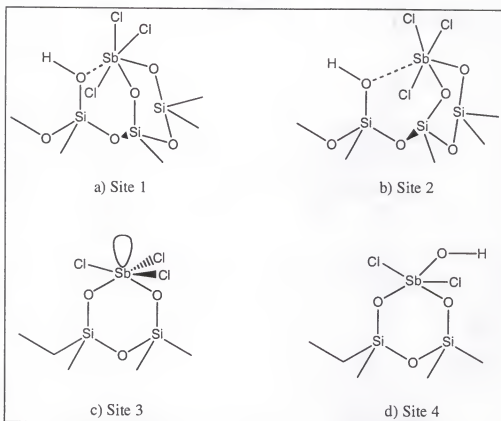


Figure 5-5. The proposed acid sites of  $(\text{silica gel})_n\text{Sb}^{\text{V}}\text{Cl}_3$ . a) The strongest site has excellent overlap between the silanol and the antimony. b) The second site is structurally similar to the first; however, due to poorer overlap, the enhancement of the Brønsted acidity is not as good. c) and d) The weakest sites are due to antimony (V) Lewis sites with varying amounts of ligating chlorine atoms.

The weaker sites are probably more akin to tethered antimony pentachloride, or perhaps antimony trichloride oxide. The proposed nature of the strong acid site is a good overlap between the open orbital on the antimony with the silanol, while the second site has a poorer overlap between the two orbitals. The third site is simply a tethered antimony (V) Lewis site, while the weakest site is a bound Lewis site with a hydroxyl or oxide in place of one or two of the chlorine ligands.

Experiments performed on  $(\text{silica gel})_n\text{P}^{\text{V}}\text{Cl}_3$  showed that this catalyst is much weaker than the antimony or aluminum chloride analog. This catalyst was not acidic enough to catalyze the alkylation of isobutane.

### Conclusion

The application of the ECW model to the promotion of Brønsted acidity with Lewis acids led to the synthesis of a new solid super acid. The acidity of this solid was determined through pyridine adsorption calorimetry,  $^{31}\text{P}$  MAS NMR of chemisorbed TEPO, and activity tests. This new solid is stronger than silica supported aluminum chloride as measured by these tests. Fourier transform IR spectroscopy was used to demonstrate that this solid possesses both Brønsted and Lewis type acid sites. These acid sites are a combination of super-acid like silanol-antimony adducts and open antimony (V) chloride Lewis centers. The high acidity of this catalyst results in high reactivity towards the base, water. Coordination of a water molecule results in irreversible hydrolysis of the antimony-chloride bonds.

## CHAPTER 6

### GENERAL CONCLUSIONS

The understanding of solid acid catalyzed reactions is limited by the techniques employed to characterize the acidity of the solids. Current analysis methods are often cumbersome, time intensive, and difficult to interpret. The work presented in this dissertation is an attempt to improve the general understanding of the role of solid acidity upon catalysis.

The work presented in Chapter 2 is a new and fast method for determining the overall strength of a solid acid. The change in chemical shift of triethylphosphine oxide was measured on a variety of solid acids. It was found to be an excellent indicator of the acid strength of a solid. The experimental conditions allowed for an estimate of the static acidity of a solid, that is the acidity a molecule experiences while adsorbed on the acid site. A comparison of this method to a differential technique allows for the identification of any energetic barriers to adsorption. Overall, this method was shown to be a new powerful tool for understanding the global acidity of a solid acid.

In Chapter 3, more spectroscopic tools were used to help qualify the acidity and nature of interaction of heteropoly acids. Heteropoly acids are a very important catalyst because of their strong acidity and additional ability to catalyze oxidation reactions. Techniques such as XRD, NMR, IR and calorimetry were used to determine that pyridine, an important probe molecule for investigating solid acidity, only penetrates the

even planes of the 12-tungstophosphoric (HPW) lattice. The acid sites, one strong site and one weak, were determined to be the face and edge centered protons in the lattice respectively. Pyridine initially penetrates the structure and coordinates to the face centered protons. The opening of the lattice by pyridine allows for more pyridine to penetrate along the fault plane. This additional pyridine interacts with the edge protons that are adjacent to the pyridinium ions formed in the first step. Solid state MAS NMR methods have shown that replacement of the protons at the edge of the Keggin unit has a significant effect on the chemical shift of the central phosphorus atom approximately 5 Å away. Magic angle spinning NMR was also used to demonstrate that proper pretreatment of the cesium salts ( $\text{Cs}_x\text{H}_{3-x}\text{PW}$ ) of HPW results in homogenous solids, as opposed to literature reports that claim that the salts are proportional mixtures of  $\text{H}_3\text{PW}$ ,  $\text{Cs}_2\text{HPW}$  and  $\text{Cs}_3\text{PW}$ .

The structure of a catalyst is important in another manner. The structure can help to stabilize the acid site, resulting in an increase in the lifetime of the catalyst during a reaction. This concept was demonstrated in Chapter 4 with the use of two sulfated silica gels. It was found that the stability of a bridging sulfate group toward deactivation by hydrolysis was much greater than the tethered sulfate group. The difference in stability can be observed in the test reaction that converts t-butanol and methanol to isobutene, methyl tertiary butyl ether (MTBE), and dimethyl ether (DME). The tethered catalyst was initially more efficient at producing the methyl *iso*-butyl ether (MIBE), MTBE and DME because of its slightly higher acid strength. However, the water produced in these reactions quickly hydrolyzed the sulfate linkage to the support resulting in the production of sulfuric acid, which was removed from the catalyst by the carrier gas. The stability of



the bridging sulfate group toward hydrolysis led to a five order of magnitude increase in life span over the tethered sulfate group, and its milder acidity resulted in a higher MTBE/MIBE ratio.

Chapter 5 combined spectroscopy, calorimetry and activity tests to study the new strong solid acid silica gel supported antimony (V) chloride. This solid was identified through the method describe in Chapter 2 to be an extremely powerful solid acid, which was confirmed through pyridine adsorption slurry calorimetry. Alkylation of isobutane with butane was used to compare the acidity of the new solid against a well known, less acid solid “super” acid (silica supported aluminum trichloride). The results of these tests show that the activity of the new solid is much greater than the standard acid.

Exploring the acidity of a solid acid is a very complex process that requires the use of many different tools. The interrelation of these tools lead to a greater understanding of the catalytic strength of a solid than any one method alone. This work has shown that the combination of a new spectroscopic method with other more traditional techniques can lead to an understanding of the way a molecule interacts with a surface. In addition, a new method for quickly screening the acidity of solid acids has been developed. This technique can be used to greatly reduce the amount of time necessary for developing solid acid catalyst, which will decrease the development time and costs of new catalyst. By combining the information obtained from several methods of characterization, the acidity of a solid, and the role that acidity plays in catalysis, can be fully understood.

## APPENDIX I

### THE BASIC THEORY OF SOLID STATE MAGIC ANGLE SPINNING NMR

#### The Fundamentals of NMR Spectroscopy

There are a large number of isotopes with nuclei that have nonzero nuclear angular momentum quantum numbers,  $I$ .<sup>157</sup> When each of these nuclei are placed in a magnetic field their nuclear magnetic vector can take on  $2I + 1$  orientations. For example, hydrogen-2, or deuterium, has  $I=1$ , therefore deuterium can have  $2(1)+1$ , or 3, orientations of its nuclear magnetic vector in a magnetic field. Each of these levels is labeled with the nuclear spin quantum number,  $m_I$ , which can have values of  $I, I-1, \dots, -I$ . Positive values of  $m_I$  align with the applied field while negative values align opposed to the field. For  $I=1/2$  nuclei  $m_I = -1/2$  is labeled  $\beta$  and  $m_I = +1/2$  is labeled  $\alpha$ . Figure A1-1 demonstrates the energy level diagrams of carbon-13 ( $I=1/2$ ) and nitrogen-14 ( $I=1$ ).

The energy of each level is given by Equation A1-1:<sup>158</sup>

$$E_{m_I} = -\gamma \hbar B m_I / 2\pi = -\mu_B \quad (\text{A1-1})$$

The small magnetic moment due to the excess  $\alpha$  spins,  $M$ , aligns with and precesses about the axis of the applied magnetic field. The frequency of the precession is proportional to the strength of the applied field,  $B_0$ , and the  $\gamma$  of the nucleus (Equation A1-2):

$$\omega_0 = \gamma B_0 \quad (\text{A1-2})$$

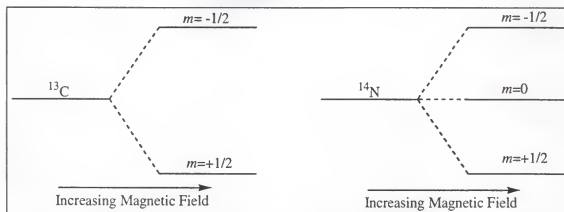


Figure A1-1. The energy level diagrams for carbon-13 (left) and nitrogen-14 (right). The NMR experiment measures the energy difference between the levels.

Where  $B_0$  is the magnetic field applied along the z-axis and  $\omega_0$  is known as the Larmor frequency of the nucleus.<sup>26</sup> Due to variations in the electronic structure near the nucleus there is a slight deviation from the applied field. This new field is called  $B_{\text{local}}$  and is fundamental to the understanding of the chemical shift. Each type of nucleus in a sample can have a different  $B_{\text{local}}$ .

The different local field at each type of nucleus gives rise to slightly different precessional frequencies. By referencing precessional frequency to a standard molecule, the chemical shift can be derived (Equation A1-3):

$$\delta = (\omega_{\text{local}} - \omega_s) / \omega_s \quad (\text{A1-3})$$

The value  $\delta$  is the chemical shift and  $\omega_s$  is the precessional frequency of a standard compound. Since  $\omega$  is field dependant while  $\delta$  is not, the chemical shift is of great use when trying to compare NMR spectra taken at different magnetic fields.

#### The Pulsed NMR Experiment

If a radio frequency field,  $B_1$ , is applied along the x-axis, the magnetization will begin to precess about the new magnetic field  $B_{\text{eff}}$  (Figure A1-2, Equation A1-4):

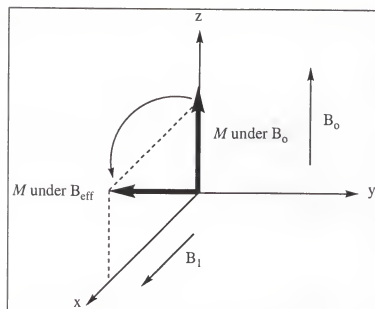


Figure A1-2. The application of a radio frequency field along the x-axis tilts  $M$  toward the xy plane. The magnetization now precesses about the new field,  $B_{\text{eff}}$ .

$$\omega_{\text{eff}} = \gamma B_{\text{eff}} \quad (\text{A1-4})$$

This can be envisioned as a tipping of  $M$  from the z-axis toward the xy plane. The efficiency of the tipping is related to how closely the frequency of the  $B_1$  field matches  $\omega_0$  (Equation A1-5):

$$B_{\text{eff}} = [(\omega_0 - \omega)^2 - \omega_1^2]^{1/2} / \gamma \quad (\text{A1-5})$$

where  $\omega$  is the precessional rate of the nuclei. When  $\omega$  is equal to the resonant frequency,  $\omega_0$ ,  $B_{\text{eff}}$  is equal to  $B_1$  and  $M$  precesses about the x axis.

In pulse NMR the  $B_1$  field is called a “hard” pulse—a short, powerful burst. During the pulse, the magnetization is tipped into the xy plane and begins to precess about the  $B_1$  field. When the pulse is turned off, the magnetization begins to return to thermal equilibrium. The rate that  $M$  returns to thermal equilibrium is governed by the rate constant  $T_1$ . As  $M$  returns to the z-axis, the magnetization in the xy plane also

decreases. The rate at which the magnetization in the xy plane decays (longitudinal relaxation) is governed by the rate constant  $T_2$ .

The intensity of the NMR signal is proportional to  $M$ . However, the relaxation constants,  $T_1$  and  $T_2$  affect the value of  $M$ . The change in  $M$  with respect to time is given by the Bloch Equation<sup>25</sup> (Equation A1-6):

$$dM/dt = \gamma \mathbf{M} \times \mathbf{B} - M_{xy}/T_2 + (M_0 - M_z)/T_1 \quad (\text{A1-6})$$

The Bloch equation is often broken down into its x, y and z components. These are collectively known as the Bloch equations.<sup>25</sup> If we allow the x and y axis to rotate at the same frequency as  $\omega_0$ , we can solve the Bloch equations to describe the observed NMR signal known as the free-induction decay (FID) (Equations A1-7 and A1-8):

$$M_y = M_0 \cos(\omega t) e^{-t/T_2} \quad (\text{A1-7})$$

$$M_x = M_0 \sin(\omega t) e^{-t/T_2} \quad (\text{A1-8})$$

The evolution of the signal along each axis is demonstrated in Figure A1-3. Fourier transform changes this data from time domain to the frequency domain and the chemical shift can then be calculated.

The NMR experiment measures the frequency at which nuclei come into resonance when placed in a magnetic field. To measure the frequency the sample must be perturbed from equilibrium. The evolution of the signal is a decaying sign wave called the FID that is acquired in time space. Fourier transform of the FID yields a frequency domain spectrum that can be referenced to a standard compound to obtain the chemical shift of the nuclei in the sample.

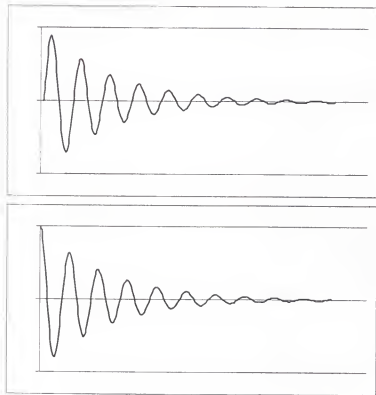


Figure A1-3. The magnetization along the x axis evolves as a decaying sin wave (top). The magnetization along y evolves as a decaying cos wave (bottom).

### Magic Angle Spinning NMR

The dipolar coupling of two nuclei has a large effect on the lineshape of the NMR signal. Dipolar couplings arise from the effect of the magnetic moment of one nucleus on the  $B_{\text{local}}$  of neighboring nuclei. The secular Hamiltonian that describes the dipolar interaction between two spins,  $i$  and  $j$ , is Equation A1-9:

$$H_D' = \sum (\hbar^2/8\pi) \gamma_i \gamma_j r_{ij}^{-3} (3\cos^2\theta - 1) (\mathbf{I}_i \cdot \mathbf{I}_j - 3I_{iz} I_{jz}) \quad (\text{A1-9})$$

Where  $i < j$ ,  $r$  is the distance and  $\theta$  is the angle between  $i$  and  $j$ ,  $\mathbf{I}_n$  is the nuclear magnetization vector of  $i$  and  $j$ , and  $I_{nz}$  is the nuclear spin operator. In the case of a liquid with rapid, random motions  $3\cos^2\theta - 1$  equals zero and the dipolar coupling is time

averaged to zero. The NMR spectrum of an  $I=1/2$  nucleus in an isotropic solution typically appears as a narrow line for each type of nucleus detected.

In the solid state, there are a large number of static dipolar interactions possible that gives rise to a slightly different  $B_{\text{local}}$  field at every nucleus (Figure A1-4). The result is that the NMR of a solid is typically very broad. The dipolar interactions can be reduced or eliminated through the use of MAS. Rapid rotation of the sample about the magic angle causes the dipolar moments to align with the magic angle. When the sample is spinning Equation A1-9 can be rewritten to the time averaged, spinning dipolar Hamiltonian, Equation A1-10:

$$H_{D,\text{ave}}^I = (\hbar^2/16\pi) (3\cos^2\beta - 1) \sum \gamma_i\gamma_j r_{ij}^{-3} (3\cos^2\beta_{ij} - 1) (\mathbf{I}_i\mathbf{I}_j - 3I_{iz}I_{jz}) \quad (\text{A1-10})$$

Where  $\beta$  is the angle between the spinning axis and the magnetic field and  $\beta_{ij}$  is the angle between spin  $i$  and  $j$ . When  $\beta$  is set equal to  $54.7^\circ$ ,  $H_{D,\text{ave}}^I$  is equal to zero. At  $54.7^\circ$  the line width of the solid is greatly reduced, allowing for the acquisition of moderately high resolution solid state NMR.

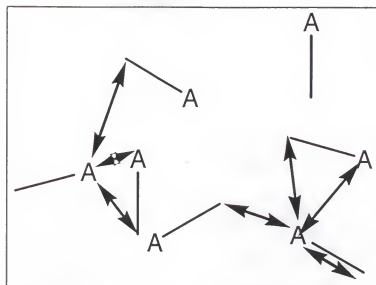


Figure A1-4. The different dipolar interactions experienced by the  $A$  nucleus in two different regions of the sample. The difference in the dipolar interactions results in a change in  $B_{\text{local}}$  and hence a change in the chemical shift of each nucleus.



## APPENDIX II

### OPERATING THE SOLID STATE BRUKER AVANCE 400 MHz NMR SPECTROMETER

#### Introduction

The Bruker Avance 400 MHz spectrometer at the University of Florida Chemistry Department is capable of performing high power solid wide line, solid MAS, and liquids high resolution NMR and imaging. The solid state NMR capabilities include a high power wide line probe; a 4 mm (rotor outer diameter) cross-polarization, triple resonance MAS probe (CP-MAS); and a 2.5 mm MAS probe designed to perform multiple quantum experiments. The selection of the probe depends on the experiments to be performed and also on the amount of sample available.

#### Probe Descriptions

The 4 mm CP-MAS probe is a triple resonance probe. It has a high power  $^1\text{H}$ - $^{19}\text{F}$  high band channel that can be used for decoupling, cross polarization, or detection; a channel ('X') tunable from  $^{13}\text{C}$  to  $^{31}\text{P}$ , and a second channel ('Y') that is tuned with the aid of special inserts. The maximum spinning speed of this probe is 16 kHz. It is a variable temperature (VT) probe capable of operation over the temperature range  $-120\text{ }^{\circ}\text{C}$  to  $+120\text{ }^{\circ}\text{C}$ . The rotors used with this probe are made out of zirconium oxide ( $\text{ZrO}_2$ , volume is approximately 80  $\mu\text{l}$ ), three different types of caps are available for use (Table A2-1).

Table A2-1. The list of rotor parts for the 4 mm CP- MAS probe and reordering information there

Part	Part Number	Approximate Cost in 1999 Dollars
Kel-F Cap	B200155 ea.	50
Barium Nitride Cap	K1927 ( for 10)	50 ea.
ZrO <sub>2</sub> Cap	B200154	250
4 mm ZrO <sub>2</sub> rotor	B0660	250

To pack the 4 mm ZrO<sub>2</sub> rotors the sample must be first ground into a powder. The 4 mm rotor is then slipped into the bottom of the loading funnel and the powder is poured into the rotor stopping to pack the solid occasionally with the packing tool. On the bottom of the packing tool is a depth gauge. The depth of the sample should be checked with this tool. When the sample has reached the height of the depth gauge, stop filling the rotor. Finally, ensure that a continuous black line traces out three quarters of the bottom of the rotor (Figure A2-1). This line allows the spin counter to determine the rotor rotation frequency. If a line is not present it can be made with a black "Sharpie" brand marker, No. 30001. There are a few special considerations necessary for packing the rotor depending on the rotor cap to be used.

The standard cap for use with this rotor is made of Kel-F, a perfluorinated polymer. This cap is useful over the temperature range -50 °C to +50 °C. Operation below this limit will cause the cap to contract and results in sample ejection from the rotor, while at temperatures above the limit, the cap becomes soft and can become deformed, allowing sample to be lost or catastrophic rotor failure to occur. To use this

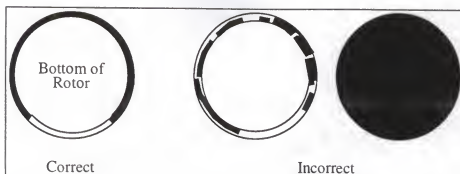


Figure A2-1. The correct way to mark the bottom of the rotor is with a solid black line three quarters of the way around the outside edge.

rotor cap, pack the sample as described above and then gently push the cap into the rotor, using a flat surface to brace the top of the cap if necessary. To unpack the rotor, first try loosening the cap with fingers (a few Kim-Wipes will prevent the flutes from cutting into skin). If the cap is too tight, use the cap remover. The cap remover is essentially two razor blades that have been attached to the top of a piece of metal with a hole in it. The rotor assembly is slipped into the cap remover, and the blades are positioned at the interface between the rotor and the cap. Extreme care must be taken to avoid pressing against any other part of the cap or the blades will cut into the cap, ruining it. Holding the rotor firmly and placing a finger over the cap, pull the rotor directly away from the cap.

A second type of cap is made out of barium nitride a white, chalk like material. Extreme care must be used with these rotor caps as barium nitride is very brittle and soft. It is unlikely that these rotors can be used more than one or two times. These rotors can be used at any temperature the probe is capable of operating at. Pack the rotor as described above. Gently lower the cap into the rotor. Almost no force should be used. If at any point it becomes difficult to insert the cap, remove it and use a razor blade to

remove some of the barium nitride from the lower portion of the cap and then try again. Repeat this process as necessary. Barium nitride is so soft that eventually enough material will be lost from the cap to make it unusable. The cap should only be removed with fingers-- the cap removal tool will destroy the cap immediately. If the cap cannot be removed, it can be destroyed with a drill and a suitably small bit (<3 mm).

The third type of rotor cap is made from zirconium oxide. The cap is opaque and white, with a hollow center and two slits on the bottom. Like the barium nitride caps, these caps can be used at any temperature that the probe can be used at. To use this cap, pack the rotor with a slightly less than usual amount of sample and then clean the exposed inside of the rotor to insure that no sample remains where the rotor blades will touch. Where Barium nitride was soft and brittle, zirconium oxide is hard and fragile. A small amount of powder between the rotor and the cap blade will result in the cracking of the blade. The cap should be pressed *straight* down into the rotor. This cap should only be removed with fingers and should be pulled straight out and never be wiggled or twisted, as this will break the blades.

Insertion of the 4 mm MAS probe should only be performed with the assistance of an individual familiar with this procedure. The first step is inserting the probe into the bore of the magnet. With the channel connectors facing to the left (toward the preamplifiers) gently push the probe all the way into the bore and secure it with the lever mounted on the shim stack. (Do not pull down on the shim stack.) Next, find the 4 mm sample injection tube (SIT). This tube is approximately 3.5 feet in length and is a pale green color. It is important to not use the 2.5 mm SIT. Lower the SIT through the top of the bore and seat it into the probe head by slowly twisting it. It will lock in place by

dropping slightly. In the MAS tube bundle, find the two long air tubes. One is the eject air and is labeled with a 'E' the other is the insert air and is labeled with a 'I.' Connect these tubes to the quick connectors with the same labels on the SIT.

The next step is connecting the drive, bearing, body air, and spin counter to the probe (Figure A2-2). The drive air connects next to the channel ports on the front of the probe. Next attach the body air by pressing the plain tube into the blue hole on the right side on the probe. Attach the spin counter (small gray cable) to the right bottom side of the probe. Finally, attach the bearing air to the left side of the probe. The bearing air is secured with a clip that is tightened down to prevent air loss. The next step is connecting the high power proton and X channel preamps to the probe, and the low power X preamp to the Y channel, if necessary. The probe is now ready to be used for room temperature experiments.

The rotor is inserted into the assembled probe/SIT by first pressing the 'insert' button on the MAS control panel located on the console. Drop the rotor into the hole on top of the SIT with the flutes toward the top. Put the SIT cap over the hole, leaving a 2 mm gap. Press the stop button. If necessary the insertion of the sample into the stator can be monitored by the change in tune of the probe. Access the acquisition window in the X\_Win2.1 program by typing 'acqu.' Typing 'wobb' activates the tuning program. Tune the empty probe and then click on the 'Wobb-SW' button in the acquisition window. Keep the tuning frequency the same, but open the tune range to 20 MHz. Now inject the sample, if the sample enters the stator the tune will change noticeably. If the rotor does not enter the stator, press the 'eject' button and reinsert the sample.

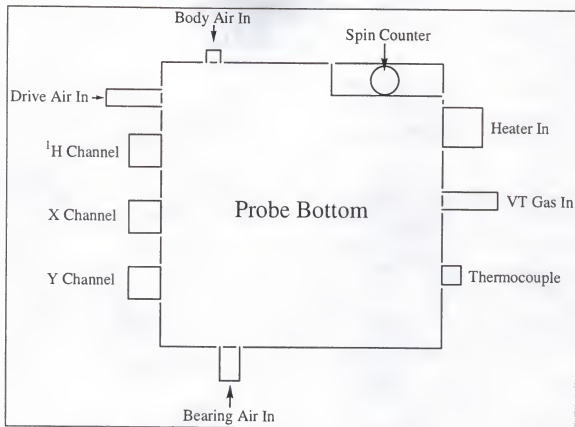


Figure A2-2. A schematic of the bottom of the 4 mm CP-MAS probe.

To spin the rotor press the 'bearing' button on the MAS controller and set the bearing air pressure to 2000 mb. Next press the 'drive' button and slowly raise the drive air until the desired spinning rate is obtained.

To eject the sample, lower the drive air to zero and slowly lower the bearing air until the spinning speed drops. Next press the 'eject' button (make sure that the SIT cap is on first!). After the rotor has been removed press stop. The contents can be removed with a copper wire or a drill bit.

This probe is also equipped with several inserts to increase the tuning range. The inserts should not be used without proper training as changing them involves taking the probe apart (Table A2-2).

Table A2-2. The available tuning inserts for the 4 mm CP-MAS probe.

Insert	X channel	Y channel
1	$^{31}\text{P}$	-
2	$^{31}\text{P}$	$^{13}\text{C}$
3	$^{13}\text{C}$	$^2\text{H}$
4	$^{13}\text{C}$	$^{15}\text{N}$

The second MAS probe that is available is the 2.5 mm probe. It has a high power channel tunable to  $^1\text{H}$  or  $^{19}\text{F}$  that can be used for decoupling, cross polarization or detection and a single 'X' channel tunable from  $^{13}\text{C}$  to  $^{31}\text{P}$ . The maximum spinning speed of this probe is 35 kHz. It is a variable temperature (VT) probe capable of operation over the temperature range  $-30\text{ }^{\circ}\text{C}$  to  $+70\text{ }^{\circ}\text{C}$ . The rotors used with this probe are also made out  $\text{ZrO}_2$  (volume is approximately 12  $\mu\text{l}$ ). The rotor caps are made from a plastic material.

The rotor is loaded in exactly the same was as the 4 mm rotor, however, a smaller funnel and packing tool is used. The packing tool also has a small drill bit on it that is used to remove the sample from the probe. The probe is installed into the magnet in a similar manner to the 4 mm probe but the 2.5 mm SIT is used (Figure A2-3).

The final probe available for solids NMR is a high power wide line. This probe has several different inserts that are used to select the tuning range. The available inserts and their tuning ranges listed in Table A2-3.

Table A2-3. The tuning inserts for the high power wide line probe.

Insert Serial Number	Tuning Range (MHz)	Nuclei in Range
HZ1930	5-34	$^{109}\text{Ag}$ , $^{14}\text{N}$
HZ2808	56-118	$^2\text{H}$
HZ03344	56-118	$^2\text{H}$
HZ2809	73-130	$^{13}\text{C}$ , $^{27}\text{Al}$
HZ03346	73-130	$^{13}\text{C}$ , $^{27}\text{Al}$
HZ2814	115-163	$^{31}\text{P}$
HZ03348	115-163	$^{31}\text{P}$

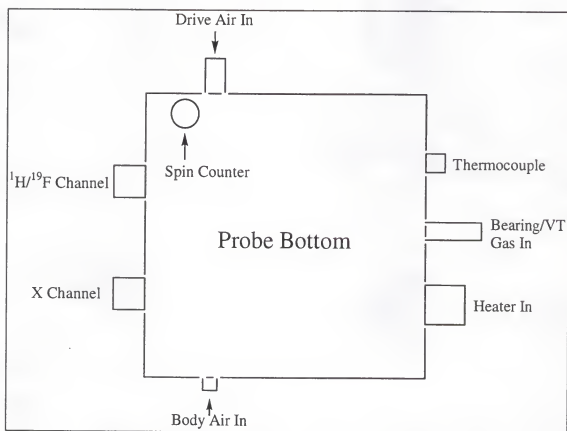


Figure A2-3. A schematic of the bottom of the 2.5 mm MAS probe.



Placing a sample in this probe is very simple. First remove the probe head by unscrewing it. The rotor head has a dewared glass portion and should be treated carefully. Next slip the sample between the coils and replace the probe head. The probe is then inserted into the bore of the magnet in the same way as the MAS probes; however, there is only one channel. This should be connected to the high power 'X' preamp.

To perform variable temperature experiments, hook up the 3 VT cables to the probe. The green VT gas is hooked up to the glass connector, the heater (gray cable) is attached to the left of the VT gas, and the thermocouple (blue cable) is hooked up to the right. The probe temperature can now be used to perform 'hot' VT by using the 'edte' window in X\_win2.1. The probe is capable of operation to +400 °C in this configuration.

Cold VT requires that the VT gas pass through a heat exchanger. The end of the green VT gas line is removed and placed aside. The open end of this tube is inserted into the VT line on the exchanger, and the VT out is hooked up to the probe. A liquid nitrogen tank is used to fill the Bruker 20 L Dewer. Next, a glass Dewer is inserted through the top of the magnet bore. This Dewer is very delicate and the up most care should be used when handling it. The Dewer fits into the ground glass joint on the top of the probe head. During the experiment, the Dewer freezes to the probe so the system must be returned to room temperature before it can be removed.

#### Glossary of Common Commands for Xwin2.1

The commands below are the minimum required to use X\_Win2.1 to do simple 1D NMR experiments. A detailed description of each command can be found in the manuals, so only a 'working' description of each command will be given.

## Command List

abs- automatic baseline correction.

ased- acquisition setup and edit. This command opens a window which allows many experimental parameters to be set including the pulse program and acquisition time.

acqu- brings up the acquisition window. The acquisition window allows the observation of the FID.

eda- edit acquisition parameters. This command is similar to ased except more parameters are available.

edasp- edit acquisition set up. This command opens a window which display a graphical representation of the amplifiers and preamplifiers used.

edc- allows the creation of a new experiment number or a new experiment name.

efp- exponential multiply FID then Fourier transform with phase correction.

em- exponential multiply. Multiplies the FID by a exponential that depends on the value in ls.

expt- experiment time.

fp- Fourier transform with phase correction.

ft- Fourier transform.

go- resumes an experiment that was interrupted with the halt command.

gs- used in the acquisition window. This command runs the pulse program continuously.

It also opens a window that allows the real time setting of many important values such as delays and pulse widths.

halt- stops an experiment without data loss. The experiment can be continued with the go command.

lb- line broadening. Sets the value used by em.

ls- left shift. Left shifts the FID by the number of points in nsp. The ls command must be used before Fourier transforming the FID.

ns- number of scans. Sets the number of transients.

nsp- number of shift points. Sets the number of shift points used by ls.

pk- phase correction. Phases the spectrum with the last phasing parameters used.

powmod- power mode. Selects either the high power or low power amplifiers.

re- allows for the change of experiment and/or process number without using edc. The format of this command is re # \$, where # is the new experiment number and \$ is the new process number. The experiment number can be changed without inputting a new process number.

setti- set title.

stop. Stops an experiment with data loss.

xwinplot- activates the plotting program. A manual with the complete description of how to operate this versatile program has been prepared by Bruker.

zg- zero and go. Starts an experiment.

## REFERENCES

1. Gogate, M. R.; Spivey, J. J.; Zoeller, J. R. "Symposium of Syngas Conversion. . ." New Orleans, March 24-29, **1996**.
2. Thomas, J. M.; Zamaraev, K. I. *Agnew. Chem. Intl. Ed. Engl.* **1994**, *33*, 308-312.
3. Guisnet, M. R. *Acc. Chem. Res.* **1990**, *23*, 392-398.
4. Trotta, R.; Miracca, I. *Catalysis Today* **1997**, *34*, 447.
5. Elkanzi, E. M. *Chem. Eng. and Process.* **1996**, *35*, 131.
6. Nikolopoulos, A. A.; Kogelbauer, A.; Goodwin, J. G. Jr.; Marcelin, G. *Catal. Lett.* **1996**, *39* 173-178.
7. Lewis, G. N. "Valence and the structure of Atoms and Molecules" **1923**, Chemical Catalogue, New York.
8. Luder, W. F.; Zuffanti, S.; "The Electronic Theory of Acids and Bases, 2<sup>nd</sup> Ed." **1961**, Dover, New York.
9. Drago, R. S.; Matwiyoff, N. A. "Acids and Bases" **1963**, Heath; Lexington, MA.
10. Huheey, J. E.; Keiter, E. A.; Keiter, R. L. "Inorganic Chemistry: Principles of Structure and Reactivity 4<sup>th</sup> Ed." **1993**, HaprerCollins College Publishers, New York.
11. Savitz, S.; Myers, A. L.; Gorte, R. J.; White, D. *J. Am. Chem. Soc.* **1998**, *120*, 5701-5703.

12. Ho, N. T.; Gander, B.; Nguyen, V. P.; Gentili, S.; Sabra, F. *J. Phys. Chem.* **1995**, *99*, 3806-3809.
13. Tanabe, K. "New Solid Acids and Bases" **1989**, Elsevier Press, New York.
14. Parrillo, D. J.; Adamo, A. T.; Kokotailo, G. T.; Gorte, R. J. *Appl. Catal.* **1990**, *67*, 107-118.
15. Nikolopoulos, A. A.; Kogelbauer, A.; Goodwin, J. G. Jr.; Marcelin, G. *J. Catal.* **1996**, *158*, 76.
16. Brunner, E. *Catal. Today* **1997**, *38*, 361-376.
17. Symons, M. C. R.; Eaton, G. *J. Chem. Soc. Faraday Trans. 1*, **1982**, *78*, 3033-3044.
18. Lunsford, J. H.; Rothwell, W. P.; Shen, W. *J. Am. Chem. Soc.*, **1985**, *107*, 1540-1547.
19. Mayer, U.; Hoffmann, H.; Kellner, R. *Monatsh. Chem.* **1988**, *119*, 1207-1221.
20. Mayer, U.; Hoffmann, H.; Kellner, R. *Monatsh. Chem.* **1988**, *119*, 1223-1239.
21. Langner, R.; Zundel, G. *J. Phys. Chem.* **1995**, *99*, 12214-12219.
22. Yamanaka, T.; Tanabe, K. *J. Phys. Chem.* **1975**, *79*, 2409.
23. Coster, D.J.; Bendada, A.; Chen, F. R.; Fripiat, J. J. *J. Catal.* **1993**, *140*, 497-509.
24. Sheng, T.; Gay, I. D. *J. Catal.* **1994**, *145*, 10.
25. Stejskal, E. O.; Memory, J. D. "High Resolution in the Solid State: Fundamentals of CP/MAS" **1994**, Oxford University Press, New York.
26. Sanders, J. K. M.; Hunter, B. K. "Modern NMR Spectroscopy: A Guide for Chemists, 2<sup>nd</sup> Ed." **1993**, Oxford University Press, New York.
27. Kolling, O. W. *Transactions of the Kansas Academy of Science* **1984**, *84*, 115-118.
28. Baltusis, L.; Frye, J. S.; Maciel, G. E. *J. Am. Chem. Soc.* **1986**, *108*, 7119- 7120.
29. Baltusis, L.; Frye, J. S.; Maciel, G. E. *J. Am. Chem. Soc.* **1987**, *109*, 40-46.

30. Riddle, F. L.; Fowkes, F. M. *Polymer Preprints (Am. Chem. Soc., Div. Polym. Chem.)* **1988**, 29, 188-189.
31. Lunsford, J. H.; Tutunjian, P. N.; Chu, P.; Zalewski, D. J. *J. Phys Chem.* **1989**, 93, 2590-2595.
32. Zalewski, D. J.; Chu, P.-J.; Tutunjian, P. N.; Lunsford, J. H. *Langmuir* **1989**, 5, 1026-1030.
33. Sang, H.; Chu, H. Y.; Lunsford, J. H. *Catal. Lett.* **1994**, 26, 235-246.
34. Guillaume, D.; Gautier, S.; Despujol, I.; Alario, F.; Beccat, P. *Catal. Lett.* **1997**, 43, 213-218.
35. Ripmeester, J. A. *J. Am. Chem. Soc.* **1983**, 105, 2925-2927.
36. Maciel, G. E.; Haw, J. F.; Chuang, I.-S.; Hawkins, B. L.; Early, T. E.; McKay, D. R.; Petrakis, L. *J. Am. Chem. Soc.* **1983**, 105, 5529-5535.
37. Haw, J. F.; Chuang, I.-S.; Hawkins, B. L.; Maciel, G. E. *J. Am. Chem. Soc.* **1983**, 105, 7206-7207.
38. Majors, P. D.; Ellis, P. D. *J. Am. Chem. Soc.* **1987**, 109, 1648-1653.
39. Xu, T.; Kob, N.; Drago, R. S.; Nicholas, J. B.; Haw, J. F. *J. Am. Chem. Soc.* **1997**, 119, 12231-12239.
40. Mayer, U.; Gutmann, V.; Gerger, W. *Monatsh. Chem.* **1975**, 106, 1235-1257.
41. Churchill, M. R.; DeBoer, B. G.; Mendak, S. J. *Inorg. Chem.* **1975**, 14, 2496-2501.
42. Riddle, F. L. Jr.; Fowkes, F. M. *J. Am. Chem. Soc.* **1990**, 112, 3259-3264.
43. Zalewski, D. J.; Chu, P.; Tutunjian, P. N.; Lunsford, J. H. *Langmuir* **1989**, 5, 1026-1030.

44. Rakiewicz, E. F.; Peters, A. W.; Wormsbecher, R. F.; Sutovich, K. J.; Mueller, K. T.  
*J. Phys. Chem.* **1998**, *102*, 2890-2896.
45. Chesnut, D. B. *J. Am. Chem. Soc.* **1998**, *120*, 10504-10510.
46. Feher, F. J.; Budzichowski, T. A.; Weller, K. J. *Polyhedron* **1993**, *12*, 591-599.
47. Biaglow, A. I.; Gorte, R. J.; Kokotailo, G. T.; White, D. J. *Catal.* **1994**, *148*, 779-786.
48. Biaglow, A. I.; Gorte, R. J.; White, D. J. *Catal.* **1994**, *150*, 221-224.
49. Biaglow A. I.; Sepa, J.; Gorte, R. J.; White, D. J. *Catal.* **1995**, *151*, 373-384
50. Fletcher, W. P.; Gilbert, C. S.; Biaglow, A. I. *Catalysis Letters* **1997**, *47*, 135-142.
51. Farcasiu, D.; Ghenciu, A. *J. Org. Chem.* **1991**, *56*, 6050.
52. Farcasiu, D.; Ghenciu, A.; Miller, G. *Journal of Catalysis* **1992**, *134*, 118-125.
53. Farcasiu, D.; Ghenciu, A. *J. Catal.* **1992**, *134*, 126.
54. Farcasiu, D.; Ghenciu, A. *J. Am. Chem. Soc.* **1993**, *115*, 10901.
55. Xu, T.; Munson, E. J.; Haw, J. F. *J. Am. Chem. Soc.* **1994**, *116*, 1962.
56. Joerg, S. D. "Extensions of the Electrostatic-Covalent and Unified Solvation Models"  
**1998** University of Florida, Gainesville, FL.
57. Klinowski, J. *Chem. Rev.* **1991**, *91*, 1459-1479.
58. Engelhardt, G.; Lohse, U.; Lippmaa, E.; Tarmak, M.; Magi, M. Z. *Anorg. Allg. Chem.*  
**1981**, *482*, 49.
59. Thomas, J. M.; Fyfe, C. A.; Ramdas, S.; Klinowski, J.; Gobbi, G. C. *J. Phys. Chem.*  
**1982**, *86*, 3061.
60. Freude, D.; Frohlich, T.; Pfeifer, H.; Scheler G. *Zeolites* **1983**, *3*, 171.
61. Samoson, A.; Lippmaa, E. *Phys. Rev.* **1983**, *28*, 6565.
62. Samoson, A.; Lippmaa, E. *Chem. Phys. Lett.* **1983**, *100*, 205.

63. Man, P. P. *Magn. Reson.* **1986**, 67, 78.
64. Man, P. P. *Magn. Reson.* **1988**, 77, 148.
65. Man, P. P.; Klinowski, J. *Chem. Phys. Lett.* **1988**, 147, 581.
66. Man, P. P.; Klinowski, J.; Trokiner, A.; Zanni, H.; Papon, P. *Chem. Phys. Lett.* **1988**, 151, 43.
67. Huggins, B. A.; Ellis, P. D. *J. Am. Chem. Soc.* **1992**, 114, 2098-2108.
68. Pearson, R. M. *J. Catal.* **1971**, 23, 388.
69. Anderson, M. W.; Barrie, P. J.; Klinowski, J. *J. Phys. Chem.* **1991**, 95, 235-239.
70. Heeribout, L.; Batamack, P.; Doremieux-Morin, C.; Fraissard, R. V. *Coll. and Surf. A* **1996**, 115, 229-237.
71. Doremieux-Morin, C.; Fraissard, J. *Spectrosc. Eur.* **1997**, 9, 8-14.
72. Parrillo, D. J.; Gorte, R. J. *J. Phys. Chem.* **1993**, 97, 8786-8792.
73. Drago, R. S.; Dias, S. C.; Torrealba, M.; Lima, L. *J. Am. Chem. Soc.* **1997**, 119, 4444-4452.
74. Chronister, C. W.; Drago, R. S. *J. Am. Chem. Soc.* **1993**, 115, 4793-4798.
75. Drago, R. S.; Petrosius, S. C.; Chronister, C. W. *Inorg. Chem.* **1994**, 33, 367-372.
76. Drago, R. S.; Kob, N. *J. Phys. Chem. B* **1997**, 101, 3360-3364.
77. Drago, R. S.; Dias, J. A.; Maier, T. O. *J. Am. Chem. Soc.* **1997**, 119, 7702-7710.
78. Kob, N.; Drago, R. S.; Young, V. *Inorg. Chem.* **1997**, 36, 5127-5131.
79. Drago, R. S.; Dias, S. C.; McGilvray; Mateus, A. L. M. L. *J. Phys. Chem. B* **1998**, 102, 1509-1514.
80. Dias, S. C. "Characterization of Zeolites and Zeotypes" **1997**, University of Florida, Gainesville, FL.



81. Dias, J. A. "Acidity of 12-Tungstophosphoric Acid and its Cesium Derivatives" **1997**, University of Florida, Gainesville, FL.
82. Scott, B. J. "A Cal-Ad Analysis of a Series of Amorphous Aluminosilicates and Gamma-Alumina" **1998**, University of Florida, Gainesville, FL.
83. Dias, J. A.; Osegovic, J. P.; Drago, R. S. *J. Catal.* Accepted 12/98.
84. Chen, D. T.; Sharma, S. B.; Filimonov, I.; Dumesic, J. A. *Catal. Lett.* **1992**, *12*, 201-212.
85. Gonzalez, M. R.; Sharma, S. B.; Chen, D. T.; Dumesic, J. A. *Catal. Lett.* **1993**, *18*, 183-192.
86. Wakabayashi, F.; Kondo, J. N.; Domen, K.; Hirose, C. *J. Phys. Chem.* **1995**, *99*, 10573-10580.
87. Weitkamp, J.; Karge, H. G.; Pfeifer, H.; Holderich, W. "Studies in Surface Science and Catalysis (Vol. 84), Zeolites and Related Microporous Materials: State of the Art 1994 (Part B)" **1994**, Elsevier Science; Amsterdam.
88. Nayak, V. S.; Choudhary, V. R. *Indian J. Technol.* **1983**, *21*, 376-8.
89. Auroux, A.; Wierzchowski, P.; Gravelle, P. C. *Thermochim. Acta* **1979**, *32*, 165-70.
90. Beyer, H. K.; Karge, H. G.; Kiricsi, I.; Nagy, J. B. "Studies in Surface Science and Catalysis (Vol. 94), Catalysis by Microporous Materials" **1995**, Elsevier Science, Amsterdam.
91. Webster, C. E.; Osegovic, J. P.; Scott, B. J.; Dias, S. C. *Micro. and Meso. Mater.* Accepted 12/98.
92. Parrillo, D. J.; Gorte, R. J. *Thermochim. Acta* **1998**, *312*, 125-132.
93. Eder, F.; Stockenhuber, M.; Lercher, J. A. *J. Phys. Chem. B* **1997**, *101*, 5414-5419.

94. Farneth, W. E.; Gorte, R. J. *Chem. Rev.* **1995**, *120*, 5701-5703.
95. Parillo, D. J.; Gorte, R. J. *J. Phys. Chem.* **1993**, *97*, 8786-8792.
96. Lide, D. R., editor "CRC Handbook of Chemistry and Physics 72nd Ed." **1991**, CRC Press, Boca Raton, FL.
97. Drago, R. S., Dias J. A., and Maier, T. O., *J. Am. Chem. Soc.* **1997**, *119*, 7702.
98. Kanda, Y.; Lee, K. Y.; Nakata, S.; Asaoka, S.; Misono, M. *Chem. Lett.* **1988**, 139.
99. Rocchiccioli-Deltcheff, C.; Thouvenot, R.; and Franck, R. *Spectrochim. Acta.* **1976**, *32A*, 587.
100. Rocchiccioli-Deltcheff, C.; Fournier M.; Franck, R.; Thouvenot, R. *Inorg. Chem.* **1983**, *27*, 207.
101. Highfield, J. G.; Moffat, J. B. *J. Catal.* **1984**, *88*, 177.
102. Southward, B. W. L.; Vaughan, J. S.; O'Connor, C. T. *J. Catal.* **1995**, *153*, 293.
103. Varga, G. M. Jr.; Papaconstantinou, E.; Pope, M. T. *Inorg. Chem.* **1970**, *9*, 662.
104. West, F. S.; Audrieth, L. F. *J. Phys. Chem.* **1955**, *59*, 1069.
105. Hodnett, B. K.; Moffat, J. B. *J. Catal.* **1984**, *88*, 253.
106. Hodnett, B. K.; Moffat, J. B. *J. Catal.* **1985**, *91*, 93.
107. Kapustin, G. I.; Brueva, T. R.; Klyachko, A. L.; Timofeeva, M. N.; Kulikov, S. M.; Kozhevnikov, I. V. *Kinet. and Catal.* **1990**, *31*, 896.
108. Jozefowicz, L. C.; Karge, H. G.; Vasilyeva, E.; Moffat, J. B. *Micropor. Mater.* **1993**, *1*, 313.
109. Lefebvre, F.; Liu-Cai, F. X.; Auroux, A. *J. Mater. Chem.* **1994**, *4*, 125.
110. Ghosh, A. K.; Moffat, J. B. *J. Catal.* **1986**, *101*, 238.
111. Kulikov, S. M.; Kozhevnikov, I. V. *Russ. Chem. Bull.* **1981**, 348.

112. Farcasiu, D.; Li, J. Q. *J. Catal.* **1995**, *152*, 198.
113. Keggin, J. F. *Nature* **1933**, *131*, 908.
114. Keggin, J. F. *Proc. Roy. Soc. A* **1934**, *144*, 75.
115. Brown, G. M.; Noe-Spirlet, M. R.; Busing, W. R.; Levy, H. A. *Acta. Cryst. B* **1977**, *33*, 1038.
116. Pope, M. T. "Heteropoly and Isopoly Oxometalates." **1983**, Springer-Verlag, Berlin.
117. Corma, A.; Martínez, A.; Martínez, C. *J. Catal.* **1996**, *164*, 422.
118. Drago, R. S.; Petrosius, S. C.; Kaufman, P. B. *J. Mol. Cat.* **1994**, *89*, 317-328.
119. Drago, R. S.; Petrosius, S. C.; Chronister, C. W. *Inorg. Chem.* **1994**, *33*, 367-372.
120. Lindqvist, I.; Olofsson, G. *Acta Chem. Scan.* **1959**, *13*, 1753-1757.
121. Osegovic, J. P.; Drago, R. S. *J. Catal.* in press.
122. Drago, R. S. "Applications of Electrostatic-Covalent Models in Chemistry" **1994**, Surfside Scientific Publishers, Gainesville, FL.
123. Drago, R. S.; Ferris, D.; Wong, N. G. *J. Am. Chem. Soc.* **1990**, *112*, 8953-8961.
124. Parry, E. P. *J. Catal.* **1963**, *2*, 371.
125. Webster, C. E.; Drago, R. S.; Zerner, M. C. *J. Am. Chem. Soc.* **1998**, *120*, 5509-5516.
126. Okuhara, T.; Mizuno, N.; Misono, M. *Adv. Catal.* **1996**, *41*, 113.
127. Kozhevnikov, I. V. *Catal. Rev.-Sci. Eng.* **1995**, *37*, 311.
128. Corma, A., *Chem. Rev.* **1995**, *95*, 559.
129. Hill, C. L.; Prosser-McCartha, C. M. *Coord. Chem. Rev.* **1995**, *143*, 407.

130. Izumi, Y.; Urabe, K.; Onaka, M.; "Zeolite, Clay, and Heteropoly Acids in Organic Reactions." **1992**, VCH, Tokyo.
131. Misono, M. *Catal. Rev.- Sci. Eng.* **1987**, 29, 269.
132. Mateev, K. I.; Kozhevnikov, I. V. *Russ. Chem. Rev.* **1982**, 51, 1075.
133. Pope, M. T.; Müller, A. "Polyoxometalates: from Platonic solids to anti-retroviral activity" **1994**, Klumer, Dordrech.
134. Pope, M. T.; Müller, A. *Angew. Chem. Int. Ed. Engl.* **1991**, 30, 34.
135. Hardwick, A.; Dickens, P. G.; Slade, R. T. C.; *Solid State Ionics* **1984**, 13, 345.
136. Nakamura, O.; Kodama, T.; Ogino, I.; Miyake, Y. *Chem. Lett.* **1979**, 17.
137. Tatsumisago, M.; Minomi, T. *J. Am. Ceram. Soc.* **1989**, 72, 484.
138. Nishimura, T.; Okuhara, T.; Misono, M. *Appl. Catal.* **1991**, 73, L7.
139. Okuhara, T.; Nishimura, T.; Misono, M. *Chem. Lett.* **1995**, 155.
140. Corma, A.; Martínez, A.; Martínez, C. *J. Catal.* **1996**, 164, 422.
141. Tatematsu, S.; Hibi, T.; Okuhara, T.; Misono, M. *Chem. Lett.* **1984**, 865.
142. Mizuno, N.; Misono, M. *Chem. Lett.* **1987**, 967.
143. Okuhara, T.; Nishimura, T.; Watanabe, H.; Misono, M. *J. Mol. Catal.* **1992**, 74, 247.
144. Mastikhin, V. M.; Kulikov, S. M.; Nosov, A. V.; Kozhevnikov, I. V.; Mudrakovsky, I. L.; Timofeeva, M. N. *J. Mol. Catal.* **1990**, 60, 65.
145. Hayashi, H.; Moffat, J. B. *J. Catal.* **1983**, 83, 192.
146. Okuhara, T.; Nishimura, T.; Ohashi, K.; Misono, M.; *Chem. Lett.* **1990**, 1201.
147. Lee, K. Y.; Arai, T.; Nakata, S.; Asaoka, S.; Okuhara, T.; Misono, M. *J. Am. Chem. Soc.* **1992**, 114, 2836.

148. Corma, A.; Martinez, A. *Catal. Rev.-Sci. Eng.* **1993**, 35, 483-570.
149. Nicolaides, C. P.; Stotijn, C. J.; van der Veen, E. R. A.; Visser, M. S. *Appl. Catal. A.* **1993**, 103, 223-232.
150. Collignon, F.; Mariani, M.; Moreno, S.; Remy, M.; Poncelet, G. *J. Catal.* **1997**, 166, 53-66.
151. McGilvray, J. M. "The Multiple Equilibria Analysis Model and its Application to the Study of Adsorption" **1997**, University of Florida, Gainesville, FL.
152. Cotton, F. A.; Wilkinson, G. "Advanced Inorganic Chemistry, 5<sup>th</sup> Ed." **1988**, John Wiley & Sons, Inc., New York.
153. Drago, R. S.; Getty, E. E. *J. Am. Chem. Soc.* **1988**, 110, 3311-3312.
154. Getty, E. E.; Drago, R. S. *Inorg. Chem.* **1990**, 29, 1186-1192.
155. Olah, G. A.; Prakash, G. K. S.; Sommer, J. "Superacids" **1985**, Wiley, New York.
156. Mirodatos, C.; Barthomeuf, D. *J. Chem. Soc., Chem. Comm.* **1981**, 39-40.
157. Drago, R. S. "Physical Methods for Chemists, 2<sup>nd</sup> Ed." **1992**, Surfside Scientific Publishers, Gainesville, FL.
158. Atkins, P. W. "Physical Chemistry 5<sup>th</sup> Ed." W. H. Freeman and Company, New York, **1990**.

## BIOGRAPHICAL SKETCH

This is a brief chronological biography of the life to date of John Philip Osegovic. John was born the fifth child of John William Osegovic and Gertrude Loretta Osegovic in Tampa, Florida on November 3, 1972. He grew up attending a variety of private schools before entering the public school system at Miles Elementary School. In 1990, he graduated from Chamberlain Senior High School. That August saw two huge changes in his life: the passing of his mother to ovarian cancer and a move to Pensacola, Florida to attend the University of West Florida. His initial course of study was zoology. However, with the encouragement of Professor Grace Chiu, he quickly changed his major to chemistry.

His father passed early in 1992 to lung cancer. In 1993, he met his future wife, Karen Marie Laug. He graduated in 1995 with a Bachelor of Arts and Sciences and began graduate school at the University of Florida that August, where he met his first Research Advisor Russell S. Drago. His ability to draw the correct structure of a solid acid catalyst led Professor Drago to 'volunteer' him for solid acid research. The next significant change in his life came on July 6<sup>th</sup>, 1996 when he married Karen Laug at the First United Methodist Church in Winter Garden, Florida.

Only 17 months later, Russell Drago died at the Florida Environmental Conference. After a period of grief, John resumed and expanded the research he had begun

under Professor Drago with the approval of the UF Chemistry Department, especially Professor C. Russell Bowers, his new advisor.

John's hobbies include writing (unintentionally) bad poems for his wife, fish breeding, bird keeping, playing all sort of games, drawing and painting, and thinking of crazy new experiments to try.

I certify that I have read this study and that in my opinion it conforms to acceptable standards of scholarly presentation and is fully adequate, in scope and quality, as a dissertation for the degree of Doctor of Philosophy.



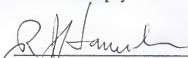
Clifford R. Bowers, Chairman  
Assistant Professor of Chemistry

I certify that I have read this study and that in my opinion it conforms to acceptable standards of scholarly presentation and is fully adequate, in scope and quality, as a dissertation for the degree of Doctor of Philosophy.



Gus Palenik  
Professor of Chemistry

I certify that I have read this study and that in my opinion it conforms to acceptable standards of scholarly presentation and is fully adequate, in scope and quality, as a dissertation for the degree of Doctor of Philosophy.



Robert J. Hanrahan  
Professor of Chemistry

I certify that I have read this study and that in my opinion it conforms to acceptable standards of scholarly presentation and is fully adequate, in scope and quality, as a dissertation for the degree of Doctor of Philosophy.



Paul A. Chadik  
Assistant Professor of Environmental Engineering  
Sciences



I certify that I have read this study and that in my opinion it conforms to acceptable standards of scholarly presentation and is fully adequate, in scope and quality, as a dissertation for the degree of Doctor of Philosophy.



---

Daniel R. Talham  
Associate Professor of Chemistry

This dissertation was submitted to the Graduate Faculty of the Department of Chemistry in the College of Liberal Arts and Sciences and to the Graduate School and was accepted as partial fulfillment of the requirements for the degree of Doctor of Philosophy.

May 1999

---

Dean, Graduate School